IMPLEMENTATION AND TESTING THE POSE COMPUTATION (POSCOM) SYSTEM

by

Melinda Harmos

A Thesis
Submitted to the College of Graduate Studies and Research
Through the Department of Industrial and Manufacturing Systems Engineering
In Partial Fulfillment of the Requirements for the
Degree of Master of Applied Science at the
University of Windsor

Windsor, Ontario, Canada
1999

0-612-52564-3

Abstract

This thesis describes the research part contributing to pose computation for accurate part positioning and reliable camera based robot workcell calibration. The pose computation technique presented here involves (1) the detection and recognition of artificial targets placed on the robot end-effector, on the fixture, and around the robot workspace; and (2) the computation of the camera pose (position and orientation) with respect to the targets using stereo triangulation. The artificial targets used for pose computation are designed for simplicity and distinctiveness so that they can be easily detected and used for pose computation. The major contribution of this technique is the use of passive vision with simple but distinctive targets for fast pose computation. Unlike many other pose computation techniques, this is based on detecting simple and unique targets. The process of target preparation and detection is described along with the formulation of stereo triangulation and pose computation. Results of target detection and stereo pose computation are also presented.

ACKNOWLEDGMENT

I would like to thank my supervisor, Dr. Waguih ElMaraghy, for his guidance and support throughout the course of this research.

I am very grateful to my husband Robert, without his support this study would not have been possible.

TABLE OF CONTENTS

LIST OF FIGURES

LIST OF TABLES

1. INTRODUCTION

1.1 General Overview

Industrial robots have been successfully employed in industry to perform a variety of tasks from welding and spray painting to material handling. However they have limited to applications which do not require very accurate robot positioning and compliant motion. Robot calibration and accurate positioning of the robot end-effector and parts within its workspace are required to allow successful execution of high accuracy robot tasks. Hence, robot and workpiece information is required, so that inaccuracies, disturbances and variations in part size (or dimensions) and position and robot kinematics (and possibly robot dynamics) can be determined and accounted for. The pose information needed for robot calibration can be obtained using many alternatives, ranging from the simple three-point-touch technique for calibration to 3-D vision sensing. In the recent years, a variety of low-cost vision sensors have appeared. With the recent advances in computer technology (in terms of increasing computing speed and expanding memory sizes) as well as the advances in solid-state technology (in terms of enhanced sensitivity and resolution and improved signal-to-noise ratios), it is becoming technically and commercially possible to use these sensors in industrial applications that require accurate and reliable 3-D measurements. It is believed that efficient algorithms need to be developed to make effective use of these sensors and to enrich the industrial robot with the required intelligence to significantly improve their performance.

1.2 Research statement and motivation

This project presents the research part contributing to the development of a sensor-integrated robotic system for automotive-body-in-white assembly using simple and low-cost off-the-shelf) vision sensors.

The pose computation technique measures the camera pose with respect to artificial targets fixed at specific locations around the robot workspace and also fixed on the end-effector and programmable fixture. The objective is to use these targets to achieve fast and accurate pose measurements. The artificial targets are designed for ease of detection and simplicity of the pose computation. Target detection is based not only on the geometry of the targets, but also on the invariance of the reflectance ratio boundaries of the targets. This technique promises to yield fast and simple target detection, simple formulation for stereo triangulation and accurate pose measurements, as will be described below in full detail.

1.3 Thesis Outline

This thesis is divided into 6 chapters and two appendixes. This chapter provides a general overview of the current work, motivations, research objectives, and the thesis outline.

Chapter 2 starts with a brief description of the camera pose computation, and presents a literature review of pose computation and stereo vision, along with the possible combination of the two.

In *Chapter 3* an overview of the pose computation system and its possible application to robot cell calibration is described. The chapter starts with presenting a general configuration of the robot cell and artificial targets, and continues by describing the different levels of pose computation and workcell calibration among the different robotic cell components.

The process of designing and detecting artificial targets is presented in *Chapter 4*. After a brief description of targets, along with their design criteria, the algorithms for detecting these features are presented along with experimental results from testing of the feature detection technique.

Chapter 5, titled "Stereo vision geometric calibration", basically presents ways of creating a calibration of the stereo vision system and describes the stereo matching of image pairs in order to get the location (x, y and z coordinate) and orientation of target.

Chapter 6 summarizes the work and gives its main conclusions and recommendations for future research.

2. LITERATURE SURVEY

2.1 Vision for 3-D Measurements

In vision based robot calibration, pose computation is a crucial step for determining the camera pose with respect to a known inertial frame, and the pose of the robot end-effector with respect to the camera or another reference frame. Pose computation is also very important in positioning parts and objects so that the execution of tasks such as assembly or welding can be carried out with the required speed and accuracy. On the other hand, range sensing has become a vital tool to various robotic applications requiring accurate and reliable 3-D measurements. Since it is proposed to employ stereo vision for pose computation, a literature review of both topics is presented along with the possible combination of stereo ranging and pose computation.

2.2 Stereo Ranging

Range sensing deals with the measurement of the distance from a reference point to objects in the scene [Jarvis, 1993]. Stereo vision is one of the most prominent ranging methods, and it is most promising and practical due to its potentially high speed and high accuracy levels. The main purpose of stereo vision analysis is to recover range (depth) information of objects in a three-dimensional (3-D) scene based on an image pair taken from two distinct views. In stereo vision, depth information is obtained from triangulation of corresponding points in the stereo image pair. Significant research has been done on stereo vision, and new stereo vision systems are still appearing [Marshall, 1992; Ross, 1993]. Further, new applications are emerging which range from automatic inspection [Marshall, 1992] and autonomous navigation of mobile robots [Bien, 1991; Kriegman, 1989], robot calibration [Bennett, 1991; Zhuang, 1991] to robot controlling system [Lantos, 1997]. The advantage of using stereo vision in industrial applications is availability, affordability and high performance of today's CCD video cameras, in addition to the ever increasing and improving computer technology in terms of speed, memory sizes and software development.

Stereo matching (correspondence between the stereo images) is a key step in stereo vision analysis. There exist two general types of stereo matching: intensity based or area-based matching [Hannah, 1989; Luo, 1995] and feature-based matching [Li, 1994; Tubaro, 1992; Venkateswar, 1995]. Feature-based stereo matching is a practical method where the speed and reliability of range finding in stereo vision depends to a great extent on the speed of feature extraction and that of establishing correspondence between the image features. The features used in the matching procedure often consist of points [Bien, 1991], edges and line segments [Brint, 1990; Marapane 1990], combinations of points and edges [Goldgof, 1992; Lee, 1994], or a hierarchy consisting of lines, vertices, edges and/or surfaces [Venkateswar, 1995]. However, although these local features are usually sparsely and irregularly distributed over the images but result in accurate depth measurement. In contrast, brightness-based processing is global and results in dense disparity maps, but such maps are difficult to achieve, particularly in passive systems. However, the features considered in most stereo vision systems and feature recognition systems are often local, very plain, and highly invariant, but not very distinct, making the correspondence task quite challenging. Hence, new techniques have recently appeared that combine both intensity- and feature-based matching [Cochran, 1992]. Others have attempted to incorporate luminance characteristics in feature-based matching [Tubaro, 1992] to integrate shape from shading techniques [Cryer, 1993] or to use disparity map along epipolar lines [Fielding, 1997]. Other advanced techniques have also appeared to solve the feature –based matching problem, by using the paradigm of prediction and verification of hypotheses [Bensrhair, 1991] or by employing relational features and searching relational graphs [Li, 1994; Parlaktuna, 1994]. Recently, a Bayaesian estimation technique was developed [Scharstein, 1998] that outperforms the techniques based on area-based matching and also the use of matching probability and compatibility coeficients for stereo matching is presented [Do, 1998].

2.3 Pose Computation

Pose computation may be regarded as determining the transformation matrix (involving three rotations and three translations) between the sensor(s) and a scene coordinate frames, given a set of corresponding image and object features and the intrinsic properties and parameters of the imaging devices (e.g. CCD cameras). The corresponding features represent the 3-D scene or object information (data relative to a known reference frame) and the image information (e.g. 2-D projective data obtained from intensity images or 3-D range data).

Most research described in the literature on pose computation has focused on solving the inverse perspective projection problem using monocular vision, where the image data consist of features such as lines and points extracted from intensity images. The inverse projection tries to obtain 3-D information from 2-D image features by applying inverse perspective transformation on these image features back to 3-D space. Significant work was reported on solving this problem with applications to object or target localization in monocular vision [Ferri, 1993; Haralick, 1989; Liu, 1990; Jacobs, 1997]. Relatively little work was done on solving the pose estimation and computation problem from range data in 3-D vision.

One major challenge associated with the inverse projection problem is establishing the correspondence between 3-D scene features and their projected image features. Generally, researchers assume that the environment is confined, and the recognition of objects of interest is complete, and the correspondences between image features and object/scene features have been obtained. However, that is not the case when dealing with a real scene or manufacturing environment. Therefore, special targets, which are more distinct than points and lines, have been used to facilitate this correspondence problem. What follows is a description of the inverse projection problem and its solution using simple features such as points and lines. The pose computation problem using specialized artificial targets will also be discussed.

2.3.1 Pose Computation by Inverse Projection and Using Simple Primitives

As described earlier, most research work on pose computation has focused on solving the inverse projection problem, where the image (projected) data consist of brightness features obtained from intensity images. Kanade, [1981] solved analytically the inverse orthographic projection problem. The orthographic projection is a sufficiently close approximation to the perspective projection in cases when the depth of the viewed object(s) is much smaller than the distance from the camera lens (i.e. the imaged surfaces are almost parallel to the image plane). However, human and camera vision can be more correctly and accurately model using the perspective projections, thus more emphasis was placed on solving the inverse perspective projection (IPP) problem.

Many different techniques have been developed for solving the pose computation problem. Many techniques attempted to find a finite number of solutions using a minimum number of point features or straight-line segments. Haralick, [1989] derived a variety of relations that govern the perspective projection using various geometric features such as points, lines and angles extracted from brightness images. Huttenlocher and Ullman, [1990] showed that the three-point had a simple solution for orthographic projections. Fischler and Bolles, [1981] showed that there might be as many as four solutions if three corresponding points were used and that solving the IPP problem required in general six point correspondences. They also proposed an analytic formulation for a unique solution using four coplanar points. An analytic solution was also proposed by Horaud, [1989] for four non-coplanar points. Similarly, Horaud, [1987] proposed analytic procedures for solving the IPP problem using three non-coplanar lines and later also Horaud, [1997] presents in detail an iterative paraperspective pose computation method for both non-coplanar and coplanar points. Dhome, [1989] gave a method for determining all the solutions using three arbitrary lines, and Sumi, [1997] proposed a new method to recognize 3D objects using segment-based stereo vision.

In many other cases, all available corresponding features, which are more than the required minimum, are used to solve the IPP problem using some optimization techniques. Roberts, [1965] proposed a classic solution in a model-based context using a minimum square-error technique for finding the transformation between the model points and the observed image points. Similarly, [Lowe, 1987; 1991] presented an elegant least-squares technique (requiring up to six pairs of image and model points) to iteratively solve for the viewpoint and object parameters from point-to-point and line-to-line correspondences. Haralick, [1989] classified the pose estimation problem into four different estimation problems from corresponding point data. They presented closed-form least-squares solutions to the over-constrained 2-D-2-D and 3-D-3-D pose estimation problems, they also gave a globally convergent iterative technique for the 2-D perspective projection (2D-PP)-3-D pose estimation problem and presented a simplified linear solution to the 2D-PP-2D-PP pose estimation problem. Liu, [1990] proposed a linear algorithm using eight or more line correspondences and a non-linear algorithm using three or more line correspondences, where line correspondences were given or derived from point correspondences. This method provided a solution for the rotation matrix and translation vector separately. Finally, there are some issues related to numerical and iterative solutions that are seldom addressed but are critical to obtain a reliable solution. These issues include the selection of the starting pose for convergence, the stability of the solution, and the efficiency of the solution in terms of computations.

Other techniques used more complex primitives than points and line segments. For example, Faugeras and Hebert, [1986] presented a method for object position computation based on surface primitives extracted from 3-D range data. Haralick, [1989] solved the IPP problem using rectangles. Richetin, [1991] solved the IPP problem using zero-curvature contour points for the localization of objects modeled by generalized cylinders. Ferri, [1993] presented analytic procedures for the perspective inversion using straight-line segments (four coplanar lines or three orthogonal line segments), as well as circular arcs and quadrics of revolution. Phong, [1995] presented a technique for optimally estimating the object 3-D poses (in terms of transformations between the camera and the object coordinate frames) from point and/or line correspondences. Recently Choy, [1997] extracted the depth information using an improved triangulation method based on stereo vision angles.

2.3.2 Pose Computation Using Artificial Targets

Simple features such as points and line drawings may not be very practical in some applications due to possible ambiguities in the correspondence between scene and image features. Therefore, special targets, which are more distinct and unique than points and lines, have been used to simplify the correspondence problem and to improve the pose computation process. Some of these targets consisted of light spots of LED patterns arranged in a specific array, and they were employed in space applications and teleoperation in nuclear and hazardous sites. Other targets, which consisted of contrast-based patterns, have also been conceived and used for pose computation, but were mostly limited to applications of autonomous vehicle navigation. Most pose computation techniques, which use such artificial targets may be regarded as model-based techniques where targets are modeled in advance and used later for on-line computation.

Numerous techniques using different types of artificial features have been reported in the literature of pose computation. In the eighties, Fukui, [1981] used a diamond-shape planar marker with known dimension to compute the camera pose with respect to the mark by relating the length of the vertical and horizontal diagonals in the image plane and the actual diagonals. Matas, [1997] placed special design patterns on the object that allowed to solve the pose computation problem easily. Magee, [1984] used a sphere marked with horizontal and vertical great circles and obtained the camera pose with respect to the sphere by computing the closest distance between the sphere's projected center and points on the projected great circles of the sphere. Abidi, [1990] used patterns of light spots, called light targets, for autonomous location of mating elements in space manipulation applications. Abidi and Chandra, [1990; 1995] also proposed a pose estimation technique based on the volume measurement of tetrahedra composed of feature-point triplets (extracted from an arbitrary quadrangular target) and the lens center of the vision system. Wang, [1993] used targets similar to bar codes for autonomous vehicle navigation. The targets consisted of two rectangular stripes of equal width and were separated by a distance equal to their width. The stripes or bars were black on a white background or vice versa. The targets were placed on a vertical plane, with their long edges being vertical. The target depth (with respect to the camera) was assumed to be constant, and the camera's optical axis and the horizontal axis of the image plane were kept horizontal and parallel to the ground. This technique proved to be reliable, accurate, fast and practical in vehicle navigation application. However, it suffered from the restricting assumptions about the scene structure and targets poses, hence could not be useful in more general applications.

Other techniques based on artificial targets were commonly used in indoor environments. Sugihara, [1988] used targets and landmarks such as vertical edges of scene objects to determine the camera position, thus avoiding sophisticated image processing. His method was based on the assumption that the scene map and that the points where vertical edges occurred were given, and the camera's optical axis was parallel to the ground. A possible location of the camera was given by a correct correspondence between the edges in the images and those given in the map through an exhaustive search. Onoguchi [1990] used stereo vision for creating a multi-information local map for the navigation of a vehicle. That stereo vision system was limited to the recognition of circles, lines and ellipses and their combinations in order to obtain the relevant depth information for navigation. Environment knowledge is built in the teaching stage which is done off-line through an operator.

2.3.3 Shading and Brightness Information

Most of the pose computation techniques described have solely relied on simple geometric features to compute the viewpoint and viewing parameters even when contrast based features were used. Shading and photometric properties have also been considered within the shape-from-shading paradigm for shape reconstruction, based on general object independent constraints [Horn, 1985]. However, these techniques have not been widely used and successfully applied for pose computation. Solving the pose computation problem using shading and photometric properties is a difficult and ill-posed one. It is not practical due to the high sensitivity of brightness-intensities to disturbances in the object poses and lighting conditions and due mainly to interreflections. However, the shading information and brightness feature properties, if effectively exploited, can be used in the correspondence part of the pose computation problem and the identification of the objects in the scene, as well as the estimation of the object pose. Although the feature identification and correspondence step can effectively use shading and image brightness information, accurate pose computation can only rely on the geometric properties of the extracted features.

In this work, stereo triangulation of specialized targets and markers to compute the camera pose (in 3-D) with respect to the observed targets or vice versa. These artificial targets have distinct features and can be quickly and accurately located in the stereo image pair. The pose computation technique employs a simple-feature based stereo matching which takes advantage of the prior knowledge about the targets' geometric and photometric properties to obtain reliable feature matching, thus providing direct and accurate 3-D pose information. The stereo vision also provides constraints that eliminate the need to solve the inverse projection problem.

3. Overview of the Pose Computation System

The pose computation module will consist of detecting special targets in the stereo image pairs, then computing the positions and orientations of these targets with respect to the camera coordinate frame, or vice versa. These targets are dark rectangular regions on bright backgrounds (or vice versa), all regions having well-defined reflectances. These targets can be either attached to the robot end effector, the programmable fixture, or fixed at specific locations around the robot workspace. These targets are designed to have simple geometries that make their detection and reconstruction easy, fast and accurate (to the sub-pixel level). Hence, they will yield fast and very accurate pose measurements. The pose information will then be fed to the calibration module, which will determine a more accurate and correct model of the robot cell, including the robots, programmable fixture and workpiece. Figure 3.1 presents the configuration of the robot workcell and the tentative locations of the targets used for pose measurements. Figure 3.2 shows the different levels of pose computation and workcell calibration among the different robotic cell components (i.e. in terms of targets fixed to these different robotic cell components).

The proposed pose computation system is novel due to the following characteristics:

- This pose computation technique uses a passive vision system that does not require special lighting, extraction of object features, or the reconstruction of object shapes from images. Instead, it relies on the detection of simple, yet unique targets, which are conveniently placed and fixed around the robot workspace.

- The target detection is simple, potentially fast and robust, hence is very practical and is likely to work effectively in the industry.
- This system will be able to cover a large volume of the workspace (between 1 m^3 and 2 m^3) at large stand-off distance in the range of 1.0 to 2.0 m, which are significantly large compared to typically short stand-off distance in laser-based sensors (e.g. 20 to 40 cm).

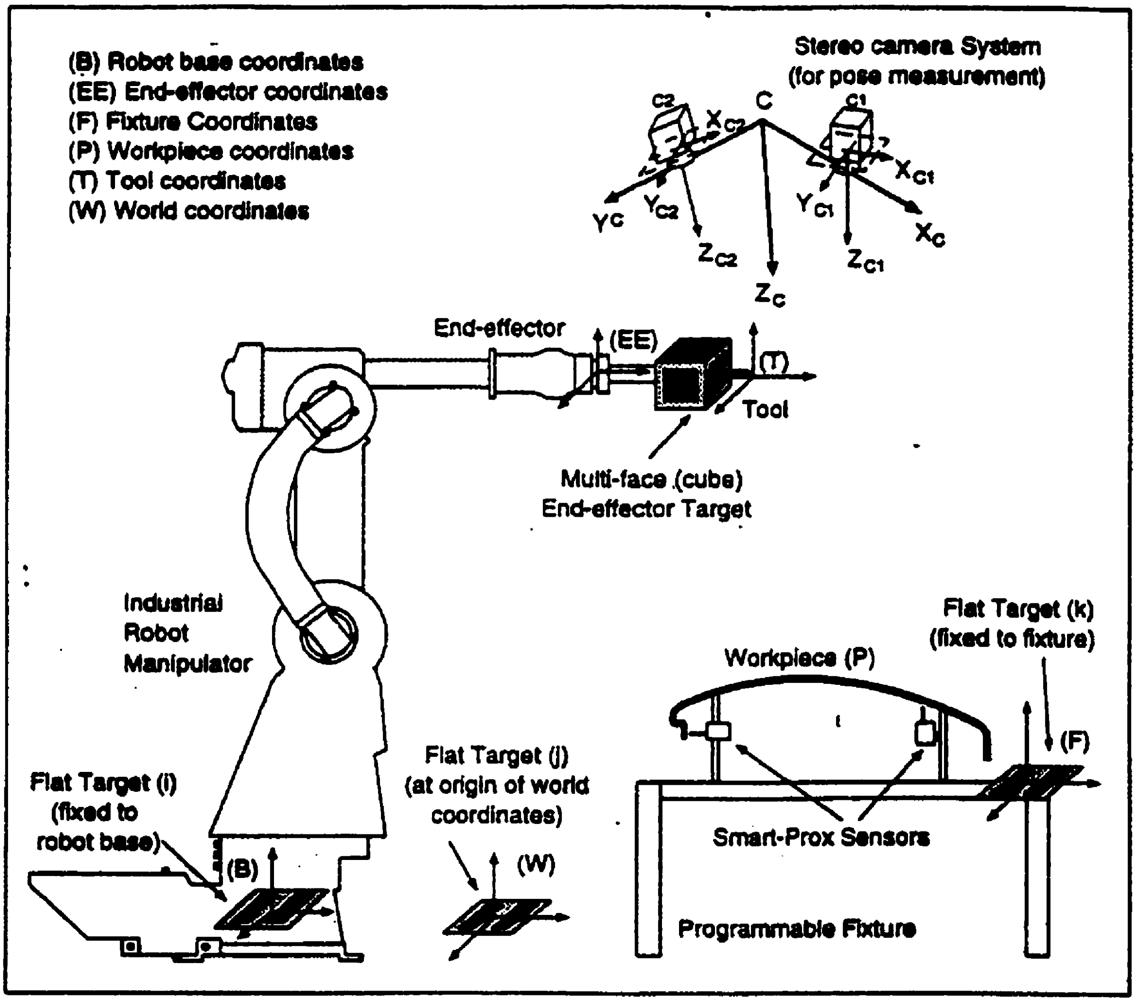

Figure 3.1 Configuration of robot cell and artificial targets used for pose computation [source: ElMaraghy, 1997]

This system has a number of advantages, as well as technical and economic benefits. First, it is passive, flexible and practical, and it uses inexpensive components. It also observes a larger workspace volume than most conventional and commercial vision sensors. Second, this system can improve the quality of manufactured products and significantly reduce their cost. For example, industrial robots have been used quite extensively in the automotive industry, but they have not been used in a flexible and efficient way.

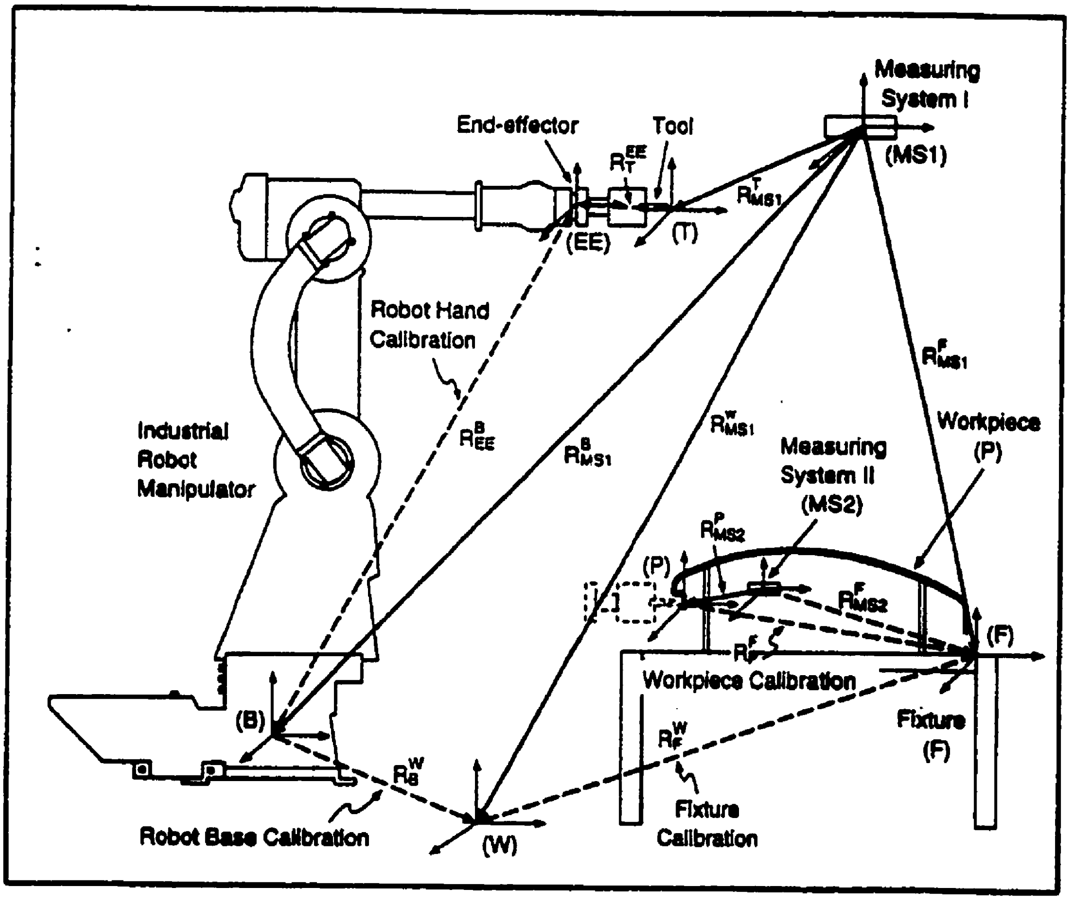

Figure 3.2 Schematics of the different robot workcell calibration steps

[source: ElMaraghy, 1997]

They could not adapt to changes and disturbances in the scene, hence resulting in a poor and inaccurate task execution, leading to low quality production. The proposed vision system would be an effective tool for industrial robots to become flexible, to be able to adjust to uncertainties and disturbances and to compensate for geometric and dimensional deviations of the parts. Besides the improved product quality, this system would significantly help reduce the number of assemblies or subassemblies that need to be rejected or reworked, resulting in substantial cost savings.

4. Artificial Feature Detection and Identification

This section describes the process of detecting specialized artificial targets placed around the robotic workcell, which will be used for pose computation. These targets are described, along with their design criteria and their brightness calibration (in terms of their reflectance ratios). The algorithms for detecting these features are then presented, along with some experimental results from the testing of the feature detection technique.

4.1 Artificial Target Description

Artificial targets are used to provide a reference pose (position and orientation) in the coordinate system in which the robot operates. By observing a single (monocular) or stereo (2 images) projection of a target or a mark, the robot should be able to determine its pose (position and orientation) in the coordinate system. The shape and characteristics of the target itself should yield enough information when it is imaged. Generally, a mathematical relationship between the target, its projection, and the camera has to be established to derive the pose computation information even from a monocular image. The use of a specifically designed target as the object of interest will greatly simplify the task of recognition and interpretation. Hence, the process of target conception and design is as important and critical as that of target detection and recognition.

Target design is constrained by the following factors concerning the application at hand:

- The target should be simple in shape so that it will be easy to install. For example, planar targets take less space and are much easier to install than three-dimensional targets.
- The target should be detectable under a variety of lighting conditions. Hence, it should have a reasonable size and not contain any fine details, since fine details may not be clearly seen from a large distance by the vision system.
- Since the robot workspace is cluttered with objects and parts, the machine vision system can easily confuse the target with other objects in the scene/robot workspace if the target is not highly distinguishable. Therefore, the system has to rely on the uniqueness of the target to effectively identify it and to reject the background.
- The system must satisfy certain accuracy requirements and must use inexpensive components.

The "flat target", consists of a pattern of rectangular stripes placed on a flat surface, and arranged in a way similar to the bar-code concept. These stripes are rectangles with known and well-specified reflectance, and with fixed and well-defined widths and separated by well-defined distances. The flat target model is similar to that used by Wang, [1993], but is more elaborate as it incorporates the brightness properties of the target regions, and is detected and used for pose computation in a different yet a more general and elaborate way (i.e. in 3-D). A sketch of a flat target is shown in Figure 4.1. Without any loss of generality, the target's bars are selected to be darker than the surrounding area, but the concept of their detection is independent of that order. Note again that the functional regions of the target are the stripes and the region separating them. The areas surrounding the stripes are not as functional in terms of the target geometry, but are also important for computing the brightness ratio and detecting the targets as well as preventing the bars and targets from merging with the background.

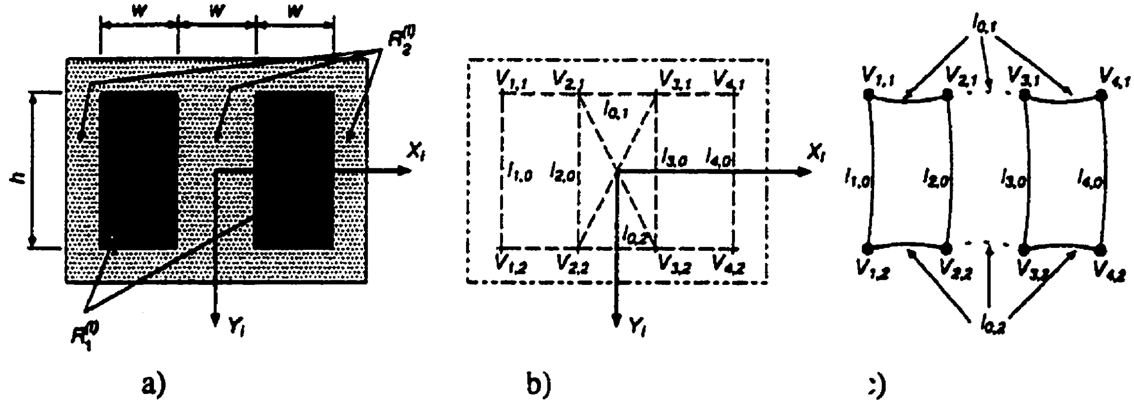

Figure 4.1 Sketches of a flat target (i): (a) target appearance; (b) target properties to be detected; (c) target graph used for modeling and reconstruction.

In Figure 4.1, (*i*) denotes the target ID, and that $R_1^{(i)}$ is the reflectance of the two stripe region, while $R_2^{(i)}$ is that of the regions separating the stripes and surrounding them. The target attributes are the eight vertices, which are the intersections of two sets of parallel lines.

The targets designed here are simple and unique. The simplicity of these targets stems from their simple rectangular shape. Their uniqueness is manifested on one hand by the unique geometry (i.e. the combination of the three bars for the flat target) and, on the other hand, by the fixed, yet well defined reflectance ratios at the boundaries of the targets regions. In fact, the geometry of the target is very important since it relates directly to the pose computation process. As for the uniqueness of the brightness characteristics, the brightness ratios are invariant to changes in scene lighting and viewing parameters. The simple and unique characteristics of these targets make their detection and identification simple and quite easy, and most important reliable and robust against lighting variations. The target data, in terms of the number of targets, their shapes, and their brightness ratio characteristics, are stored as part of the priori knowledge of the robot workcell to be used by the vision system.

4.2 Target Modeling and Calibration. Equipment used

One way of creating a large number of targets with the same and extremely simple geometry was by using different shades of gray for each target created. In a given image each pixel has an associated row/column address and a gray-level value which can be retrieved for further analysis. If an 8-bit representation is used, values range between 0 (black) and 255 (white). For the "flat targets" a combination between white (255) and shades of gray starting with 0 (black), 15, 31,...255 was created. The white (255) was used as background for the two rectangular stripes that forms the "flat target". The rectangular stripes were created in different shades of gray starting with 0 which is black for the first target and always increasing the gray level with 16 for the following targets. This resulted in 17 targets. The other approach in modeling targets was using a certain level of gray for the background and different levels of gray than the background for the functional areas of targets. For the background the 127 gray, and for the rectangular stripes grays from 0 (black) to 111 in increments of 16 were used. The resulting number of targets to be tested was 17 using the first approach, and 7 more targets using the second approach. To create the targets Power Point (97) was used which has the capability of controlling the gray levels and also the dimensions of the targets. As dimensions the unit of one inch was used for the width of rectangular stripes and the gap between them, the length of the rectangular stripes being the double of the width.

a)

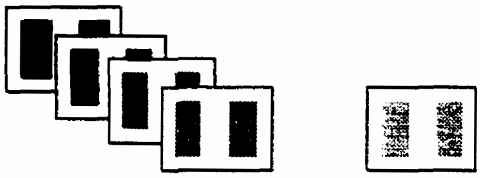

b)

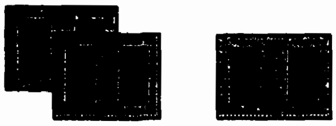

Figure 4.2 Examples of target design.

a) Targets created on white background.

b) Targets created on gray (127) background.

Using these 24 targets, brightness measurements were done and the results stored in a database to be used later for matching. This information consists mainly of brightness information in terms of brightness ratios at the boundaries of the target regions. Brightness is defined as the amount of radiant energy (light) which an imaging system receives per unit apparent area. Brightness is equivalent to irradiance which can also be defined as the amount of incident radiant energy per unit area of the receiving surface [Horn, 1986]. This brightness ratio information is obtained interactively by selecting points at the boundaries of the targets, then reading the brightness gradient and the brightness ratio at each selected point. The user-selected points do not always fall on the exact target edge. Hence a small routine is added to determine the actual edge point before computing the gradient and brightness ratio. A number of points is selected at the boundaries of each target region, then the value of the brightness ratios and the standard deviation is computed. The standard deviation value is used to select the tolerance value for labeling a detected edge as a target edge.

The first set of targets was made by printing the rectangular regions with gray shades on white paper using a laser printer HP LaserJet 4/4M. After conducting measurements and actually testing these targets for the recognizability by the Poscom system the conclusion was that the resolution of maximum 600 DPI given by this printer is not good enough to create reliable targets.

The second set of targets was made by using Conica 812, resulting in prints characterized by 3600 DPI. For each target and each camera measurements were done using different camera settings, camera modes ($\gamma=1$ or $\gamma=0.45$), and positions. The detection of targets relies on the brightness-related information collected from the images. The criteria in deciding how many and which targets out of the 24 test targets will be considered to be used at once in the system was based on the brightness ratios and the requirement that the brightness fields that are characteristic to each target not to intersect each other, so that targets are not going to be confused with each other.

For each case and each camera a number of 16 probes were taken along the edges of the functional regions of the targets. The recorded information that was recorded includes the minimum brightness, maximum brightness, the ratio of these two, as well as the gradient magnitude.

Camera used to get the analized image

Camera mode (can be set from the swich on the back of camera)

Apperture (can be set from the switch on the back of camera)

Minimum brightness

Maximum brightness

Ratio of min. and max.

Gradient magnitude

Target 3:
Background: white (255)
Strips: gray (31)

camera A gamma 0.45
case 2 (App 4)
Target 3

MinBr. [W/m²]	MaxBr. [W/m²]	Ratio	Grad.m
22.1	114.7	0.193	296.377
22	114.7	0.192	291.967
22	115.1	0.192	303.002
21	113.6	0.185	359.263
20.5	112.6	0.182	316.766
20.2	104.1	0.194	218.178
20.4	110.4	0.185	313.804
19.8	112.8	0.175	322.991
21.4	113	0.189	309.946
21	115.1	0.182	337.285
22.2	115.7	0.192	292.562
21.4	114.7	0.186	299.086
21.4	113.8	0.188	316.299
21.9	113.6	0.193	312.159
21.5	113.6	0.189	344.599
20.7	111.3	0.186	303.241
	min	0.175	218.178
	max	0.194	359.263
	avr.	0.188	308.595

Figure 4.3 The format of table and data recorded

Figure 4.3 shows the table that was used for recording each of the measurements for each target. These measurements were collected in a database and were used later on for target matching. Measurements are included in the Appendix A.

The calibration measurements were done using a pair of converging black-and-white CCD cameras and an image processing software.

Cameras. Two identical PULNiX black-and-white CCD cameras (model TM-7CN) are used along with a Matrox frame grabber to acquire intensity images of the scene. This camera type contains a ½" interline transfer imager with a resolution of 768(H)x494(V) sensor cells and excellent low light sensitivity. It is also equipped with back panel switches to adjust the gamma mode (1.0/0.45), the capture and transfer mode

(Frame/Field), and the gain control mode (AGC/MGC) as well as the gain constant for for the MGC. As a short explanation of the terms above, it should be mentioned that the video signal is proportional to the scene brightness to the power gamma.

The gamma = 1 (linear) mode gives a linear relationship between the scene brightness and the video signal (converted to image intensities). This mode is meant to be used in machine vision applications where the image intensities are assumed to be proportional to the scene brightness. The gamma = 0.45 results in a video signal that is approximately proportional to the scene brightness to the power 0.45 (can be regarded as the square root of the scene brightness), and is designed for surveillance applications where the video signal is directly fed to a CRT-type video monitor, which in turn displays the signal with a 2.2 power factor. Frame mode is the standard interlace mode of horizontal line transfer. For each frame, the odd lines are first transferred, then the second field when the even lines of video are transferred. This mode is used for normal operations and for integration applications. The field mode of operation works as follows: during each transfer, two adjacent lines are combined together and then shifted out. This is used in applications that involve shuttering because, during shuttering, the camera's sensitivity is reduced due to the reduction of integration time. Automatic gain control (AGC) is the feature that allows to condition the video signal depending on the scene brightness by increasing the resulted image brightness readings, but one of the disadvantages is that the effect of noise may be increased.

Image processing software. The software used is ***Image Workframe (IWF).*** This is a PC-based software used for image analysis and developing computer vision applications.

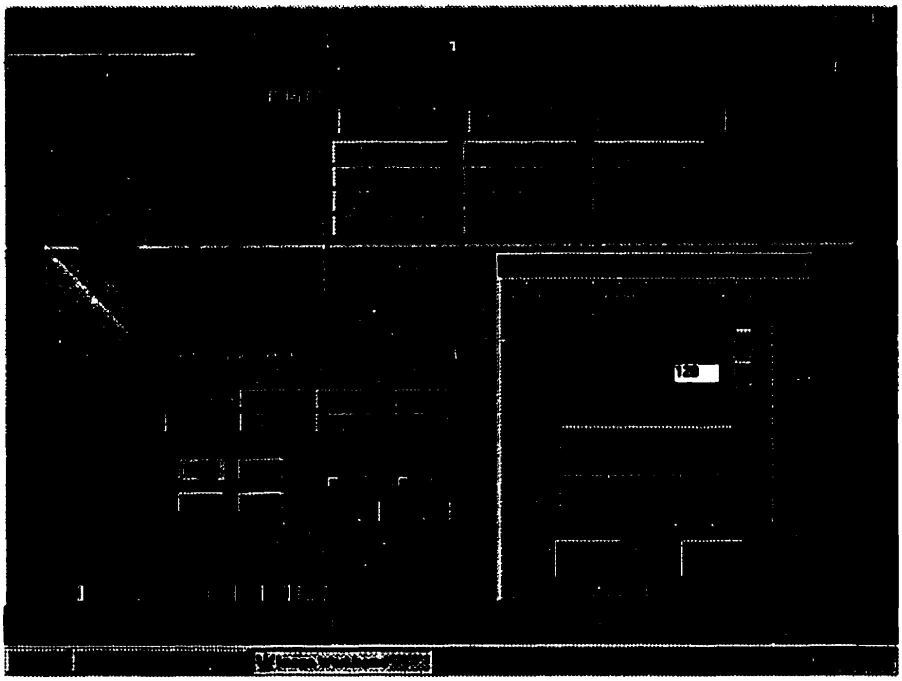

Figure 4.4 Image Workframe (IWF) Image processing software. Basic tools.

This software offers a wide selection of basic tools, as presented in figure 4.4. Subselections expand with each choice: for example, after selecting '*Capture*' there are choices for getting of a live image (*Live* or *Input device-0*), capturing a single frame/field to a buffer (*Snap*), transferring the image from frame buffer to memory (*Copy*) or getting multiple video inputs (*Stereo*). The program also offers image statistics functions such as '*Read Pixel*' which gives an average image intensity in a 3 by 3 patch around a selected pixel, or '*Histogram*' which leads to the gray palette manager that allows to manipulate the lookup table. An image histogram is displayed along with the possibility to view the effects of thresholding. When selecting '*Threshold*', and applying the threshold value to the image, the original brightness values are destroyed and a thresholded image is created. The '*Sobel edge*' operator is a first order differential operator which performs edge detection. After thresholding the differential image, and performing a thinning operation, a one-pixel-wide edge appears.

Besides the basic tools presented above, the IWF software also has more complicated functions that starts with brightness ratio measurements at the edges in any direction ('TargtTesting'), capturing one ('CaptureImage') or more than one (stereo) images ('*CaptureStereo*'), and ends with pattern recognition in one ('*FindPattren1*') or two ('*FindPattren2*') images.

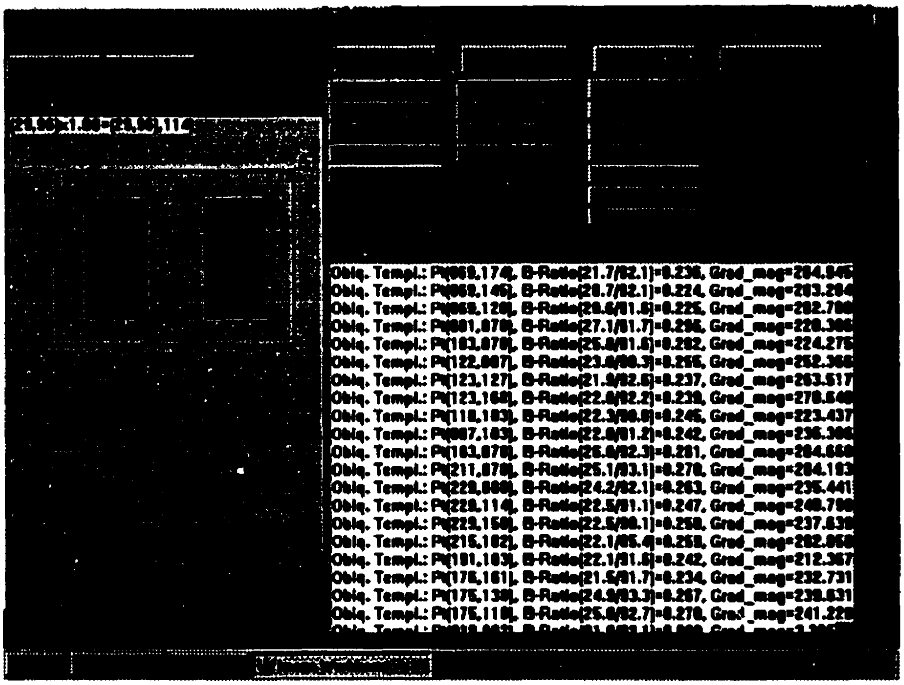

Figure 4.5 Image Workframe (IWF) Calibration tools.

In Table 4.1 each column represents the average brightness ratios resulting from measurements carried out under different conditions. However, for targets with the rectangular strips of very light gray (gray level bigger than 223), the contrast between the background and the rectangles is very low, and the brightness ratio is unusable.

Target 1	Target 2	Target 3	Target 4	Target 5	Target 6	Target 7	Target 8	Target 9	Target 10	Target 11	Target 12	Target 13	Target 14
0.149	0.157	0.190	0.233	0.280	0.338	0.348	0.407	0.470	0.560	0.583	0.672	0.727	0.811
0.142	0.157	0.186	0.226	0.282	0.332	0.334	0.403	0.455	0.568	0.574	0.680	0.725	0.806
0.142	0.163	0.183	0.239	0.272	0.320	0.329	0.385	0.455	0.562	0.562	0.677	0.738	0.802
0.144	0.161	0.180	0.223	0.259	0.320	0.354	0.377	0.461	0.558	0.563	0.676	0.732	0.809
0.140	0.166	0.178	0.216	0.257	0.316	0.346	0.390	0.452	0.557	0.553	0.688	0.742	0.806
0.142	0.177	0.181	0.219	0.248	0.322	0.328	0.398	0.486	0.560	0.562	0.666	0.743	0.799
0.137	0.159	0.179	0.216	0.250	0.328	0.329	0.409	0.486	0.564	0.562	0.657	0.741	0.809
0.137	0.165	0.175	0.214	0.257	0.328	0.316	0.394	0.480	0.556	0.565	0.662	0.730	0.805
0.134	0.158	0.181	0.220	0.260	0.332	0.336	0.416	0.468	0.568	0.570	0.654	0.725	0.808
0.136	0.176	0.177	0.228	0.255	0.329	0.333	0.409	0.465	0.563	0.588	0.664	0.717	0.805
0.148	0.169	0.194	0.222	0.266	0.330	0.348	0.415	0.452	0.557	0.573	0.660	0.716	0.811
0.147	0.155	0.190	0.240	0.284	0.329	0.358	0.401	0.481	0.553	0.580	0.668	0.705	0.812
0.148	0.163	0.186	0.237	0.261	0.332	0.341	0.396	0.471	0.550	0.579	0.672	0.718	0.807
0.143	0.157	0.182	0.224	0.265	0.320	0.333	0.413	0.483	0.563	0.577	0.683	0.718	0.800
0.145	0.160	0.180	0.220	0.259	0.325	0.330	0.405	0.481	0.582	0.576	0.680	0.724	0.817
0.145	0.166	0.178	0.222	0.253	0.324	0.323	0.390	0.462	0.572	0.576	0.680	0.731	0.814

Table 4.1 Brightness ratio averages for camera A.

Seven targets can be used by the system at the same time. The brightness ratios for the selected seven targets are presented in Figure 4.6.

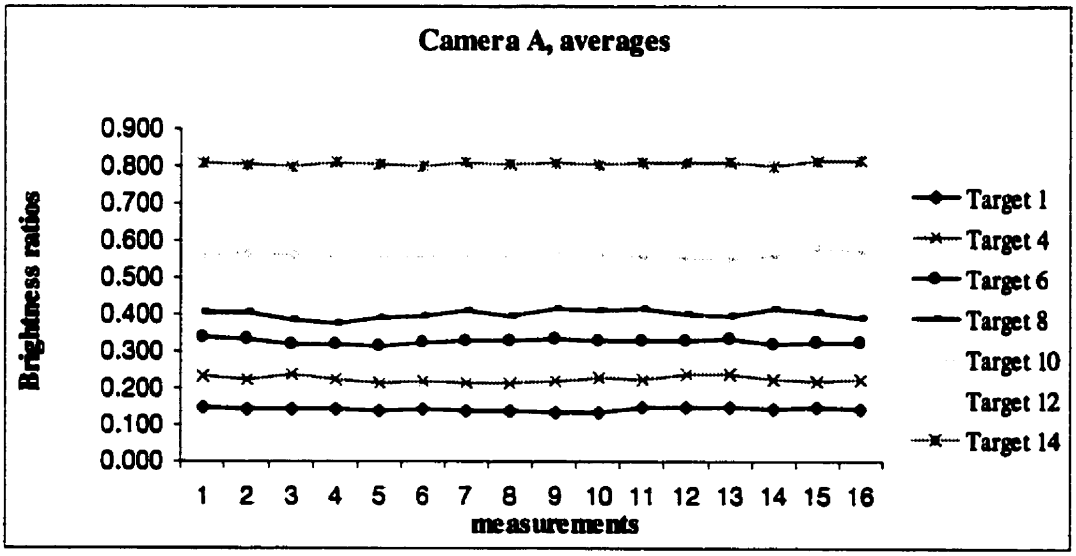

Figure 4.6 Brightness ratios resulted from measurements done with camera A.

The same set of measurements was done for the second camera. The results are represented in Table 4.2 and Figure 4.7.

Target 1	Target 2	Target 3	Target 4	Target 5	Target 6	Target 7	Target 8	Target 9	Target 10	Target 11	Target 12	Target 13	Target 14
0.154	0.184	0.199	0.221	0.262	0.320	0.340	0.397	0.477	0.557	0.599	0.717	0.751	0.831
0.147	0.188	0.182	0.224	0.263	0.318	0.344	0.394	0.465	0.573	0.586	0.698	0.747	0.820
0.142	0.173	0.185	0.220	0.270	0.337	0.333	0.390	0.459	0.559	0.572	0.696	0.749	0.819
0.134	0.164	0.193	0.224	0.272	0.326	0.342	0.383	0.454	0.542	0.568	0.702	0.748	0.811
0.139	0.163	0.188	0.219	0.274	0.324	0.332	0.381	0.454	0.556	0.575	0.701	0.756	0.818
0.133	0.159	0.197	0.211	0.285	0.334	0.314	0.418	0.475	0.557	0.570	0.693	0.762	0.826
0.161	0.161	0.210	0.205	0.270	0.325	0.319	0.443	0.487	0.562	0.575	0.678	0.755	0.833
0.160	0.169	0.197	0.204	0.273	0.326	0.315	0.423	0.480	0.562	0.571	0.688	0.747	0.823
0.156	0.179	0.190	0.204	0.257	0.323	0.321	0.388	0.481	0.549	0.600	0.691	0.753	0.819
0.164	0.187	0.188	0.198	0.263	0.322	0.321	0.379	0.465	0.558	0.602	0.695	0.737	0.822
0.161	0.173	0.190	0.210	0.260	0.317	0.323	0.402	0.471	0.550	0.607	0.698	0.728	0.821
0.154	0.173	0.201	0.213	0.266	0.316	0.350	0.401	0.467	0.562	0.589	0.707	0.724	0.823
0.148	0.175	0.194	0.212	0.269	0.328	0.343	0.400	0.450	0.545	0.598	0.713	0.738	0.822
0.145	0.160	0.197	0.215	0.271	0.332	0.353	0.397	0.445	0.542	0.604	0.704	0.743	0.821
0.151	0.168	0.198	0.215	0.275	0.328	0.347	0.396	0.445	0.548	0.601	0.699	0.747	0.823
0.147	0.167	0.198	0.214	0.272	0.327	0.337	0.392	0.451	0.544	0.615	0.709	0.754	0.822

Table 4.2 Brightness ratio averages for camera B

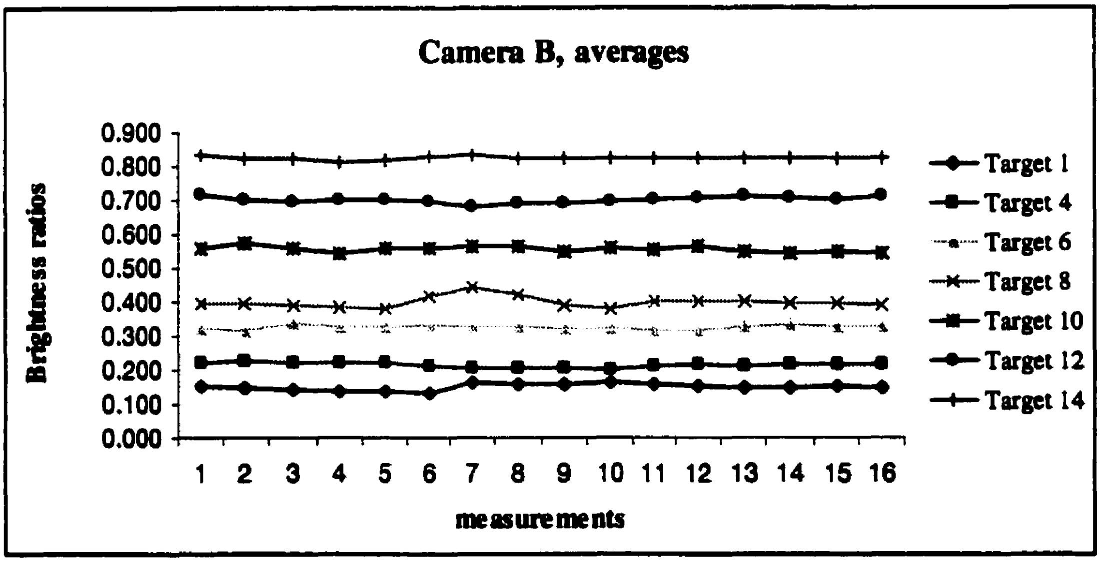

Figure4.7 Brightness ratios resulted from measurements done with camera B

After deciding which targets and how many of them to use at once, the measurements done with camera A and camera B were compared (Table 4.3).

A	**Target 1(A)**	**Target 4(A)**	**Target 6(B)**	**Target 8(A)**	**Target 10(A)**	**Target 12(A)**	**Target 14(A)**
min (br. Ratio)	0.118	0.183	0.298	0.353	0.53	0.622	0.758
max (br. Ratio)	0.165	0.266	0.368	0.485	0.606	0.744	0.847
Avr. (br. Ratio)	0.143	0.225	0.326	0.400	0.562	0.671	0.807
B	**Target 1(B)**	**Target 4(B)**	**Target 6(B)**	**Target 8(A)**	**Target 10(B)**	**Target 12(B)**	**Target 14(B)**
min (br. Ratio)	0.12	0.183	0.309	0.365	0.488	0.635	0.79
max (br. Ratio)	0.196	0.246	0.32	0.485	0.61	0.752	0.849
Avr. (br. Ratio)	0.150	0.213	0.346	0.399	0.554	0.699	0.822
overall min.	0.118	0.183	0.298	0.353	0.488	0.622	0.758
overall max.	0.196	0.266	0.368	0.485	0.61	0.752	0.849
overall avr.	**0.146**	**0.219**	**0.336**	**0.400**	**0.558**	**0.685**	**0.815**
	Min. GR (1)	Min. GR (4)	Min. GR (6)	Min. GR (8)	Min. GR (10)	Min. GR (12)	Min. GR (14)
Gradient (A and B)	145.829	147.497	119.096	119.574	64.722	21.889	14.283

Table 4.3 Summary or measurement results for the A and B cameras.

The results of the measurements suggest that the system can handle seven targets at once without confusing them.

Another set of measurements was done to find the effects of target lamination/plastification. A comparation was made among the measurements resulted in testing a plain target, target covered with reflectant tape and target covered with mate or nonreflectant tape. It was concluded that covering the surface of targets using eighter shiny or mate tape has an effect of slightly reducing the brightness of the images by an approx. 2-3%. Test results are annexed. One inconvenience of covering targets with reflectance tape is that incident lighting is uncontrollably reflected, resulting in a negative effect on recognition.

These targets are only experimental, and they should be made of, or printed on, flat rigid plastic material.

4.3 Target Detection

The concept of target detection is based on the invariance of the reflectance ratio in neighboring smooth surface patches [Nayar, 1993]. Unlike classical segmentation techniques (e.g. edge detection or thresholding), the proposed method uses the brightness information, otherwise often wasted, to quickly and reliably identify the targets. This results in reliable stereo matching and pose computation.

The target detection algorithm consists of two steps: a coarse search and fine search routines. The coarse search step aims at identifying seed points of the target edges, by scanning for high gradient points. The coarse search step aims at identifying seed points of the target edges, by scanning for high gradient points. This search process scans the image along a scan lines oriented at specified directions, typically horizontally, and labeling points of maximum gradient within a N x 1 window, where N is the typical edge width. If the labeled edge point matches the brightness properties of the modeled target edges, then it will be considered as a seed point from which the fine search process takes over. Otherwise, that edge point is ignored and the search continues.

When a seed point is found, the fine search process starts along the tangent of this seed edge point, looking for similar edge points on either of its sides. Similar edge points should have the same brightness ratio, the same gradient value at the edge point, and the same edge orientation. The seed point and the detected neighboring points are then grouped and fitted (using a least-square fit) into a straight line segment, which is then labeled with its slope (in image coordinates), y-intercept value, end points, brightness attributes and its target-model association, referred to as target index.

Once the image is completely scanned, all the labeled line segments present are then grouped based on similarity of brightness information to reconstruct the targets in the image. That is accomplished by organizing the detected lines into a graph structure representing the targets. In this process, the line segments with the same target-model and brightness attributes are first grouped, then sub-categorizing them based on parallelism, i.e. dividing them into a maximum of two sets of parallel lines. The graph is then constructed with vertices representing the nodes of the graph and the line segmenting the arcs connecting the graph nodes.

4.4 Experimentation of Target Detection

The robustness of target detection method was investigated against illumination variation, shadows, and target changes in orientation.

4.4.1 Illumination Variation

The illumination at a point on a surface is the luminous flux incident on an infinitesimal element of the surface centered at the given point divided by area of the surface element. The illumination at a point on a surface due to a point source of light is proportional to the luminous intensity of the source in the direction of surface point and to the cosine of the angle between this direction and the surface normal direction. It is inversely proportional to the square of the distance between the surface point and the source. Luminous flux is the radiant power evaluated according its capacity to produce visual sensation. In the process of image formation the lens plays a major role. The lens is characterized by its f-number (aperture) which is the ratio of its focal length to the diameter of lens. Aperture allows the control of the amount of light that passes through the lens. To check the effects of illumination variation the aperture of the cameras used in this study was changed, and the system's ability to recognize the target was observed. The aperture change has an influence on the brightness that is defined as the amount of radiant energy (light) which an imaging system receives per unit apparent area. Brightness is also equivalent to irradiance, which can also be defined as the amount of incident radiant energy per unit area of the receiving surface.

Two examples were chosen to illustrate how well the program recognizes the target. The first example the target recognition under good illumination conditions Figure 4.8.

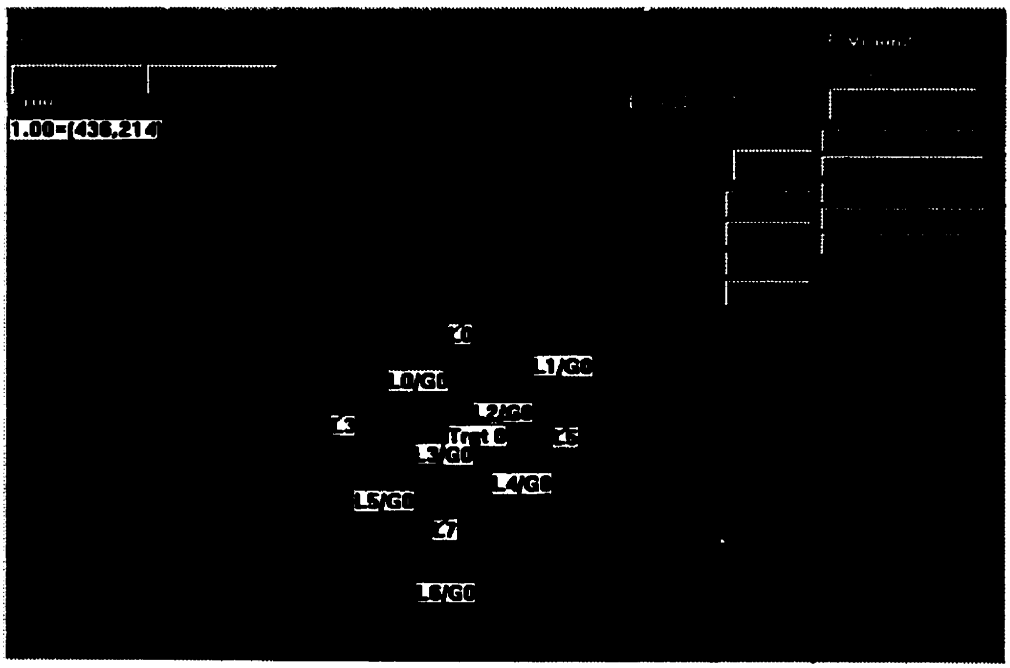

Figure 4.8 Testing the effects of illumination changes. Recognition of target with favorable illumination.

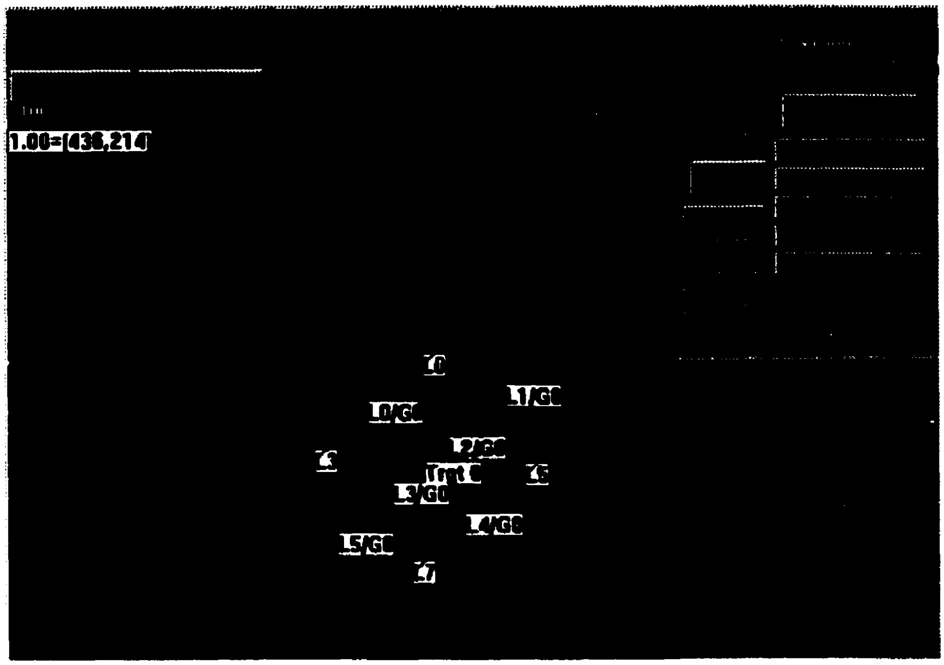

Figure 4.9 Testing the effects of illumination changes. Recognition of target when illumination is low.

It was observed and concluded that the target recognition program performs well even under unfavorable illumination conditions. This good feature results from the fact that the recognition algorithm is based on the brightness ratio values at edges which do not change even when illumination conditions are altered.

4.4.2 Shadowing

Shadow is considered as an area of the target that does not have the features that are used in target recognition. Features used in target recognition are the geometry of the target and the well-defined reflectance ratios at the boundaries of target regions. To create shadows on the target strips of paper with different reflectance than the functional regions of target were used.

Figure 4.10 shows that the target was successfully recognized when strips of paper covered part of it.

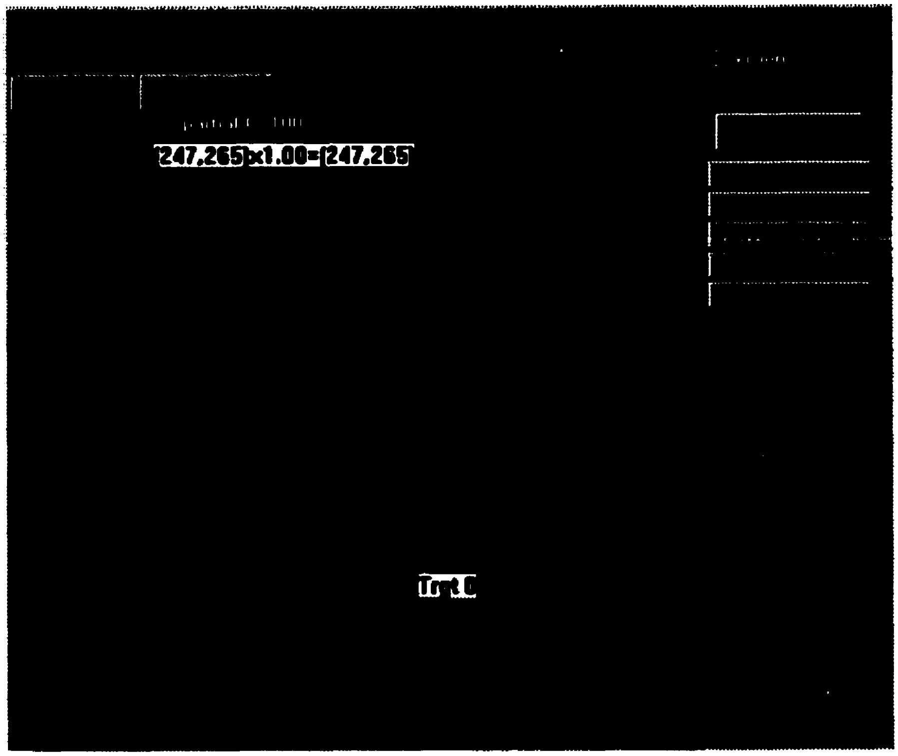

Fig. 4.10 Testing the target for shadows.

It is concluded that if functional areas of the target are not fully covered, then the target is recognized well, but if, for example, an edge is totally hidden and can not be used for recognition then the target is not recognized. This can be explained with the fact that in the recognition process edge points are grouped in line segments, and collinear line segments are combined into a line that is labeled with the target index.

4.4.3 Changes in Orientation

The target recognition system is extremely sensitive to the changes in orientation. The tests that were done in this respect show that the target recognition can not be completely reliable. Figures 4.11 and 4.12 show the most frequent problem in recognition. Having the same conditions (lighting, camera settings, and aperture) and only some small change in orientation of target can influence the recognition process in an undesired way.

In Figure 4.11 the target is perfectly recognized. Around the two rectangular stripes the recognized edge points are shown. Also the lines are correctly recognized and grouped. The recognition of the target is successful.

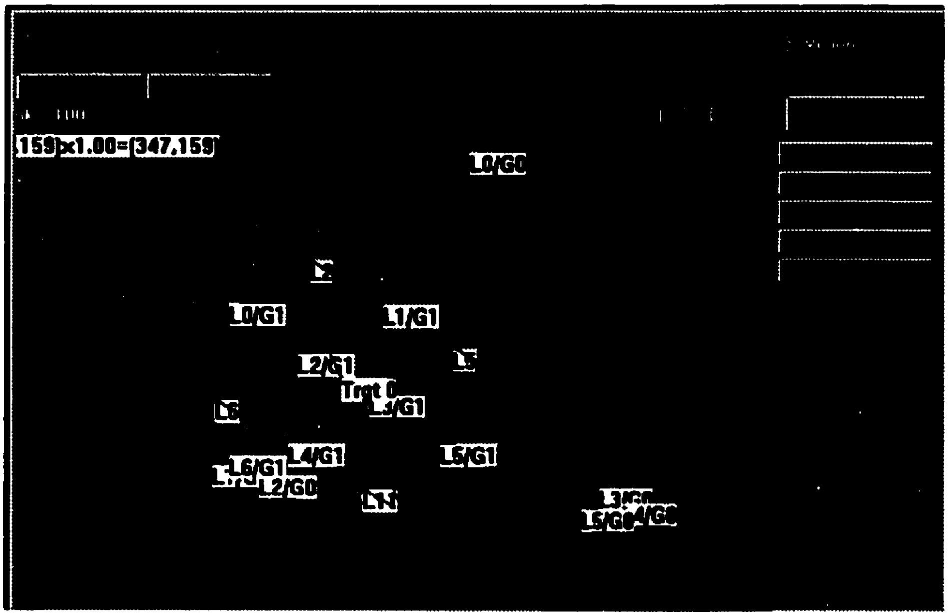

Figure 4.11 Successful recognition of target.

In Figure 4.12, the conditions that were used to get the image were the same as in Figure 4.11. The edge points and the lines are recognized well, but an error occurs in the grouping of the lines. Although this case is fairly straightforward, the target is not recognized well; instead of one two targets are accepted.

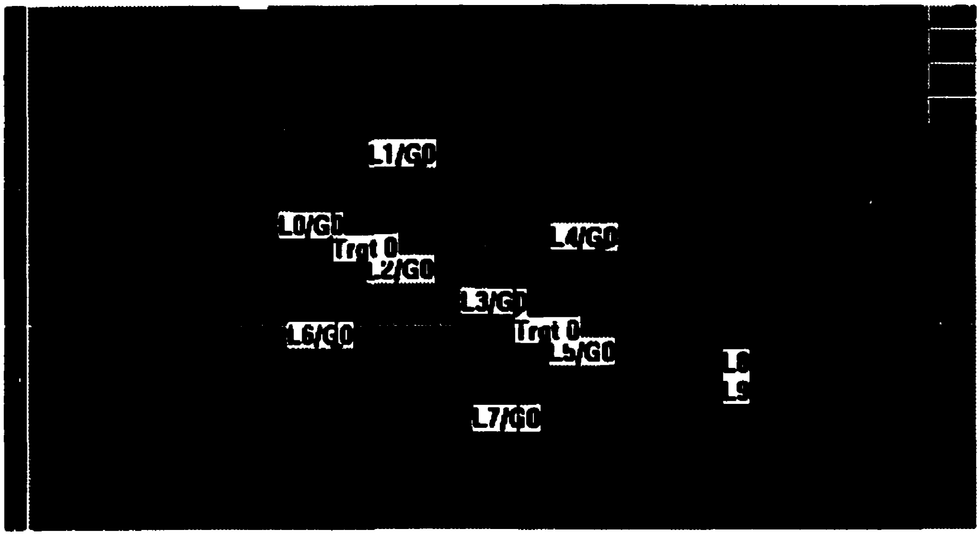

Figure 4.12 Error that occurred most often in the recognition (1).

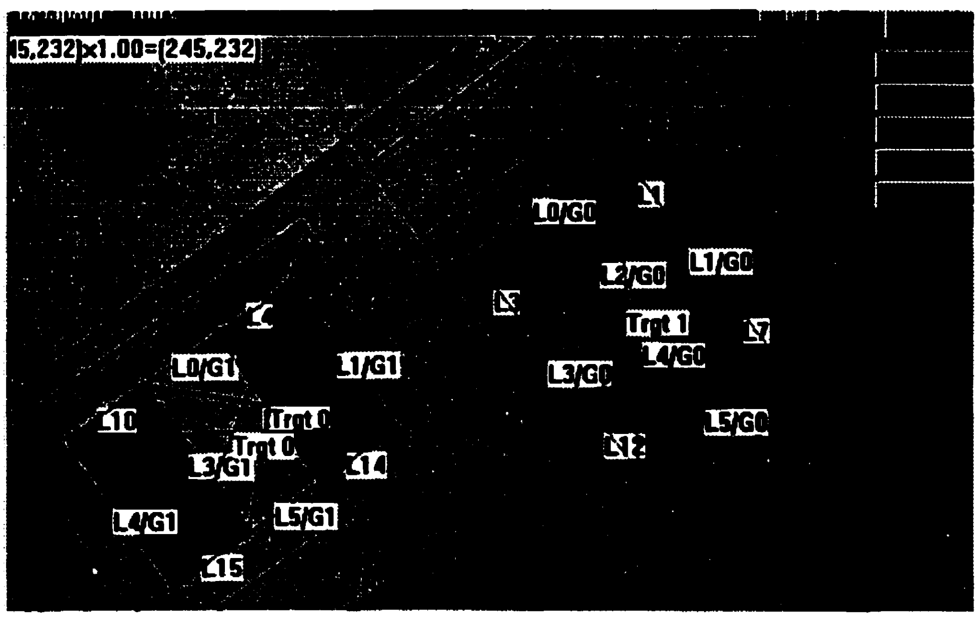

Figure 4.13 Error that occurred most often in the recognition (2).

Another problem often occurring is when besides the actual target a second target is accepted as target, which cannot create any usable output in terms of industrial applications.

In the case of Fig. 4.13, the problem is that one of the targets noted "Trgt 0" in the figure should not be accepted by the system as target. The edge points are recognized well, the lines are also grouped well but an error appears and an extra target is accepted.

Considering these problems, the target recognition software should be improved before recommending its use for applications where the orientation of targets changes a lot. In this study as targets are fixed on the fixture their orientation will not change; the only thing open to change is their position.

5. Pose Computation

5.1 Stereo Vision Geometric Calibration

Three dimensional vision applications, such as robot vision, require modeling of the relationship between the two-dimensional images and the three-dimensional world. Camera calibration is a process, which accurately models this relationship. The problem of camera calibration is to compute the camera intrinsic and extrinsic parameters based on a number of points whose object coordinates in the (x, y, z) coordinate system are measured and whose image coordinates f, and g are known. The extrinsic parameters give information regarding the camera position and orientation with respect to the world coordinate system, while the intrinsic parameters include focal length, scale factors to go from pixels to units of length, as well as values expressing the different types of possible lens distortions. The term "camera calibration" refers to finding values of these parameters for a given camera setup so that the coordinates x,y, and z can be calculated. In this area there has been much previous work. The techniques proposed to solve this problem range from simple linear equation solving to complex non-linear optimization approaches. An optimized two-step calibration algorithm is developed by Bacakoglu [1997], that starts with a linear calibration and based on these results constructs the homogeneous 4X4 transformation matrix. Another camera calibration method is the three-step camera calibration method [Bacakoglu, 1997] which first approximates the calibration parameters using the linear least-squares method then finds the optimal rotation matrix from the calibration parameters and as last step a nonlinear optimization is performed to handle lens distortion. An extension of the two-step calibration is the four-step calibration procedure [Heikkila, 1997] which ads a step to compensate for distortion caused by circular features, and a step for correcting the distorted image coordinates. Han [1992] presents a method of calculating the viewing parameters of a camera using a specially designed circular pattern,

To find the calibration and lens correction coefficients, the calibration algorithm provided by Sensor Adaptive Machines Inc. (SAMI) [56] was used. The provided routine is very easy to implement and requires no prior knowledge of the focal lengths of the cameras, the distance between them, or their relative angular orientation. To use it a table containing a large number of x, y, z, values and the corresponding pixel locations in each image was created for approximately 100 samples taken uniformly throughout the volume to be calibrated. A short description of the algorithm [56] used by this calibration routine given the following camera model mapping (x,y,z) to undistorted pixel (f,g):

$$f(u)=\frac{a(0)\cdot x+a(1)\cdot y+a(2)\cdot z+a(3)}{a(8)\cdot x+a(9)\cdot y+a(10)\cdot z+1} \tag{5.1}$$

$$f(u) = f+D(f)(df,order,f,g) \tag{5.2}$$

$$g(u)=\frac{a(4)\cdot x+a(5)\cdot y+a(6)\cdot z+a(7)}{a(8)\cdot x+a(9)\cdot y+a(10)\cdot z+1} \tag{5.3}$$

$$g(u) = g+D(g)(dg,order,f,g) \tag{5.4}$$

- (f,g) is frame buffer pixel coordinate(column,row) with arbitrary origin.
- (x,y,z) is world coordinate ie(mm).
- a(k) k = 0...10 are unknown camera parameters.
- D(f)(df,order,f,g) is a polynomial lens distortion model in f with a set of (order+1)(order+2)/2 parameters,df.
- D(g)(dg,order,f,g) is a polynomial lens distortion model in, g, with a set of (order+1)(order+2)/2 parameters,dg.

A third order lens distortion model, for example, has the following form:

$D(d,3,f,g)=d(0)+d(1)f+d(3)f^2+d(4)fg+d(5)g^2+d(6)f^3+d(7)f^2g+d(8)fg^2+d(9)g^3$

This algorithm finds the set of parameters, a (k), df and dg that minimizes the least squared error.

The solution is determined in stages:

1. Find the a(k) parameters based on the set of (x(i),y(i),z(i)) and (f(i),g(i)) i = 1...n
2. With the a(k) parameters and (x(i),y(i),z(i)) find F(i),G(i) using xyz_fg model above; compute difference(DF(i),DG(I)) as (F(i)-f(i),G(i)-g(i))
3. Estimate lens distortion parameters df and dg, from difference (DF(i),DG(i))
4. Compute new pixel coordinates, (FF(i),GG(i)) as [f(i) + D(f)(df,3,f(i),g(i)), g(i) + D(g)(dg,3,f(i),g(i)))
5. Iterate a second time: repeat step 1, but use (FF(i),GG(i))
6. Repeat steps 2, 3 and 4.

5.2 Collecting the calibration data

To collect the world coordinates x,y,z, and the corresponding pixel locations in the images resulting from camera A and camera B besides the two cameras, the Poscom image processing software and a measuring device was used.

The steps in collecting the calibration data included:

1. Recognizing the target using the target recognition algorithm based on the brightness ratios of targets.
2. Collecting the pixel locations of targets in image A and image B.
3. Finding the x,y and z coordinates of target.

5.2.1 Target recognition

The target recognition algorithm has as output the pixel location of the center of the target P_0 so the corresponding x,y and z had to be measured. The center location of target was found difficult to find, by measurements so, for the data collection purposes, the pixel locations of the four external corners P_1, P_2, P_3 and P_4 and the corresponding x,y,z coordinates were considered. The target recognition program when used for the stereo images, first activates image A and finds the target and corresponding target data (pixel locations of corners), then activates image B and repeats the entire process to get the target data.

5.2.2 Collecting the pixel locations

To get the resulting target data in a file that can be used later in a spreadsheet or for further calculations, two small functions were written which store these data in an ASCII file. These functions were needed due to the fact that the same recognition algorithm was repeated two times, first for image A and second for image B and the target data resulting from testing the image A was overwritten by the target data resulting from testing image B. The functions are as follows:

- 'collectpoints1()'
- 'collectpoints2()'

```
void collectpoints1 ()
 {
 FILE *fin, *fout;
  char buffer[100];
  fin=fopen("pointdata.dat", "r");
        fout=fopen("pixel_location.dat", "w");
  while( (fgets(buffer, 100, fin)) != NULL)
  {
    //fgets(buffer, 90, fin);
    fprintf(fout, "%s", buffer);
    }
 fclose(fin);
fclose(fout);
 }

void collectpoints2()
```

```
{
 FILE *fin, *fout;
 char buffer[100];

 fin=fopen("pointdata.dat", "r");

        fout=fopen("pixel_location.dat", "a");
 while( (fgets(buffer, 100, fin)) != NULL)
   fprintf(fout, "%s", buffer);
fclose(fin);
fclose(fout);
}
```

5.2.3 Collecting the x,y,z coordinates

To collect the x,y,z coordinates of the target in the scene which correspond to the f,g pixel locations in the images resulted from both cameras it was considered that depending on the instrument used for the measurements there are at least three ways that this measurement can be taken:

- Using a ruler that has 1 mm divisions,
- Using a vernier,
- Using the CMM machine.

Each coordinate finding technique (using a ruler, vernier or CMM) has its own advantages and disadvantages that are going to be discussed later. For all three ways of measuring x,y,z coordinates the cameras were positioned side by side at different heights (z coordinates), and the targets positioned in the common field of view of cameras.

Data collection using a ruler. In this case the measuring device is a ruler with 1mm divisions. The center of the coordinate system is situated at the level of cameras at a center point between them. Graph paper glued to the work plane was used to help in measuring. The advantages of this method are the really inexpensive measuring device and that it can be done everywhere without any special setup. The accuracy due to the measuring device (ruler) is 1mm, but due to human interpretation error it can be much lower.

Data collection using a vernier. The setup for the measurements is the same as in case of measuring with a ruler. As instruments of measurement the following were used:

- Mitutoyo vernier (digital), with a resolution of 1/50, measures up to 15cm.
- Kanon vernier (analog), with a resolution of 1/50, measures up to 60 cm.

As the flat target measured had no features like corners or walls, a block of 60x60x10mm glued to the workplan at a well-defined position with respect to the cameras coordinate system was used so that its surfaces were used to help doing measurements.

This way of data collection is time consuming and even though the precision of the vernier is higher than the precision of the rulers the resulting data do not necessarily present a better resolution.

Collecting data with CMM. CMMs are machines that give physical representations of a three dimensional rectilinear Cartesian coordinate system.

The components of a coordinate measuring system are shown in Figure 5.1

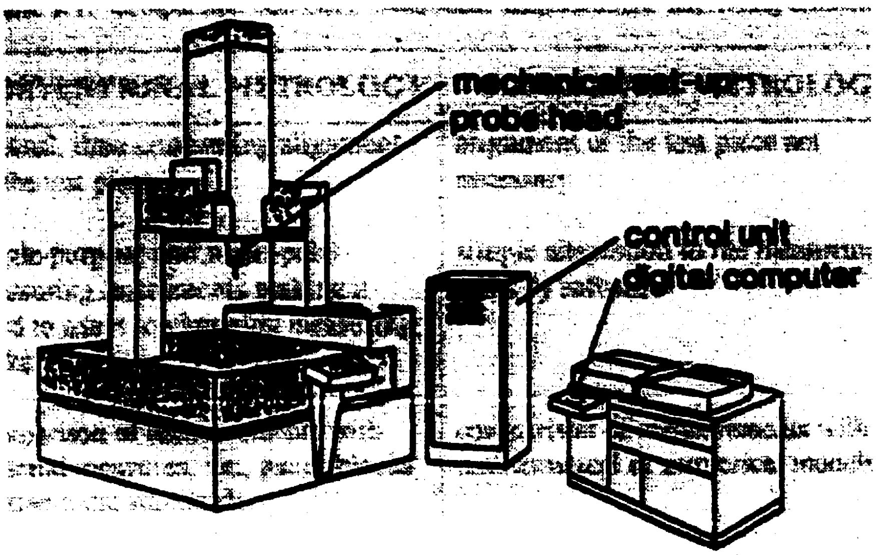

Figure 5.1 System components of a CMM

A CMM consists of the following essential system components:

1. mechanical set-up with the three axes, and the displacement transducers,
2. probe head,
3. optional remote control unit, and
4. digital computer with peripheral equipment (printer, plotter), and software to calculate and represent results.

A measurement with a CMM follows these steps:

1. Calibration of the stylus or probe tip with respect to the probe head reference point,
2. Metrological determination of the workpiece position (workpiece related coordinate system X_W, Y_W, Z_W) in the measuring machine related coordinate system X_M, Y_M, Z_M,

3. Measurement of the surface points on the workpiece in the measuring machine related coordinate system,
4. Evaluation of the geometric parameters of the workpiece, and
5. Representation of the measurement results after coordinate transformation into the workpiece related coordinate system.

The target used by the vision system is a flat surface and has two rectangular stripes. As CMMs cannot be used to do measurements of points on a surface, the setup shown in Figure 5.2 was used when actually taking the measurements. This setup consists of two parts: i) the upper block, which has an opening with the shape, and size of the target, and ii) the lower block, to which the target printed on a paper is attached. To assure that the upper block fits all the time in the same way over flat target attached to the lower block dowel holes and dowel pines were used to create the connection.

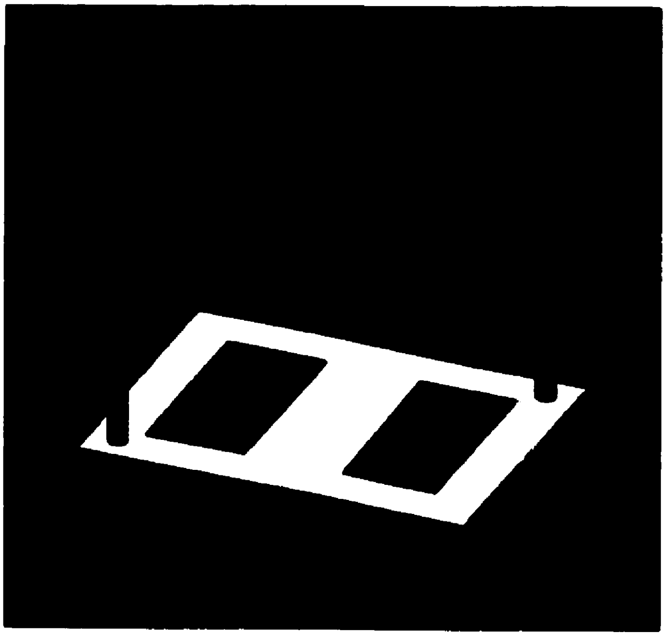

Figure 5.2 Target used for measurements done with the CMM

Steps in collecting the measurement data using the CMM include:

1. Positioning the block with the target attached to it in the field of view of both cameras.
2. Fixing this block to the CMM-s work piece table.
3. Taking the stereo image using the IWF image processing software and CCD cameras.
4. Recognizing the target in both images.
5. Slowly positioning the upper block over the target.
6. Collecting the measurements.

Each corner point of the target is considered as an intersection among three planes, one of them being the plan of the target and the other two being two of the four inside planes of the upper blocks. Each of these surfaces was probed eight times and the best-fit planes were considered to get the intersection point, which was actually the target point.

To find the expected precision of measurements the upper and lower blocks were measured before starting any data recording. The measurements were done to test the surfaces and to see what kind of machining errors are present. The results of these measurements showed that, due to machining, an error of $3 \div 7\mu$ is present. For this set of measurements the target was redesigned to have the dimensions of the upper blocks opening. The new target was printed intending to eliminate the errors due machining. The new target was glued to the lower block's surface using. The positioning of target was done manually, and this procedure cannot be considered error free, so some errors would still appear. An error of 3 ÷ 7μ has to be considered as measurement error. The probe tip that has 1mm radius was used along with two 10mm extensions. The extensions were needed due to the limited accessibility of target when in the field of view of both cameras. The probe tip is designed so that when measurements are done along the major axes the error is minimized. In this case, due to limited space it was assumed that error up to 5 μ may occur because of the deflections of probe tip at the time of measurements. The setup for data collection is presented in Figure 5.3.

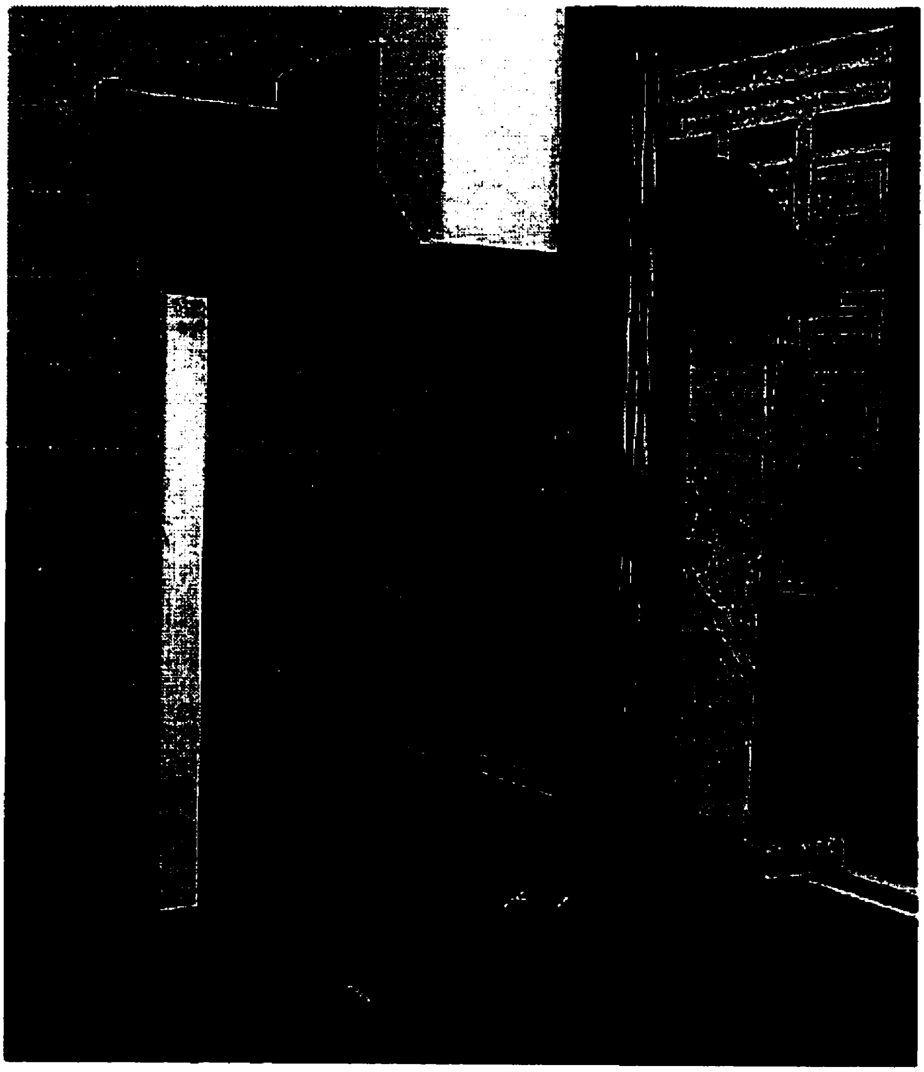

Figure 5.3 Data collection using the CMM.

In the setup from Figure 5.3 height measurement, which is the distance from the targets surface to the cameras, was conducted by taking sets of points at the level of the CMM's table, on the targets surface, and on the structure that had the cameras attached.

To find the actual distance between the target and cameras, the file containing the measurements from above was passed to the program called "Surfacer". With the help of one of the basic features offered by this software, the height measurement was calculated for different camera positions.

The data collected with the above three methods (ruler, vernier, CMM) was used to calculate the calibration coefficients that were saved in separate files so that the coefficients resulting from each calibration method could be accessed later.

5.3 Stereo Matching and Triangulation

Stereo vision is one of the most prominent ranging methods, it is promising and practical due to its potentially high-speed and high accuracy levels. The main purpose of stereo vision analysis is to recover range (depth) information of objects in a three-dimensional (3-D) scene based on an image pair taken from two distinct views. In stereo vision, depth information is obtained from triangulation of corresponding points in the stereo image pair. A stereo image pair refers to two perspective projection images taken of the same scene from slightly different positions. The common area appearing in both images of the stereo pair is usually 40% to 80% of the total image area. A point p on one image and a point q on a second image are said to form a corresponding point pair (p,q) if p and q are each a different sensor projection of the same three-dimensional point. Triangulation refers to the process of determining the (x, y, z) coordinates of a three-dimensional point from the observed position of two perspective projections of the point. The centers of perspectivity and the perspective projection planes are assumed known. [Haralick, 1993].

The triangulation procedure is the determination of a 3D point from the intersection of more than two rays. Consider the case when the lens geometric distortions are totally compensated and assuming that (f_L, g_L) and (f_R, g_R) is the perspective projection of a 3D point (x, y, z). The triangulation procedure makes use of the parallax, which is the displacement in the perspective projection of a point caused by a translational change in the position of observation. The basic stereo triangulation procedure (Haralik, 1993) when we consider the position of the left camera lens is at:

$$\begin{pmatrix} -b_x / 2 \\ 0 \\ 0 \end{pmatrix} \tag{5.5}$$

Considering the position of the right camera lens it is at:

$$\begin{pmatrix} b_x / 2 \\ 0 \\ 0 \end{pmatrix} \tag{5.6}$$

Assuming that the image plan is at a distance f in front of each camera lens, and that both cameras are oriented identically, with the x-axis of the camera reference frame oriented along the line defined by the position of the camera lenses. Let (x, y, z) be an 3D point and (f_L, g_L) and (f_R, g_R) be its perspective projection on the left and right images, respectively. Then:

$$\begin{pmatrix} f_L \\ g_L \end{pmatrix} = \frac{f}{x} \begin{pmatrix} x + b_x / 2 \\ y \end{pmatrix} \tag{5.7}$$

$$\begin{pmatrix} f_R \\ g_R \end{pmatrix} = \frac{f}{x} \begin{pmatrix} x - b_x / 2 \\ y \end{pmatrix} \tag{5.8}$$

In this situation g_L=g_R so that the y-parallax is zero. The solution for (z, y, z), given (f_L, g_L) and (f_R, g_R), can be obtained from the difference f_L-f_R, which is called x-parallax.

$$f_L - f_R = \frac{f}{z}\left[x + \frac{b_x}{L} - \left(x - \frac{b_x}{L} \right) \right] = \frac{f}{z}(b_x) \tag{5.9}$$

Hence:

$$z = \frac{f \cdot b_x}{f_L - f_R} \tag{5.10}$$

Once the depth z is determined, the (x, y) coordinates are easily determined from the perspective projection equations:

$$\begin{pmatrix} x \\ y \end{pmatrix} = \frac{z}{f} \begin{pmatrix} f_L \\ f_L \end{pmatrix} - \begin{pmatrix} b_x / 2 \\ 0 \end{pmatrix} = \frac{z}{f} \begin{pmatrix} f_R \\ f_R \end{pmatrix} + \begin{pmatrix} b_x / 2 \\ 0 \end{pmatrix} \tag{5.11}$$

The equation (5.1) to determine the depth from the x-parallax is a classic relation that in a real-world situation is actually close to being useless, for three simple reasons [Haralik, 1993]:

1. The observed perspective projections are subject to measurement errors, so that $g_L \neq g_R$ for corresponding points.

2. The camera reference frames for the left and right images may often have slightly different orientations.

3. When there are two different cameras that take the left and right images, it is almost always the case that the camera constant $f_R \neq f_L$.

Considering the triangulation model represented through Equations 5.1 to 5.4 (*5.1 Stereo Vision Geometric Calibration*) which is taking in consideration the camera parameters and the lens distortion model in f respectively g, the world coordinates of a 3D point can be determined. First, the camera parameters and distortion parameters are calculated when geometrically calibrating the cameras. Then using these coefficients, the x, y, and z are calculated.

The program written in Borland C++ is presented in Appendix C; it uses the output file from the calibration program, which contains all the camera and calibration coefficients. The triangulation algorithm uses two input files. One of them is a file that contains the pixel locations of corresponding points, and the other file has all the calibration coefficients. In the first stage, there is a memory allocation part that locates in the memory positions where matrixes C[4x3], V[3x3] and vectors w[3], b[4] used in the mathematical part are going to be stored. The next part is solving a set of mathematical equations that lead to a matrix representation C[4x3] that is decomposed using the singular value decomposition (SVD) function [Press, 1990] and results in the output (x, y, z) written in an ASCII file. For the orientation of target, the position of two corners A, B of target are calculated using the above method the gradient of straight line going through these two points was: $m=(y_2-y_1)/(x_2-x_1)=\tan\alpha$ (5.12).

Where *m* is the gradient of line, (x_1,y_1) and (x_2,y_2) the coordinates of two points and α is the angle which is the orientation of target. These functions are implemented in *Image Workframe (IWF)* (Image processing software) and can be accessed through the buttons under the 'Stereo'. There are two options: the first of them is "X,Y,Z " that calculates the (x, y, z) coordinates of corresponding targets and writes them in a file called "coord.dat" and also gives an output on the screen with the calculated data. The other option would be "Orientation" that calculates the orientation of target. Figure 5.4 shows where the position and orientation finding algorithms can be accessed.

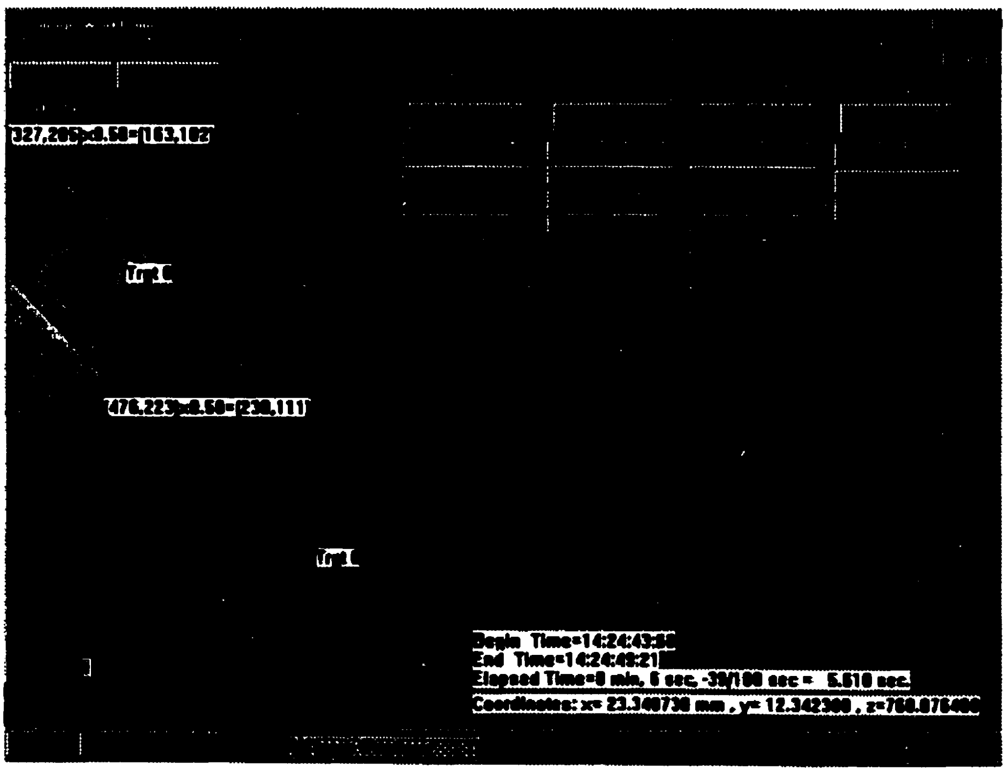

Figure 5.4 The software development that calculates the position of the target.

5.4 Experimentation of Finding the Targets Position

Once the stereo triangulation is completed, the accuracy of the position and orientation has to be tested. For this experiment the setup in Figure 5.5 was used. This is the same setup that was used for collecting the calibration data using a ruler or vernier (5.2.2). In this setup the cameras are positioned on a fixture at a certain height above the targets. The targets are placed on a surface covered by graph paper. The graph paper was used to help position the target at a well defined (x, y, z). First, the target was positioned on a well-defined location and under a well-defined orientation.

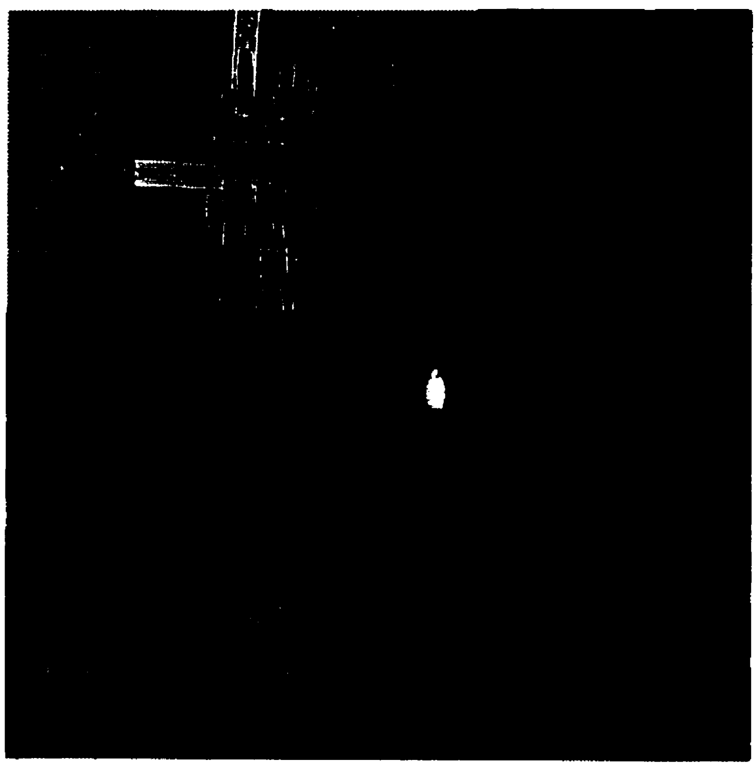

Figure 5.5 Testing the accuracy of position and orientation finding.

Then, stereo image was taken of the scene and, after recognizing the targets in both images and finding the corresponding points for the target, the position and orientation was found with the help of the algorithms.

The position and orientation of the two PULNIX CCD cameras were kept the same, as they were when the calibration data was collected. In this fixed position the two cameras were moved up and down on the fixture this way the height was adjusted.

Table 5.1 shows the true position values against the computed values for six different target positions and the three sets of calibration data.

	Position	Coeffs # 1 (ruler)	Coeffs # 2 (vernier)	Coeffs # 3 (CMM)
1	(20, 140, 600)	(21.64, 140.7, 603.12)	(22.56, 143.09, 604.19)	(21.09, 139.71, 601.02)
2	(40, 140, 600)	(42.13, 141.42, 603.64)	(41.97, 143.23, 602.71)	(40.59, 140.09, 599.06)
3	(10, 150, 600)	(10.89, 149.27, 602.87)	(8.98, 152.07, 602.84)	(10.19, 150.43, 600.95)
4	(20, 140, 650)	(22.45, 143.11, 652.17)	(23.81, 142.7, 649.93)	(20.71, 139.29, 651.05)
5	(40, 140, 650)	(38.05, 141.24, 652.88)	(41.98, 140.06, 651.67)	(41.01, 141.1, 651.18)
6	(10, 150, 650)	(9.08, 152.45, 653.09)	(11.28, 152.79, 651.28)	(10.94, 151.02, 651.73)

Table 5.1 Comparison of calculated position against true position.

In Table 5.1 all data are presented in mm. The average of the absolute deviations in the x, y, and z directions between the true value and the calculated value under different setups show that this procedure of locating and positioning the artificial target is a good method.

The results show that the compounded position values are close to the true values, indicating that the method used to calculate positions is valid.

6. Discussion

This thesis presented a new method for camera-based pose computation using simple artificial targets, off shelf cameras and an image-processing software.

The artificial targets were designed for easy detection and simplicity of the pose computation. The targets detected here are simple and unique. The simplicity of these targets stems from their simple rectangular shapes. A large number of targets were tested to determine their brightness information in terms of brightness ratios at the boundaries of the target regions and also to find out the maximum number of targets that can be used in the same time by the system. The results of the measurements were stored in a database to be used later for matching.

The robustness of the target detection algorithm was investigated against illumination variation, shadows, and target changes in orientation. Real situations were chosen to create an image of the capabilities offered by the target recognition algorithm. Finally this algorithm proved to be suitable for the purposes of this research.

The geometric calibration of the camera system is a procedure that computes the cameras parameters based on a number of points whose object coordinates in the (x, y, z) coordinate system were measured and whose image coordinates (pixel locations) were known. Three possibilities are presented for collecting the calibration data. The calibration data consist of a large number of 3D positions (x, y, z), and the corresponding pixel locations in both images. The calibration coefficients resulted from each of the approaches were saved in data files to be used later for the position finding of targets.

Stereo vision is one of the most promising and practical ranging methods due to its potentially high-speed and high accuracy levels. Triangulation refers to the process of determining the x, y, and z coordinates of a three-dimensional point from the observed position of two perspective projections of the point. Using the stereo triangulation model presented in chapter 5 equations 5.1 to 5.4 a C++ algorithm was developed to find the position and orientation of the artificial targets placed in various positions in the cameras field of view. This algorithm is implemented in *Image Workframe (IWF)* image processing software as a development and can be accessed by clicking on one of the buttons offered under the *"Stereo"* tools. The position finding algorithm is optionally taking into consideration one of the files containing the calibration coefficients. Results of position detection are also presented. This addition to the software offers to the user an extra feature that opens the door for more complicated applications of the software for such as calibration of a robotic workcell.

In this work stereo vision was used to find x, y, and z coordinates of a three dimensional point from the observed position of two perspective projections of the point. The position-finding technique presented here is based on relatively chip components as an image processing software, computer, and simple surveillance cameras. This technique can be used to find robot and workpiece information, that can be used further for robot calibration and accurate positioning of the robot, end effector and parts within its workspace, to allow successful execution of high accuracy robotic tasks. This is suggested as a topic for future research.

References

[1] Abidi M. A. and Chandra T., "Pose Estimation for Camera Calibration and Landmark Tracking," In *Proc. of the IEEE Int. Conf. on Robotics and Automation*, pp. 420-426, Cincinnati, Ohio, May 1990.

[2] Abidi M. A. and Chandra T., "New Efficient and Direct Solution for Pose Estimation Using Quadrangular Targets: Algorithm and Evaluation," *IEEE Trans. on Pattern analysis and Machine Intelligence*, Vol. 17, no 5, pp. 534-538, 1995.

[3] Abidi M. A. and Gonzalez R. C., "The Use of Multisensor Data for robotic Applications," *IEEE Trans. on Robotics and Automation*, Vol. 6, no. 2, pp. 159-177, 1990.

[4] Bacakoglu H., Kamel M., "Optimized two-step camera calibration method," In *Proc. of IEEE International Conference On Robotics and Automation*, Vol. 2, pp. 1347-1352.

[5] Bacakoglu H., Kamel M., "Three-step camera calibration method," *In IEEE Transactions on Instrumentation and Measurement*, Vol. 46, no. 5, pp.1165-1172, 1997.

[6] Bennett D. J., Geiger D., and Hollerbach J. M., "Autonomous Robot Calibration for Hand-Eye Coordination," *Int. J. of Robotics Research*, Vol. 10, no. 5, pp. 550-559, October 1991.

[7] Bensrhair A., Miche P., and Debrie R., "Fast Stereo Matching for Implementation in a 3-D Vision Sensor," In *Proc. of the Int. Conf. on Industrial Electronics, Control and Instrumentation –IECON '91*, pp. 1779-1783, Kobe, Japan, Oct. 28-Nov. 1 1991.

[8] Bien Z., Kwon H.Y., Youn J., and Suh I. H., "Closed from 3D Self-Positioning Algorithm for a Mobile Robot Using Vision and Guide-Marks," *Robotica*, Vol. 9, no. 3, pp. 265-274, July-September 1991.

[9] Brint A. T. and Brady M., "Stereo Matching of Curves," *Image and Vision Computing*, Vol. 8, no. 1, pp. 50-56, February 1990.

[10] Choy I., Sin Y., Park J., "Depth information on moving objects using stereo vision," *Proceedings of SPIE The Int. Soc. for Opt. Engineering Visual Information Processing*, Vol. 3074, pp. 284-291, 1997.

[11] Cochran S. D. and Medioni G., "3-D Surface Description from Binocular Stereo," *IEEE Transactions on Pattern Analysis and Machine Intelligence*, Vol. 14, no. 10, pp. 981-994, October 1992.

[12] Cryer J. E., Tsai P.-S., and Shah M., "Integration of Shape from X Modules: Combining Stereo and Shading," In *Proc. Of the IEEE Conf. on Computer Vision and Pattern Recognition*, pp. 720-721, New York, NY, 1993.

[13] Do K. H., Kim Y. S., Uam T. U., Ha Y. H., "Iterative relaxational stereo matching based on adaptive support between disiparities," *Pattern recognition*, Vol. 31, no. 8, pp. 1049-1059, 1998.

[14] Dhome M., Riechtin M., Lapresté J. T., and Rives G., "Determination of the Attitude of 3D Objects from a Single Perspective View," *IEEE Transactions on Pattern Analysis and Machine Intelligence*, Vol. 11, no. 12, pp. 1265-1278, 1989.

[15] ElMaraghy W. H., Private Communication, IMS Center, University of Windsor, 1997.

[16] Faugeras O. D. and Hebert M., "The Representation, Recognition, and Locating of 3-D Objects," *The Int. J. of lrobotic Research*, Vol. 5, no. 3, pp. 27-52, 1986.

[17] Ferri M., Mangili F., and Viano G., "Projective Pose Estimation of Linear and Quadratic Primitives in Monocular Computer Vision," *CVGIP: Image Understanding*, Vol. 58, no. 1, pp.66-84, 1993.

[18] Fielding G., Moshe K., "Applying the Hungarian method to stereo matching," *Proc. of the IEEE Conference on Decision and Control*, part 2, Vol. 2, pp. 1928-1933, 1997.

[19] Fischler M. A. and Bolles R. C., "Random Sample Consensus: A Paradigm for Model Fitting with Applications to Image Analysis and Automated Cartography," *Communications of the ACM*, Vol. 24, no. 6, pp. 381-395, 1981.

[20] Fukui I., "TV Image Processing to Determine the Position of a Robot Vehicle," *Pattern Recognition*, Vol. 14, no. 1, pp. 101-109, 1981.

[21] Goldgof D. B., Lee H., and Huang T. S., "Matching and Motion Estimation of Three-Dimensional Point and Line Sets Using Eigenstructure without Correspondences," *Pattern Recognition*, Vol. 25, no. 3, pp. 271-286, March 1992.

[22] Han M. H., Rhee S., "Camera calibration for three dimensional measurement," *Pattern Recognition*, Vol. 25, no. 2, pp. 155-164, 1992.

[23] Hannah M. J., "System for Digital Stereo Matching," *Photogrammetric Engineering and Remote Sensing*, Vol. 55, no. 12, pp. 1765-1770, December 1989.

[24] Haralick R. M., "Determining Camera Parameters from the perspective projection of a rectangle," *Pattern Recognition*, Vol. 22, no. 3, pp. 225-230, 1989.

[25] Haralick R. M., "Monocular Vision Using Inverse Perspective Geometry: Analytic Relations," In *Proc. of the IEEE Conf. on Computer Vision and Pattern Recognition*, pp. 370-378, San Diego, CA, June 1989.

[26] Haralick R. M. and Joo H., Lee C. -N., Zhuang X., Vaidya V.G., and Kim M.B., "Pose Estimation from Corresponding Point Data." *IEEE Trans. on Pattern Analysis and Machine Intelligence*, Vol. 19, no. 6, pp. 1426-1446, 1989.

[27] Haralick R. M. and Shapiro L., *Computer and Robot vision*, Addison-Wesley Publishing Company, 1992.

[28] Heikkila J., Olli S., "Four-step camera calibration procedure with implicit image correction," In *Proc. of the IEEE Conf. on Computer Vision and Pattern Recognition*, pp.1106-1112, 1997.

[29] Horaud R., "New Methods for Matching 3-D Objects with Single Perspective Views," *IEEE Trans. on Pattern analysis and Machine Intelligence*, Vol. PAMI-9, no. 3, pp. 401-412, 1987.

[30] Horaud R., Conio B., Leboulleux E., and Lacolle B., "An Analytic Solution for the Perspective 4-Point Problem," *Computer Vision Graphics, and Image Processing*, Vol. 47, pp. 33-44, 1989.

[31] Horaud R., Dornaika F., Lamiroy B., Christy S., "The link between weak perspective, paraperspective, and full perspective," *Int. J. of Computer Vision*, Vol. 22, no. 2, pp. 173-189, 1997.

[32] Horn B. K. P., *Robot Vision*. The MIT Press, Cambridge, MA, 1986.

[33] Huttenlocher D. P. and Ullman S., "Recognizing Solid Objects by Alignment with an Image," *Int. J. of Computer Vision*, Vol. 5, no. 2, pp. 195-212, 1990.

[34] Jacobs D. W., Basri R., "3-D to 2-D recognition," *In Proc. of the IEEE Computer Society Conference on computer vision and pattern recognition*, pp. 547-553, 1997.

[35] Jarvis R. A., "Range Sensing for Computer Vision," In A. K. Jain and P. J. Flynn, editors, *Three-Dimensional Object Recognition Systems*, Advances in Image Communication 1, pp. 17-56. Elsevier Science Publishers B.V., Amsterdam, The Netherlands, 1993.

[36] Kanade T., "Recovery of the Three-Dimensional Shape of an object from a Single View," *Artificial Intelligence (Special Volume on Computer Vision)*, Vol. 17, no. 1-3, pp. 293-331, 1981.

[37] Kriegman D. J., Triendl E., and Bindford T. O., "Stereo Vision and Navigation in Buildings for Mobile Robots," *IEEE Trans. On Robotics and Automation*, Vol. 5, no. 6, pp. 792-803, December 1989.

[38] Lantos B., Klatsmanyy P., Ludvig L., Tell F., "Intelligent control system of a robot with dexterous hand," *IEEE International Conference on Intelligent Engineering Systems*, INES, pp129-134, 1997.

[39] Lee S.-H. and Leou J.-J., "Dynamic Programming Approach to Line Segment Matching in Stereo Vision," *Pattern Recognition*, Vol. 27, no. 8, pp. 961-986, August 1994.

[40] Li Z.-N., "Stereo Correspondence Based on Line Matching in Hough Space Using Dynamic Programming," *IEEE Trans. on Systems, Man and Cybernetics, Vol. 24, no. 1, pp. 144-152, January 1994.*

[41] Liu Y., Huang T. S., and Faugeras O. D., "Determination of Camera Location from 2-D to 3-D Line and Point Correspondences," *IEEE Trans. on Pattern Analysis and Machine Intelligence*, Vol. 12, no. 1, pp. 28-37, 1990.

[42] Lowe D. G., "Three-Dimensional Object Recognition from Single Two-Dimensional Images," *Artificial Intelligence*, Vol. 31, pp. 355-395, 1987.

[43] Lowe D. G., "Fitting Parameterized Three-Dimensional Models to Images," *IEEE Trans. on Pattern Analysis and Machine Intelligence*, Vol. 13, no. 5, pp. 441-450, 1991.

[44] Luo A. and Burkhardt H., "Intensity-bades Cooperative Bi-directional Stereo Matching with Simultaneous Detection of discontinuities and Occlusions," *Int. J. of Computer Vision*, Vol. 15, no. 3, pp. 171-188, July 1995.

[45] Magee M. J., "Determining the Position of a Robot Using a Single Calibration Object," In *Proc. of the IEEE Int. Conf. on Robotics and Automation*, pp. 140-149, 1984.

[46] Marshall A. D. and Martin R.R., "Automatic inspection of three-dimensional geometric features," In *Winter Annual Meeting of the ASME*, pp. 53-67, Anaheim, CA, November 8-13 1992.

[47] Matas J., Soh L. M., Kittler J., "Object recognition using a tag," *IEEE International Conference on Image Processing*, Vol. 1, pp. 877-879.

[48] Nayar S. K. and Bolle R. M., "Refelectance ratio: A Photometric Invariant for Object Recognititon," In *Proc. of the IEEE fourth Int. Conf. on Computer Vision*, pp. 280-285, Berlin, Germany, May 1993.

[49] Onofuchi K. and Watanabe M., "A Visual Navigation System Using a Multi-Information Local Map," In *Proc. of the IEEE Int. Conf. on Robotics and Automation*, pp. 767-775, Cincinnati, Ohio, May 1990.

[50] Parlaktuna O., On S., and Akcay N., "Feature-based Stereo Matching Algorithm," In *Proc. of the 7th Mediteranean Electrotechnical Conf. – MELECON*, Vol. 1, pp. 153-155, Antalya, TURKEY, August 1994.

[51] Phong T. Q., Horaud R., Yassine A., and Tao P. D., "Object Pose from 2-D to 3-D Point and Line Correspondences," *Int. J. of Computer Vision*, Vol. 15, pp. 225-243, 1995.

[52] Richetin M., Dhome M., Lapresté J. T., and Rives G., "Inverse Perspective Transform Using Zero-Curvature Contour Points: Application to the Localization of Some Generalized Cylinders from a Single View," *IEEE Trans. on Pattern Analysis and Machine Intelligence*, Vol. 13, no. 2, pp. 185-192, 1991.

[53] Roberts L. G., "Machine Perception of Three-Dimensional Solids," In J. T. Tippett et al., Editor, *Optical and Electro-Optical Information Processing*, pp. 159-197. The MIT Press, Cambridge, MA, 1965.

[54] Ross B., "Practical Stereo Vision System," In *Proc. of the IEEE Conf. on Computer Vision and Pattern Recognition*, pp. 148-153, New York, N. Y., 1993.

[55] Scharstein D., Szeliski R., "Stereo matching with nonlinear diffusion," *International Journal of computer vision*, Vol. 28, no. 2, pp. 155-174, 1998.

[56] Sensor Adaptive Machines Incorporated, "Calibrate.cpp," Routine that determines the sensor calibration coefficients, 1997.

[57] Sumi Y., Tomita F., "Three-dimensional object recognition using stereo vision," *Systems and Computers in Japan*, Vol. 28, no. 13, pp. 19-26, 1997.

[58] Trivedi M. M., Abidi M. A., Eason R. O., and Gonzalez R. C., "Developing Robotic Systems with Multiple Sensors," *IEEE Trans. on Systems, Man, and Cybernetics*, Vol. 20, no. 6, pp. 1285-1300, November/December 1990.

[59] Tubaro S., "Precise Stereoscopic System with Two Video Cameras," *European Trans. on Telecommunications and Related Technologies*, vol. 3, no. 3, pp. 275-280, July 1992.

[60] Venkateswar V. and Chellappa R., "Hierarchical Stereo and Motion Correspondence Using Feature Groupings," *Int. J. of Computer Vision*, Vol. 15, no. 3, pp. 245-269, July 1995.

[61] Wang S. H., *Machine Vision with its Application to Autonomous Vehicle Navigation*, Master's Thesis, Department of Mechanical and Industrial Engineering, University of Manitoba, Winnipeg, Manitoba, Canada, October 1993.

[62] Zghal H. and ElMaraghy H. A., "Extraction of Brightness Features for Stereo Analysis in Robot Vision," *Submitted for publication in Image and Vision Computing,* August 1997.

[63] Zhuang H., Roth Z. S., and Wang K., "Robot Calibration by Mobile Camera Systems," In *Winter Annual Meeting of the ASME,* pp. 65-72, Atlanta, GA, December 1-6 1991.

APPENDIX A

TARGET BRIGHTNESS CALIBRATION (MEASUREMENTS)

Using the designed artificial targets (*Chapter 4*) brightness measurements were done and the results stored in a database to be used later on for matching. This information consists mainly of brightness information in terms of brightness ratios at the boundaries of the target regions. This brightness ratio information is obtained interactively by selecting points at the boundaries of the targets.

The table from figure A.1 was used to record the target calibration measurements. These measurements were done for two purposes:

1. Since the target recognition algorithm is relying on the brightness ratio and gradient magnitude information's these were collected for every target and saved in a spreadsheet. This information is needed by the recognition algorithm in order to recognize the artificial targets. Whenever a target is used in the vision system the corresponding data (in terms of brightness ratio and gradient magnitude) is taken from the spreadsheet and used.
2. To decide how many and which artificial targets can be used by the vision system in the same time without the possibility of targets being confused.

Camera used to get the analized image

Camera mode (can be set from the swich on the back of camera)

Apperture (can be set from the switch on the back of camera)

Minimum brightness

Maximum brightness

Ratio of min. and max.

Gradient magnitude

Target 3:
Background: white (255)
Strips: gray (31)

camera A		gamma 0.45	
case 2	(App 4)		
Target 3			
MinBr. $[W/m^2]$	MaxBr. $[W/m^2]$	Ratio	Grad.m
22.1	114.7	0.193	296.377
22	114.7	0.192	291.967
22	115.1	0.192	303.002
21	113.6	0.186	359.263
20.5	112.6	0.182	316.766
20.2	104.1	0.194	218.178
20.4	110.4	0.186	313.804
19.8	112.8	0.175	322.991
21.4	113	0.189	309.946
21	115.1	0.182	337.286
22.2	115.7	0.192	292.562
21.4	114.7	0.186	299.086
21.4	113.8	0.188	316.299
21.9	113.6	0.193	312.159
21.5	113.6	0.189	344.599
20.7	111.3	0.186	303.241
	min	0.175	218.178
	max	0.194	359.263
	avr.	0.188	308.596

Figure A.1 The format of table and data recorded.

In the figure A.1 is also shown what kind of information were recorded for every set of measurement. These informations's are:

- ***Which camera*** was used to record the image (camera A or camera B).
- The ***camera settings***:

  Apperture (allows the control of the amount of light that passes through the lens),

  Camera modes (capture or transfer mode). The cameras are equipped with back panel switches to adjust the gamma mode (1.0/0.45). The gamma = 1 (linear) mode gives a linear relationship between the scene brightness and the video signal (converted to image intensities). The gamma = 0.45 results in a video signal that is approximately proportional to the scene brightness to the power 0.45.

- ***Brightness measurements:*** minimum, maximum, and the ratio of brightness measurements for the functional and nonfunctional areas of the artificial targets. Brightness is defined as the amount of radiant energy (light) which an imaging system receives per unit apparent area.

- ***Gradient magnitude:*** The idea underlining most edge detection techniques is the computation of a local derivative operator. The magnitude of the first derivative can be used to detect the presence of an edge. The first derivative at any point in an image can be obtained by using the magnitude of the gradient at that point. The gradient of an image f(x,y) at location (x,y) is defined as the two dimensional vector (Haralick, 1993):

$$G[f(x,y)] = \begin{bmatrix} G_x \\ G_y \end{bmatrix} = \begin{bmatrix} \frac{\partial f}{\partial x} \\ \frac{\partial f}{\partial y} \end{bmatrix} \tag{A.1}$$

For edge detection we are interested in the magnitude of this vector, generally referred as the gradient and denoted by:

$$G[f(x,y)] = [G_x^2 + G_y^2]^{1/2} = \left[\left(\frac{\partial f}{\partial x}\right)^2 \quad \left(\frac{\partial f}{\partial y}\right)^2 \right]^{1/2} \tag{A.2}$$

The table 4.1 and 4.2 and figures 4.6, 4.7, and 4.8 (*Chapter 4*) resulted from the data presented on the following pages.

camera A	gamma 1		
case 1	(App 8)		
Target 1			
MinBr $[W/m^2]$	MaxBr $[W/m^2]$	Ratio	Grad.m
11	80.8	0.136	220.741
9.9	78.2	0.127	247.504
11	80.9	0.136	222.545
10.8	80.2	0.135	241.655
10.7	79.1	0.136	245.248
11.1	76.1	0.146	229.701
10.7	75	0.143	220.763
10.6	72.8	0.145	193.962
10	81.3	0.123	235.916
9.9	78.2	0.127	247.504
9.8	81.3	0.121	260.005
10.8	82.8	0.13	269.89
11.2	82.3	0.136	244.374
10.9	83.1	0.131	265.806
11	80.9	0.136	222.545
9.7	78.6	0.124	243.45
	min	0.121	193.962
	max	0.146	265.806
	avr.	0.1333	240.726

camera A	gamma 0.45		
case 1	(App 8)		
Target 1			
MinBr $[W/m^2]$	MaxBr $[W/m^2]$	Ratio	Grad.m
12.5	79.2	0.158	239.031
12.4	79.2	0.156	224.01
12.2	79.4	0.154	237.042
12.7	76.8	0.165	225.16
12.1	76.8	0.157	227.179
12.3	79.5	0.155	246.481
12.8	80.1	0.16	237.772
12.7	81.7	0.155	232.232
12.1	76.8	0.157	227.179
12.3	80.4	0.153	253.408
11.7	80.3	0.146	262.057
11.2	80	0.14	266.581
10.7	74.2	0.145	210.858
9.9	78.4	0.127	239.502
10.9	81	0.135	281.283
11.3	81.2	0.139	281.514
	min	0.127	210.858
	max	0.165	281.514
	avr.	0.1501	243.206

camera A	gamma 1		
case 2	(App 4)		
Target 1			
MinBr $[W/m^2]$	MaxBr $[W/m^2]$	Ratio	Grad.m
15.2	102.4	0.148	321.104
14.1	102.2	0.138	331.772
13.6	101.7	0.133	279.415
13.6	101.5	0.134	328.623
12.9	101.2	0.128	360.324
12.5	100.1	0.125	315.286
11.5	100.5	0.115	319.614
12	101.6	0.118	332.391
12.6	101.9	0.123	363.902
13.2	102.1	0.13	388.243
16.1	102	0.158	312.439
16.2	102	0.159	314.835
15.3	101.1	0.151	344.192
15.7	101.5	0.155	315.03
15	101.6	0.147	281.746
15.6	100.7	0.155	300.902
	min	0.115	279.415
	max	0.159	388.243
	avr.	0.1386	325.614

camera A	gamma 0.45		
case 2	(App 4)		
Target 1			
MinBr $[W/m^2]$	MaxBr $[W/m^2]$	Ratio	Grad.m
17.4	114.3	0.152	334.809
16.6	114.3	0.145	329.03
15.9	111.3	0.143	331.186
15.3	109.4	0.14	319.936
15.1	108.8	0.139	348.619
15	104.8	0.143	311.223
13.7	104.6	0.131	311.584
14	107	0.131	331.134
14.4	110.1	0.131	352.681
14.9	112.6	0.132	356.009
18.4	111.3	0.165	326.953
17.6	111.6	0.157	297.657
17.7	111.8	0.158	302.421
17.8	111.5	0.16	361.512
17.8	109.6	0.163	318.744
17.4	107.9	0.161	320.481
	min	0.131	297.657
	max	0.165	361.512
	avr.	0.1469	328.374

camera A	gamma 1		
case 1	(App 8)		
Target 2			
MinBr $[W/m^2]$	MaxBr $[W/m^2]$	Ratio	Grad.m
12.5	90	0.139	275.984
12.7	88.2	0.144	282.265
12.9	91.6	0.141	284.558
12.9	88.4	0.146	277.707
14.4	91.9	0.156	205.857
12.8	89.7	0.142	264.062
12.8	89.3	0.144	256.493
16	92.6	0.172	276.911
13.5	91.8	0.147	292.819
15.3	91.4	0.167	272.452
17.2	93	0.185	247.417
12.6	91.4	0.138	296.183
12.6	91.6	0.138	283.743
13.2	91	0.145	233.12
13.5	91.8	0.147	292.819
15.3	91.4	0.167	272.452
	min	0.138	205.857
	max	0.185	296.183
	avr.	0.1511	269.679

camera A	gamma 0.45		
case 1	(App 8)		
Target 2			
MinBr $[W/m^2]$	MaxBr $[W/m^2]$	Ratio	Grad.m
14.6	87.9	0.167	265.413
14.8	88.5	0.167	277.292
14.4	89.4	0.161	278.699
14.5	88.2	0.164	254.307
14.5	88.2	0.165	248.746
17.2	90.8	0.189	271.566
15.3	91.2	0.168	288.857
14.9	88.3	0.169	272.602
15.9	88.3	0.18	233.792
19.4	89.8	0.216	225.296
14.9	88.7	0.169	288.502
14.5	89.3	0.163	275.682
15	89.3	0.168	259.612
14.4	88.7	0.162	254.664
14.7	89.5	0.164	279.109
15.1	89.5	0.169	274.838
	min	0.161	225.296
	max	0.216	288.857
	avr.	0.1713	265.561

camera A	gamma 1		
case 2	(App 5.6)		
Target 2			
MinBr $[W/m^2]$	MaxBr $[W/m^2]$	Ratio	Grad.m
15.6	100.6	0.155	306.298
15.5	101.2	0.153	261.076
17.1	101.3	0.169	297.651
15.4	98.3	0.157	314.626
15.2	100.4	0.151	339.586
15.4	96.8	0.159	257.853
15.4	99.9	0.154	295.065
15.5	101.1	0.153	295.075
14.7	101.7	0.144	359.549
15.8	101.4	0.155	347.934
16.2	101.2	0.161	273.315
15.7	101.1	0.155	280.892
15.3	100.8	0.151	303.746
15.2	101.1	0.15	289.799
14.7	99.6	0.148	297.139
15.6	100.6	0.155	306.298
	min	0.144	257.853
	max	0.169	359.549
	avr.	0.1544	301.62

camera A	gamma 0.45		
case 2	(App 5.6)		
Target 2			
MinBr $[W/m^2]$	MaxBr $[W/m^2]$	Ratio	Grad.m
17.9	108.3	0.165	313.417
17.5	107.3	0.163	298.178
19.6	108.1	0.181	314.964
18.7	106.8	0.175	329.891
20.5	107.3	0.191	297.686
23.5	108.3	0.217	266.274
17.8	104.3	0.17	316.589
17.3	104.8	0.165	316.452
16.7	104.4	0.16	310.118
17.3	105.5	0.164	298.993
17	107.5	0.159	345.054
17.4	107	0.162	357.868
21.2	108.1	0.196	295.062
18.3	107.1	0.171	276.579
19.3	107.3	0.18	332.702
18.4	107.1	0.172	338.718
	min	0.159	266.274
	max	0.217	357.868
	avr.	0.1744	312.909

camera A gamma 1
case 1 (App 8)
Target 3

MinBr $[W/m^2]$	MaxBr $[W/m^2]$	Ratio	Grad.m
14.5	82.8	0.175	201.642
13.9	82.4	0.169	201.012
13.4	84.6	0.159	261.476
13.6	84	0.162	223.172
12.9	84.3	0.153	256.033
12.9	81.8	0.157	244.512
13	78.3	0.166	227.549
12.6	80.5	0.157	239.531
14.5	83	0.175	260.198
12.9	82.6	0.157	225.339
12	82.3	0.146	275.732
14.3	82.9	0.172	217.033
14.1	82	0.172	215.203
13.2	83.2	0.159	250.825
13.2	83.9	0.158	258.768
13.2	83.3	0.159	268.141
	min	0.146	201.012
	max	0.175	275.732
	avr.	0.1623	239.135

camera A gamma 0.45
case 1 (App 8)
Target 3

MinBr $[W/m^2]$	MaxBr $[W/m^2]$	Ratio	Grad.m
15.3	81.5	0.188	255.558
14.8	81.2	0.183	260.902
15.1	80.8	0.187	254.734
15.3	82.3	0.186	268.548
14.9	79.5	0.187	224.162
14.3	75.8	0.188	215.658
14	76	0.184	214.037
15.2	80.7	0.188	259.361
14.8	82	0.181	256.771
14.8	82.3	0.18	268.677
17.5	80.9	0.216	208.876
16.9	81	0.208	216.879
15.3	80.3	0.191	250.927
15.2	81	0.187	218.36
15.2	80.6	0.189	234.297
14.3	78.6	0.182	227.206
	min	0.18	208.876
	max	0.216	268.677
	avr.	0.1891	239.685

camera A gamma 1
case 2 (App 4)
Target 3

MinBr $[W/m^2]$	MaxBr $[W/m^2]$	Ratio	Grad.m
20.7	102.1	0.202	297.516
20.2	102	0.198	295.587
19.8	101.9	0.194	297.407
19	101.5	0.187	301.994
19.2	101.7	0.188	328.712
18.7	101.8	0.184	288.14
18.4	102	0.181	303.224
18.3	101.2	0.181	307.408
18.2	102.2	0.178	311.925
19.3	102.2	0.189	293.2
22.5	102.1	0.221	276.885
20	102.4	0.195	301.728
19.9	102.4	0.194	307.701
19.1	101.6	0.188	290.421
18.7	101.7	0.184	295.748
18.8	101.4	0.186	322.589
	min	0.178	276.885
	max	0.221	328.712
	avr.	0.1906	301.262

camera A gamma 0.45
case 2 (App 4)
Target 3

MinBr $[W/m^2]$	MaxBr $[W/m^2]$	Ratio	Grad.m
22.1	114.7	0.193	298.377
22	114.7	0.192	291.967
22	115.1	0.192	303.002
21	113.6	0.185	359.263
20.5	112.6	0.182	316.766
20.2	104.1	0.194	218.178
20.4	110.4	0.185	313.804
19.8	112.8	0.175	322.991
21.4	113	0.189	309.946
21	115.1	0.182	337.285
22.2	115.7	0.192	292.562
21.4	114.7	0.186	299.066
21.4	113.8	0.188	316.299
21.9	113.6	0.193	312.159
21.5	113.6	0.189	344.599
20.7	111.3	0.186	303.241
	min	0.175	218.178
	max	0.194	359.263
	avr.	0.1877	308.595

camera A gamma 1
case 1 (App 8)
Target 4

MinBr $[W/m^2]$	MaxBr $[W/m^2]$	Ratio	Grad.m
16.2	84.7	0.191	267.25
17.6	85.1	0.207	264.613
23	86.4	0.266	214.224
19.5	86.5	0.225	221.197
17.2	86.8	0.198	259.197
17.6	83.4	0.211	240.023
16.7	85.3	0.196	257.415
16.1	82.1	0.197	234.184
16.3	77.5	0.21	192.34
16.5	81.8	0.202	235.048
15.3	83.7	0.183	261.441
20.9	86.7	0.24	219.234
21	85.9	0.244	222.069
18.8	86.6	0.217	204.261
18	85.2	0.212	187.326
16.7	82	0.204	226.311
	min	0.183	187.326
	max	0.266	267.25
	avr.	0.2127	231.635

camera A gamma 0.45
case 1 (App 8)
Target 4

MinBr $[W/m^2]$	MaxBr $[W/m^2]$	Ratio	Grad.m
20.8	86.6	0.24	203.091
21.2	86.7	0.244	223.477
19.9	87.1	0.229	281.22
19.3	85	0.228	254.755
19	83.2	0.228	249.678
18.5	81	0.228	215.331
18.6	79.2	0.235	212.723
18.5	81.2	0.228	213.26
20.1	83.8	0.24	229.59
19.8	83.4	0.237	230.867
20	84.3	0.237	236.805
20.5	84.5	0.242	198.838
19.9	85.3	0.234	208.388
19.7	85.1	0.231	198.705
18.9	84	0.225	216.903
18.7	81	0.231	217.578
	min	0.225	198.705
	max	0.244	281.22
	avr.	0.2336	224.451

camera A gamma 1
case 2 (App 4)
Target 4

MinBr $[W/m^2]$	MaxBr $[W/m^2]$	Ratio	Grad.m
25.3	102.7	0.246	283.924
24	102.3	0.234	281.981
25.9	102.8	0.252	263.782
22.5	101.8	0.222	291.199
22.8	101.7	0.224	303.809
22.7	101.5	0.224	311.061
21.7	101.6	0.214	293.096
22.3	101.9	0.219	298.964
21.7	102	0.213	306.282
22.8	102	0.224	294.305
23.9	102.2	0.234	317.258
26.9	103	0.262	269.781
26.4	103	0.256	280.382
23.8	102.6	0.232	293.928
22.4	102	0.22	280.211
23.4	101.8	0.23	290.899
	min	0.213	263.782
	max	0.262	317.258
	avr.	0.2316	291.304

camera A gamma 0.45
case 2 (App 4)
Target 4

MinBr $[W/m^2]$	MaxBr $[W/m^2]$	Ratio	Grad.m
29.4	115.5	0.255	269.109
25.3	115.7	0.219	282.04
24.4	116.1	0.21	331.655
24.4	112.2	0.218	338.386
24.3	113.2	0.215	334.672
24.1	112.6	0.214	310.785
24.2	111.3	0.217	302.892
24.5	115.3	0.212	306.83
25	115.1	0.217	330.36
29.7	119	0.249	288.107
27.8	119.4	0.233	302.633
25.8	118.8	0.217	322.527
24.7	116.3	0.212	308.429
24.6	113.9	0.216	319.633
24.6	111.5	0.221	277.409
24.6	110	0.224	291.383
	min	0.21	269.109
	max	0.255	338.386
	avr.	0.2218	307.303

camera A gamma 1
case 1 (App 8)
Target 5

MinBr [W/m^2]	MaxBr [W/m^2]	Ratio	Grad.m
22.6	90.6	0.25	270.361
22.1	90.6	0.244	246.855
21.4	90.6	0.236	260.903
20	88.2	0.226	230.892
20.6	92	0.224	290.185
19.9	92.1	0.216	282.49
21.3	91.8	0.231	267.61
23.6	90	0.263	187.5
23.1	90.1	0.256	185.905
22.6	88.2	0.257	216.665
21	83.7	0.251	214.023
20.5	86.7	0.236	223.917
19.1	84.8	0.225	224.067
20.2	83.5	0.242	209.48
22.8	89.2	0.256	232.566
22.8	88.7	0.257	227.142
	min	0.216	185.905
	max	0.263	290.185
	avr.	0.2419	235.661

camera A gamma 0.45
case 1 (App 8)
Target 5

MinBr [W/m^2]	MaxBr [W/m^2]	Ratio	Grad.m
24.8	87	0.285	222.222
25.2	87.2	0.289	215.335
24.3	87.7	0.278	227.162
24.4	87	0.28	226.291
24.1	85.9	0.281	228.246
22.5	84	0.267	222.56
22.5	85.4	0.263	213.432
21.6	80.6	0.268	201.149
22.1	81.4	0.271	203.207
22.6	82.8	0.273	213.774
24.6	89	0.276	267.452
23.2	88.7	0.261	244.136
22.5	86.9	0.258	250.889
22.5	84.1	0.267	209.996
22.5	87.5	0.257	226.879
23.1	89.7	0.258	257.883
	min	0.257	201.149
	max	0.289	267.452
	avr.	0.2708	226.913

camera A gamma 1
case 2 (App 5.6)
Target 5

MinBr [W/m^2]	MaxBr [W/m^2]	Ratio	Grad.m
30.1	101.4	0.297	244.163
33.2	101.5	0.327	216.155
30.7	101.4	0.303	240.731
28	101.1	0.277	248.665
26.4	101.2	0.261	253.964
24.2	96.7	0.25	248.399
24.7	98.6	0.25	255.001
24.2	97.8	0.248	241.531
27	101.5	0.267	279.251
24.2	101.6	0.239	316.014
24.9	101.6	0.245	324.562
34.8	101.3	0.344	208.193
28.6	101.2	0.283	228.166
27.6	95.4	0.289	223.767
24.9	95.3	0.261	242.165
23.2	95.8	0.242	253.892
	min	0.239	208.193
	max	0.344	324.562
	avr.	0.2739	251.539

camera A gamma 0.45
case 2 (App 5.6)
Target 5

MinBr [W/m^2]	MaxBr [W/m^2]	Ratio	Grad.m
31.7	109.4	0.289	238.971
28.7	107	0.268	223.083
28.7	106.1	0.27	267.645
26.4	104	0.254	284.804
25.6	98	0.262	243.541
26.2	100.7	0.26	250.421
26.8	105.1	0.255	239.011
26.4	106	0.249	285.821
26.5	107	0.247	289.586
27.3	108.4	0.252	291.509
30.9	106.8	0.29	238.115
31.5	107.3	0.294	233.998
28.3	102.4	0.276	247.911
26.2	100.8	0.26	260.09
25.6	97.7	0.262	257.683
25.1	99.2	0.253	232.868
	min	0.247	223.083
	max	0.294	291.509
	avr.	0.2651	256.566

camera A gamma 1
case 1 (App 8)
Target 6

MinBr [W/m^2]	MaxBr [W/m^2]	Ratio	Grad.m
30.1	93	0.324	209.403
30.2	93.5	0.323	217.099
28.8	93.6	0.308	213.166
32	94.4	0.339	213.584
29.7	94.7	0.314	228.977
30.3	94.1	0.322	194.806
31.2	94.5	0.33	205.868
28.6	92.5	0.31	220.251
27.9	90.4	0.309	221.212
28.1	91.3	0.307	214.765
28	91.3	0.306	219.839
27.2	91.2	0.299	222.631
29.4	92.5	0.318	228.739
28.7	94.7	0.303	245.544
30.4	94.9	0.32	187.56
29.9	95.7	0.313	262.55
	min	0.299	187.56
	max	0.339	262.55
	avr.	0.3153	219.126

camera A gamma 0.45
case 1 (App 8)
Target 6

MinBr [W/m^2]	MaxBr [W/m^2]	Ratio	Grad.m
32.4	97.3	0.333	182.482
31.3	96.4	0.325	201.139
31.1	96.8	0.322	204.534
29.7	94.9	0.313	240.621
28.3	90	0.314	224.351
28.6	84.3	0.339	189.645
28.8	88.7	0.325	211.681
28	85.4	0.327	186.986
28.6	88.8	0.322	223.211
27.3	91.8	0.298	223.902
29.3	95	0.308	241.322
32.2	95.4	0.337	209.18
32.1	95.2	0.337	199.966
29	90.7	0.32	220.301
29.1	88.3	0.329	198.923
28.4	89.7	0.316	219.264
	min	0.298	182.482
	max	0.339	241.322
	avr.	0.3228	211.094

camera A gamma 1
case 2 (App 5.6)
Target 6

MinBr [W/m^2]	MaxBr [W/m^2]	Ratio	Grad.m
37.4	103	0.363	229.151
35	102.5	0.342	243.016
33.4	99.4	0.336	228.931
33.5	101.1	0.331	247.957
32.5	101.3	0.321	252.966
30.9	101.7	0.303	264.261
35.4	102.3	0.346	246.403
36.7	103	0.356	255.525
36.8	103	0.357	211.104
37.9	103	0.368	234.052
34.7	99.1	0.35	227.799
34.3	97.2	0.353	212.995
33.2	98.1	0.338	236.627
33.1	98.2	0.337	211.805
33.9	99.1	0.342	224.193
36	102.1	0.353	240.039
	min	0.303	211.104
	max	0.368	264.261
	avr.	0.3435	235.427

camera A gamma 0.45
case 2 (App 5.6)
Target 6

MinBr [W/m^2]	MaxBr [W/m^2]	Ratio	Grad.m
39	117.4	0.332	224.715
39.4	116.8	0.337	242.928
35.9	114.7	0.313	253.709
32.4	108.9	0.298	263.638
33.5	106.2	0.316	241.748
33.3	103.4	0.322	228.228
33.5	107.5	0.311	250.493
34.4	107.9	0.319	258.115
37.5	110.9	0.338	250.488
39.3	115.1	0.341	263.266
41.4	116.3	0.356	234.606
37.5	115.5	0.325	240.471
38.3	114.3	0.335	227.917
34.9	108.9	0.32	246.616
32.6	106.1	0.307	254.06
32.4	103.4	0.313	250.452
	min	0.298	224.715
	max	0.356	263.638
	avr.	0.3239	245.716

camera A	gamma 1		
case 1	(App 8)		
Target 7			
MinBr [W/m^2]	MaxBr [W/m^2]	Ratio	Grad.m
22.7	70.1	0.324	174.823
20.9	71.1	0.294	214.046
22	70.4	0.312	151.677
27.1	71.6	0.379	146.712
24.9	71.4	0.348	152.176
22.3	72.2	0.31	160.158
21.4	70.9	0.301	193.231
20.4	66.9	0.304	149.078
20.7	68.8	0.3	159.606
20.8	67	0.311	158.716
25.7	70.7	0.363	146.923
22.8	66.4	0.344	141.844
21.9	68.7	0.319	165.936
22	68.8	0.321	144.978
21.4	67.4	0.317	146.257
21.2	67.4	0.314	164.614
	min	0.294	141.844
	max	0.379	214.046
	avr.	0.3226	160.674

camera A	gamma 0.45		
case 1	(App 8)		
Target 7			
MinBr [W/m^2]	MaxBr [W/m^2]	Ratio	Grad.m
27.8	73.4	0.379	157.34
26.5	72.8	0.364	154.949
25.4	73.1	0.348	138.82
24	70.3	0.342	160.819
25.1	72.1	0.348	143.72
24.1	71.2	0.338	168.82
23.8	69.8	0.341	113.172
23.1	70.4	0.329	166.991
23.1	71	0.325	157.248
24.9	72.8	0.342	167.078
23.8	74	0.322	171.057
27.9	73.5	0.379	151.826
26	73.8	0.352	149.079
24.5	73.6	0.333	202.001
23.6	71.4	0.331	184.975
23.2	73	0.318	199.876
	min	0.318	113.172
	max	0.379	202.001
	avr.	0.3432	161.736

camera A	gamma 1		
case 2	(App 5.6)		
Target 7			
MinBr [W/m^2]	MaxBr [W/m^2]	Ratio	Grad.m
32.5	101.9	0.319	305.939
34.9	102.2	0.341	231.003
34.7	101.6	0.341	300.627
39.1	101.3	0.386	219.795
37.2	101.3	0.367	205.239
35.5	101	0.352	248.851
33.5	100.7	0.333	250.686
32.1	101.7	0.316	268.091
33.2	100.3	0.331	251.943
33.1	101.4	0.326	214.981
37.4	101	0.371	198.48
36.9	100.8	0.366	228.351
36.1	100.6	0.359	238.134
35.5	101.6	0.35	231.003
33.3	99.7	0.334	239.412
33.7	101.3	0.333	209.662
	min	0.316	198.48
	max	0.386	305.939
	avr.	0.3453	240.137

camera A	gamma 0.45		
case 2	(App 5.6)		
Target 7			
MinBr [W/m^2]	MaxBr [W/m^2]	Ratio	Grad.m
44.7	121	0.37	228.273
40.2	119.6	0.336	292.568
38.1	120.6	0.316	297.406
36.5	118	0.31	293.764
35.3	110.6	0.319	241.875
36.4	117.6	0.31	280.486
40.9	120.4	0.34	281.775
38.2	120.8	0.316	335.009
46.5	120	0.387	226.591
42.1	119.2	0.353	227.678
39.4	117	0.337	265.18
39.3	114.6	0.343	250.518
36.2	108.9	0.333	228.459
37.8	115.9	0.326	240.05
38.7	115.3	0.336	271.689
38.4	117.4	0.327	275.661
	min	0.31	226.591
	max	0.387	335.009
	avr.	0.3349	264.811

camera A	gamma 1		
case 1	(App 8)		
Target 8			
MinBr [W/m^2]	MaxBr [W/m^2]	Ratio	Grad.m
24.6	65.8	0.374	144.896
25.2	68.4	0.369	126.398
24.8	70.2	0.353	183.432
25.4	70.5	0.361	177.981
26.5	70.9	0.374	182.869
26.6	68.9	0.386	154.848
27.6	68.1	0.405	146.301
26.5	68.3	0.388	157.43
26	68.4	0.38	159.162
27.8	70.3	0.396	128.065
27.4	70.7	0.387	156.247
27.4	71.6	0.383	152.034
26.7	70.2	0.38	161.02
26.4	66.8	0.395	140.523
25.7	66.7	0.386	136.958
25.8	69.9	0.369	163.372
	min	0.353	126.398
	max	0.405	183.432
	avr.	0.3804	154.472

camera A	gamma 0.45		
case 1	(App 8)		
Target 8			
MinBr [W/m^2]	MaxBr [W/m^2]	Ratio	Grad.m
27.6	67.3	0.41	127.861
27.6	71	0.389	157.228
27.2	71.4	0.381	167.112
27.7	73.7	0.376	179.296
28.5	69.5	0.41	134.657
30.9	72.7	0.425	137.672
30.9	71.8	0.43	141.542
28.5	73.5	0.387	172.072
28.9	73.2	0.395	160.637
27	71.4	0.378	178.479
26	71.1	0.366	188.278
26.9	73.4	0.366	196.76
27.2	71.4	0.38	179.619
32.8	73	0.45	124.595
30.4	71.2	0.427	142.522
27.9	72.2	0.386	166.34
	min	0.366	124.595
	max	0.45	196.76
	avr.	0.3973	159.667

camera A	gamma 1		
case 2	(App 5.6)		
Target 8			
MinBr [W/m^2]	MaxBr [W/m^2]	Ratio	Grad.m
39.7	91.5	0.433	171.202
42.2	92.3	0.457	165.577
35.7	90.7	0.394	199.86
35.4	92.8	0.381	226.164
35.9	94.3	0.38	236.787
35.5	93	0.381	205.09
35.2	93.4	0.377	184.652
37.3	93.3	0.4	214.468
38.4	93.9	0.409	208.923
35.2	92.2	0.382	206.005
39.2	93	0.422	158.468
40.3	92.4	0.436	170.768
36.4	91	0.4	185.111
36.9	95.6	0.385	206.005
36.7	94.2	0.389	208.742
36.7	94	0.39	202.858
	min	0.377	158.468
	max	0.457	236.787
	avr.	0.401	196.918

camera A	gamma 0.45		
case 2	(App 5.6)		
Target 8			
MinBr [W/m^2]	MaxBr [W/m^2]	Ratio	Grad.m
48.4	117.6	0.411	255.585
46.7	117.6	0.397	258.38
46.7	114	0.41	231.293
43.8	113.1	0.388	227.597
45.2	114.7	0.394	232.234
46.3	116.3	0.398	268.893
49.1	116.5	0.422	252.834
46.8	117.4	0.399	254.996
57.6	120.6	0.478	181.628
56.9	118.6	0.48	210.412
58	119.6	0.485	203.157
50	119.4	0.419	254.947
50.6	120	0.422	237.837
48.3	114.2	0.423	200.879
47.8	115	0.416	224.005
49.2	118.4	0.416	231.508
	min	0.388	181.628
	max	0.485	268.893
	avr.	0.4224	232.887

camera A gamma 1
case 1 (App 8)
Target 9

MinBr [W/m²]	MaxBr [W/m²]	Ratio	Grad.m
33.1	73.1	0.453	142.338
33.6	72.8	0.462	138.392
32.7	73.2	0.447	118.388
33.2	72.4	0.458	150.757
32.4	72.6	0.446	166.762
33.8	72.9	0.464	146.504
33.6	72.8	0.462	138.392
35.6	74.1	0.481	114.725
34	73.9	0.461	142.736
33.5	73.4	0.456	133.288
32.1	70.7	0.454	124.568
32.1	71.9	0.447	138.311
31.9	72	0.443	123.944
35.7	74.6	0.479	105.401
38	74	0.514	115.038
35.8	73.7	0.486	104.42
	min	0.443	104.42
	max	0.514	166.762
	avr.	0.4633	131.496

camera A gamma 0.45
case 1 (App 8)
Target 9

MinBr [W/m²]	MaxBr [W/m²]	Ratio	Grad.m
31.7	69.5	0.457	125.015
30.9	73	0.423	150.997
32.3	73.7	0.438	155.819
33.2	76.2	0.436	150.97
32.9	77.6	0.425	175.157
39	79.2	0.493	134.105
39.1	79.3	0.493	129.036
35.3	78.9	0.448	176.33
33	76.5	0.432	170.886
32.8	75	0.437	164.361
32.1	74.9	0.429	172.703
38.4	79.5	0.483	130.943
34.5	78	0.443	142.753
33.3	75.2	0.443	143.385
31.9	75.6	0.422	152.785
31	73.4	0.423	138.373
	min	0.422	125.015
	max	0.493	176.33
	avr.	0.4453	150.851

camera A gamma 1
case 2 (App 5.6)
Target 9

MinBr [W/m²]	MaxBr [W/m²]	Ratio	Grad.m
41.3	87.5	0.472	143.782
40	90.9	0.44	177.981
41.8	92.2	0.453	162.635
41.4	91.4	0.453	167.287
40.8	91.8	0.445	194.587
43.9	89.1	0.492	150.357
42.4	89	0.477	132.473
45.2	89.5	0.505	146.235
40.4	89.7	0.451	194.023
41	90.9	0.451	156.955
41	91	0.45	207.523
45.4	89.5	0.507	145.385
43.6	89.8	0.486	145.94
45.7	90	0.508	139.994
40.8	86.6	0.471	149.466
39.5	89.3	0.443	170.824
	min	0.44	132.473
	max	0.508	207.523
	avr.	0.469	161.59

camera A gamma 0.45
case 2 (App 5.6)
Target 9

MinBr	MaxBr [W/m²]	Ratio	Grad.m
66.2	133.2	0.497	238.251
64.6	131	0.493	251.635
62.6	129.6	0.483	244.378
60.5	122.4	0.495	207.942
60.2	122.2	0.492	194.467
60.7	122.6	0.495	248.574
63.2	123.6	0.511	233.818
62.1	127.7	0.486	242.752
71.1	134.7	0.528	195.334
66.2	128.8	0.514	211.934
61.7	129.8	0.475	225.589
60.9	125.5	0.486	202.79
62.1	121.6	0.511	162.384
58.6	116.6	0.503	187.017
63.1	122.6	0.515	192.849
63.4	127.9	0.495	212.215
	min	0.475	162.384
	max	0.528	251.635
	avr.	0.4987	215.746

camera A gamma 1
case 1 (App 8)
Target 10

MinBr [W/m²]	MaxBr [W/m²]	Ratio	Grad.m
39.8	70.8	0.562	94.621
40.1	70.6	0.567	92.34
38.9	71.5	0.545	120.378
38.7	72.3	0.536	122.643
39.4	72.4	0.544	116.04
41.4	73.8	0.561	106.382
41.1	72.9	0.563	107.95
39.9	72.5	0.55	126.19
38.9	71	0.547	135.72
38.2	71.5	0.534	132.014
38.3	71	0.54	123.561
38.1	70.6	0.54	115.93
37.7	71.2	0.53	116.893
40.3	72.5	0.556	104.42
40.3	72.3	0.558	110.581
39.8	71.4	0.558	106.112
	min	0.53	92.34
	max	0.567	135.72
	avr.	0.5494	114.611

camera A gamma 0.45
case 1 (App 8)
Target 10

MinBr [W/m²]	MaxBr [W/m²]	Ratio	Grad.m
41.8	75.7	0.552	117.391
42.6	75.6	0.564	127.552
44.5	79.3	0.561	116.119
43.4	78.6	0.552	123.291
42.7	78.7	0.542	124.423
41.2	75.4	0.546	112.511
40.1	74.7	0.536	114.58
39.3	72.8	0.539	117.843
40.4	71.1	0.568	89.163
40.4	71.7	0.563	94.621
40.2	72.7	0.553	120.395
39.8	72.7	0.547	124.116
40.7	75	0.542	122.944
42.1	76.8	0.548	127.955
46.4	78	0.595	101.184
43.1	77.7	0.555	100.238
	min	0.536	89.163
	max	0.595	127.955
	avr.	0.5539	114.644

camera A gamma 1
case 2 (App 5.6)
Target 10

MinBr [W/m²]	MaxBr [W/m²]	Ratio	Grad.m
48	88.6	0.541	163.65
47.6	87.5	0.544	160.975
47.7	86.5	0.552	131.184
49.1	87.2	0.563	123.631
48.1	88	0.547	139.171
48.4	88.4	0.548	136.471
49	88.9	0.552	142.669
50.2	89.8	0.559	141.844
50.1	87.8	0.571	117.498
50.1	87.2	0.575	110.742
49.7	89.7	0.554	152.139
47.6	88.2	0.54	146.733
48.4	86.4	0.56	132.114
49.5	84.5	0.586	119.078
49	85.6	0.573	129.34
49.4	86.4	0.572	126.347
	min	0.54	110.742
	max	0.586	163.65
	avr.	0.5586	135.849

camera A gamma 0.45
case 2 (App 5.6)
Target 10

MinBr [W/m²]	MaxBr [W/m²]	Ratio	Grad.m
76	130.2	0.584	168.965
70.8	119	0.595	151.57
70.4	119.4	0.589	153.678
69.5	120	0.579	164.557
70.5	118.8	0.594	165.847
70.7	121.2	0.583	173.792
79.5	131	0.606	173.181
70.1	121.8	0.576	160.832
78	133.6	0.584	195.424
76.3	132.1	0.578	198.269
77.1	132.7	0.581	185.736
74.7	127.8	0.585	172.467
74.7	131.9	0.566	182.65
72.8	129.6	0.562	181.588
73.6	122.2	0.602	146.098
72.7	120.4	0.604	138.353
	min	0.562	138.353
	max	0.606	198.269
	avr.	0.5855	169.438

camera A gamma 1
case 1 (App 8)
Target 11

MinBr [W/m²]	MaxBr [W/m²]	Ratio	Grad.m
24.3	43.7	0.555	60.202
23.7	43.6	0.543	60.202
23	43.6	0.527	78.924
22.5	43.2	0.521	79.438
21.2	39.4	0.538	57.073
21.8	41	0.533	60.229
22.2	42.7	0.521	73.165
22.8	42.6	0.535	68.33
23.8	43.1	0.551	65.244
27.5	43.4	0.633	49.244
23.6	42.1	0.561	66.037
23.2	41.7	0.556	70.441
22.2	40.2	0.554	62.442
22.8	40.4	0.564	62.442
23.6	41.9	0.564	69.573
23.7	41.8	0.568	70.008
	min	0.521	49.244
	max	0.633	79.438
	avr.	0.5515	65.8121

camera A gamma 0.45
case 1 (App 8)
Target 11

MinBr [W/m²]	MaxBr [W/m²]	Ratio	Grad.m
27	46.3	0.583	64.536
25.9	46.3	0.56	59.74
24.7	45.4	0.545	78.199
24.5	44.8	0.546	81.931
23.8	43.7	0.546	74.225
23.2	43.2	0.538	60.898
23.6	42.9	0.55	66.267
24.5	44.3	0.552	71.104
24.9	44.9	0.556	73.88
25.3	45.3	0.558	75.964
25.3	44.5	0.568	70.49
25.5	43.2	0.59	62.751
25.2	43.4	0.58	63.124
24.6	42	0.586	60.343
24.3	41	0.592	57.134
26.6	44.6	0.598	65.965
	min	0.538	57.134
	max	0.598	81.931
	avr.	0.5655	67.9094

camera A gamma 1
case 2 (App 5.6)
Target 11

MinBr [W/m²]	MaxBr [W/m²]	Ratio	Grad.m
56.2	97.8	0.574	123.593
55.8	97.8	0.571	126.644
53.7	98.3	0.547	127.082
53	97.9	0.541	144.625
51.5	97.7	0.527	149.386
51.6	96.5	0.534	161.02
51	96.5	0.529	160.441
49.1	92	0.533	149.81
49.1	92.2	0.533	144.912
51.2	91.8	0.558	134.285
52.5	97	0.541	139.751
55.2	96.8	0.57	144.037
55	96.9	0.568	150.278
54.9	96.6	0.568	150.278
53.3	95.2	0.56	153.812
51.8	93.5	0.554	136.497
	min	0.527	123.593
	max	0.574	161.02
	avr.	0.5505	143.528

camera A gamma 0.45
case 2 (App 5.6)
Target 11

MinBr [W/m²]	MaxBr [W/m²]	Ratio	Grad.m
58.5	94.7	0.618	134.379
58.1	93.7	0.621	115.552
57.9	92.4	0.627	117.127
54.6	85	0.642	83.213
54.4	90.5	0.601	114.623
61.2	95.4	0.641	106.48
61.9	95.4	0.649	113.741
61	95.4	0.639	119.846
62	97.3	0.638	111.281
58	96.2	0.603	117.82
59.9	96.2	0.623	117.417
57.5	95.6	0.602	141.116
58.3	95.2	0.612	135.572
55.4	93.8	0.591	126.571
52.7	89.6	0.588	115.012
54.1	93	0.582	127.355
	min	0.582	83.213
	max	0.649	141.116
	avr.	0.6173	118.569

camera A gamma 1
case 1 (App 8)
Target 12

MinBr [W/m²]	MaxBr [W/m²]	Ratio	Grad.m
28.3	43.5	0.651	60.387
29.4	44	0.668	53.686
29	43.5	0.667	57.24
29.6	43.2	0.685	37.519
29.7	43.5	0.683	47.708
29.1	44.1	0.66	42.948
28.1	43.7	0.642	58.408
27.9	43	0.649	58.068
26.7	42.9	0.622	55.244
26.3	41.7	0.629	54.399
27.4	42.8	0.639	53.992
27.1	42.5	0.639	47.869
28.4	42.5	0.669	50.895
30.4	44.9	0.678	43.031
28.8	43.9	0.657	54.863
29.3	44.3	0.662	52.676
	min	0.622	37.519
	max	0.685	60.387
	avr.	0.6563	51.7968

camera A gamma 0.45
case 1 (App 8)
Target 12

MinBr [W/m²]	MaxBr [W/m²]	Ratio	Grad.m
31	45.8	0.677	51.951
30.3	45.9	0.661	54.151
29.4	45.9	0.64	65.273
29.2	46.3	0.631	64.298
28.8	43.7	0.658	53.369
28.5	45.3	0.63	63.355
28.8	45.8	0.629	58.784
28.3	45.5	0.622	61.183
29.1	45.7	0.637	59.384
30.9	47.4	0.653	55.51
30.6	47.1	0.648	52.008
30	46	0.651	54.024
29.5	46.8	0.63	64.182
29.4	45.5	0.647	60.653
29.3	44.4	0.66	48.487
29.7	45	0.661	56.484
	min	0.622	48.487
	max	0.677	65.273
	avr.	0.6459	57.6935

camera A gamma 1
case 2 (App 5.6)
Target 12

MinBr [W/m²]	MaxBr [W/m²]	Ratio	Grad.m
62	97.1	0.639	113.665
65.9	98.1	0.672	100.392
64.9	98	0.662	119.815
64.7	98.2	0.659	126.729
64.6	97.2	0.665	128.412
62.8	97.1	0.647	122.006
61.9	96.2	0.643	121.948
62.5	94.4	0.662	109.251
61.9	96.7	0.64	115.056
62	97.1	0.639	113.665
63.8	96.6	0.66	115.037
67.6	98.7	0.685	103.448
66.7	97.8	0.682	103.15
66.3	98.6	0.673	116.554
66.1	97.3	0.679	118.862
65.5	96.3	0.68	110.23
	min	0.639	100.392
	max	0.685	128.412
	avr.	0.6617	114.889

camera A gamma 0.45
case 2 (App 5.6)
Target 12

MinBr [W/m²]	MaxBr [W/m²]	Ratio	Grad.m
69.4	96.4	0.72	100.485
70.5	98	0.72	97.84
72.4	98.2	0.738	73.74
71.6	98.2	0.729	80.794
73.1	98.3	0.744	77.092
71.6	98.3	0.728	80.794
69	96.8	0.713	94.336
68.7	96.2	0.714	95.509
67.7	94.7	0.715	97.298
68.8	93.9	0.733	89.535
65.4	94.4	0.693	101.859
66.4	95.2	0.697	107.496
67.3	95.2	0.707	101.926
71	96.8	0.734	76.255
69.3	95.6	0.725	71.241
68.1	95.2	0.716	101.972
	min	0.693	71.241
	max	0.744	107.496
	avr.	0.7204	90.5108

camera A		gamma 1	
case 1	(App 8)		
Target 13			
MinBr (W/m^2)	MaxBr (W/m^2)	Ratio	Grad.m
32.8	45	0.73	36.569
32.3	45.3	0.714	41.58
32.3	44.7	0.722	49.183
32.8	44.9	0.73	49.244
31.8	43.8	0.725	38.024
31.6	43.5	0.727	34.563
32.2	43.9	0.734	41.118
31.6	44.3	0.714	48.647
31.4	44	0.714	45.137
30.9	45.1	0.686	45.51
32.5	45	0.722	42.375
30.5	43.4	0.701	47.56
31.1	42.2	0.737	37.492
31.2	43.4	0.718	37.714
30.8	43.4	0.709	37.898
30.6	42.8	0.715	36.732
	min	0.686	34.563
	max	0.737	49.244
	avr.	0.7186	41.8341

camera A		gamma 0.45	
case 1	(App 8)		
Target 13			
MinBr (W/m^2)	MaxBr (W/m^2)	Ratio	Grad.m
32.8	48.8	0.671	50.315
32.8	49.1	0.669	56.236
33.1	47.2	0.701	52.889
32.8	48.5	0.678	55.316
32.3	46.9	0.689	59.443
32.4	46.6	0.696	46.457
32.2	46.6	0.692	40.838
31.5	46.3	0.681	53.454
32.1	47.2	0.679	58.695
31.9	46.9	0.68	59.372
32.4	47.9	0.677	57.821
32.8	48.7	0.674	55.245
31.4	47.5	0.662	48.606
30.9	46.3	0.667	52.72
31	45.7	0.679	48.459
31.4	46	0.683	47.187
	min	0.662	40.838
	max	0.701	59.443
	avr.	0.6799	52.6908

camera A		gamma 1	
case 2	(App 5.6)		
Target 13			
MinBr (W/m^2)	MaxBr (W/m^2)	Ratio	Grad.m
76.5	101	0.758	86.379
75.8	101.2	0.749	82.026
77.3	101.2	0.764	88.972
75.7	100.4	0.755	90.168
75	99.4	0.755	99.039
74.7	98.5	0.758	88.155
74.9	98	0.764	76.937
73.5	98.2	0.748	73.122
74.1	99.2	0.747	107.924
74.7	99.8	0.748	99.966
72.9	100.9	0.722	94.972
71.5	100.6	0.711	87.401
72	100.2	0.719	94.856
72.3	99.1	0.729	94.785
72.1	98	0.736	72.836
72.5	96.1	0.755	76.869
	min	0.711	72.836
	max	0.764	107.924
	avr.	0.7449	88.4004

camera A		gamma 0.45	
case 2	(App 5.6)		
Target 13			
MinBr (W/m^2)	MaxBr	Ratio	Grad.m
79.3	106.2	0.747	99.592
82.1	107	0.768	81.931
79.5	104.2	0.763	84.759
78.1	102.4	0.763	89.242
77.1	96.5	0.799	60.055
76.9	97.1	0.792	65.542
74.4	96.4	0.772	68.262
76.6	98.5	0.778	82.148
76.8	101	0.76	80.012
78.6	104.4	0.753	96.77
78.7	105.9	0.744	87.929
78.3	106.6	0.734	95.866
77.8	103.1	0.755	91.577
75.7	99.7	0.759	91.337
75.3	97.5	0.772	83.071
73.5	95.4	0.771	70.566
	min	0.734	60.055
	max	0.799	99.592
	avr.	0.7644	83.0412

camera A		gamma 1	
case 1	(App 8)		
Target 14			
MinBr (W/m^2)	MaxBr (W/m^2)	Ratio	Grad.m
35.3	43.8	0.806	26.398
34.5	43.1	0.8	34.401
34.2	42.4	0.808	28.589
34.1	42.6	0.802	28.512
33.6	41.7	0.806	27.287
34.5	42.8	0.806	32.573
33.9	43	0.789	35.246
34.2	42.8	0.8	29.901
34.5	43	0.802	29.761
36.3	44.2	0.821	26.119
36	44.2	0.814	33.93
35.3	43.9	0.803	27.656
35.1	43.6	0.806	31.657
34	43.2	0.788	29.065
34.7	42.3	0.821	25.874
34.2	42.4	0.807	22.777
	min	0.788	22.777
	max	0.821	35.246
	avr.	0.8049	29.4841

camera A		gamma 0.45	
case 1	(App 8)		
Target 14			
MinBr (W/m^2)	MaxBr (W/m^2)	Ratio	Grad.m
37.3	47.7	0.782	35.154
35	45.2	0.774	37.892
35.2	45.3	0.778	31.296
35	45.2	0.774	37.892
35.2	45.3	0.778	31.296
37.1	48.5	0.766	35.562
36.6	46.6	0.786	35.58
35.1	46.1	0.762	39.25
35.8	46.3	0.774	31.761
35.1	46.3	0.758	44.508
37.1	48.5	0.766	35.562
37.7	48.6	0.775	39.823
36.5	47.7	0.766	33.903
35.4	46.2	0.768	34.894
36.3	46.2	0.787	36.817
34.9	45.1	0.774	31.197
	min	0.758	31.197
	max	0.787	44.508
	avr.	0.773	35.7742

camera A		gamma 1	
case 2	(App 5.6)		
Target 14			
MinBr (W/m^2)	MaxBr (W/m^2)	Ratio	Grad.m
82.2	99.9	0.823	61.081
82.2	100.5	0.819	71.383
81.1	99.6	0.814	66.079
81	98.9	0.819	72.012
80.3	98.7	0.813	62.164
80.8	98.5	0.82	61.628
80.3	96.9	0.829	49.074
81.6	98.1	0.832	63.053
81.5	98.5	0.827	64.684
81.2	98.9	0.821	47.216
82.2	100.1	0.821	50.476
84	100.3	0.838	51.786
81.8	99.4	0.823	65.72
81.3	99	0.822	71.606
81	98.4	0.824	62.728
80.9	97.9	0.826	51.288
	min	0.813	47.216
	max	0.838	72.012
	avr.	0.8232	60.7486

camera A		gamma 0.45	
case 2	(App 5.6)		
Target 14			
MinBr (W/m^2)	MaxBr (W/m^2)	Ratio	Grad.m
86.6	104.2	0.831	53.327
87.2	105.1	0.83	63.768
83.5	103.5	0.807	68.238
83.5	99.6	0.839	57.003
80.3	97.3	0.825	62.05
79.3	98.5	0.805	62.704
79.3	95.6	0.83	57.845
79	95.6	0.827	64.232
79.5	96.1	0.827	61.447
79.2	96.8	0.818	68.264
82.6	98.2	0.842	51.522
83.7	100.8	0.83	54.128
87.5	104.9	0.834	56.357
87.5	106.6	0.821	55.163
85.4	102.4	0.834	68.378
84	99.2	0.847	54.274
	min	0.805	51.522
	max	0.847	68.378
	avr.	0.8279	59.9188

camera B gamma 1
case 1 (App 8)
Target 1

MinBr [W/m^2]	MaxBr [W/m^2]	Ratio	Grad.m
8	57.7	0.138	172.847
7.3	55.2	0.132	162.992
8.1	57.8	0.141	172.35
6.9	56.3	0.123	173.833
7.6	56.5	0.135	145.829
7.1	55.3	0.128	164.88
7.1	56.9	0.124	157.763
9	58.4	0.154	167.375
8.6	58.5	0.147	176.169
9.4	58.7	0.161	165.066
8.7	58.4	0.149	146.536
8.6	56.3	0.152	180.115
8	56.7	0.142	193.215
7.6	55.3	0.137	181.28
8	52.9	0.152	153.942
7.9	54.8	0.145	146.402
	Min	0.123	145.829
	Max	0.161	193.215
	Avr.	0.1413	166.287

camera B gamma 0.45
case 1 (App 8)
Target 1

MinBr [W/m^2]	MaxBr [W/m^2]	Ratio	Grad.m
9.6	63.3	0.152	183.553
9	62.6	0.143	170.027
7.5	62.8	0.12	188.645
7.8	62.7	0.124	174.955
7.7	61.3	0.125	155.534
7.2	60.3	0.12	177.535
12.3	62.9	0.196	164.29
11	63.2	0.174	178.578
11.4	63.1	0.181	175.142
8.6	62.6	0.138	156.457
9.7	63.6	0.153	177.115
8.9	61.3	0.145	192.334
8.3	62.3	0.133	215.075
7.5	60.5	0.124	211.906
8.3	57.8	0.144	165.331
8.3	60.3	0.138	155.535
	Min	0.12	155.534
	Max	0.196	215.075
	Avr.	0.1444	177.626

camera B gamma 1
case 2 (App 5.6)
Target 1

MinBr [W/m^2]	MaxBr [W/m^2]	Ratio	Grad.m
15.6	96.8	0.161	304.433
14.4	96.8	0.149	257.944
15.9	96.8	0.165	301.629
13.7	94.6	0.145	275.082
14	92.5	0.152	266.764
13.8	94.6	0.146	270.162
12.9	93.6	0.137	286.17
13.3	95.5	0.139	287.081
13.3	96.8	0.137	290.898
16.4	96.8	0.169	291.993
15.7	96.8	0.162	300.104
15.9	96.8	0.164	254.126
16.1	95.8	0.168	277.06
14.4	95.7	0.151	315.506
14	96.8	0.144	306.061
14.8	95.5	0.155	274.431
	Min	0.137	254.126
	Max	0.169	315.506
	Avr.	0.1528	284.965

camera B gamma 0.45
case 2 (App 5.6)
Target 1

MinBr [W/m^2]	MaxBr [W/m^2]	Ratio	Grad.m
17.6	106.9	0.165	267.442
17.1	103.3	0.165	254.877
14.9	105.3	0.142	299.919
14.8	101.9	0.145	289.866
14.8	103.1	0.143	287.226
13.4	98.4	0.136	282.925
18.9	101	0.187	295.385
17.9	104.5	0.171	310.164
16.7	106.1	0.158	307.271
19.9	106.1	0.188	269.258
17.5	98.4	0.178	300.751
15.7	101.9	0.154	327.185
15.4	104.9	0.147	342.605
17.1	101.7	0.168	276.276
17.1	103.4	0.165	246.295
15.2	102.6	0.148	309.164
	Min	0.136	246.295
	Max	0.188	342.605
	Avr.	0.16	290.413

camera B gamma 1
case 1 (App 8)
Target 2

MinBr [W/m^2]	MaxBr [W/m^2]	Ratio	Grad.m
10.3	61.4	0.168	157.276
11.5	61.2	0.188	164.536
8.9	60	0.148	170.9
8.8	58.1	0.151	179.584
8.2	57.3	0.143	173.63
8.9	58.9	0.152	156.187
8.9	57.9	0.155	162.65
10.2	60.4	0.169	176.692
10.9	60.8	0.18	171.805
10.9	61.4	0.177	177.326
9.3	60.6	0.154	180.717
9.3	59.3	0.157	180.288
9.4	59	0.158	172.412
8.8	56.3	0.156	141.349
10.9	61.4	0.177	177.326
9.3	60.6	0.154	180.717
	Min	0.143	141.349
	Max	0.188	180.717
	Avr.	0.1617	170.212

camera B gamma 0.45
case 1 (App 8)
Target 2

MinBr [W/m^2]	MaxBr [W/m^2]	Ratio	Grad.m
11.5	63.4	0.181	163.541
12.3	64.1	0.192	168.774
11.6	63.2	0.184	166.78
9.9	63.8	0.155	200.651
10	63.4	0.157	194.874
9.3	63.8	0.146	165.168
9.3	62.1	0.149	172.278
10.2	64.2	0.158	162.232
12.2	64.1	0.19	181.398
11.5	63.9	0.18	182.844
11.3	63.3	0.179	196.907
12.2	64.1	0.19	170.051
11.8	64.4	0.184	177.907
9.3	64	0.145	181.558
9.2	64.5	0.143	181.873
8.8	63.3	0.14	184.376
	Min	0.14	162.232
	Max	0.192	200.651
	Avr.	0.1671	179.452

camera B gamma 1
case 2 (App 5.6)
Target 2

MinBr [W/m^2]	MaxBr [W/m^2]	Ratio	Grad.m
19.1	96.8	0.197	281.232
17.4	96.8	0.179	275.963
16.1	93.8	0.171	286.63
16.4	92.8	0.176	265.992
16.6	95.7	0.173	274.499
16	94.4	0.169	280.488
16	96.6	0.166	291.661
16.2	96.8	0.167	268.752
16.3	96.6	0.169	287.367
18	96.8	0.186	289.645
16.7	96.8	0.172	267.79
17	96.8	0.175	285.917
17.7	96.8	0.183	265.545
16.5	96.8	0.17	269.921
16.4	96.8	0.17	254.925
16.6	96.8	0.172	276.5
	Min	0.166	254.925
	Max	0.197	291.661
	Avr.	0.1747	275.178

camera B gamma 0.45
case 2 (App 5.6)
Target 2

MinBr [W/m^2]	MaxBr [W/m^2]	Ratio	Grad.m
19.5	102.9	0.19	242.786
20.1	104.6	0.192	264.31
20.1	105.6	0.19	272.877
18.9	108.6	0.174	298.502
18.6	103.5	0.18	309.843
17.6	105.1	0.167	309.051
18.7	106.9	0.175	279.441
19.4	107.2	0.181	251.11
18.8	106.1	0.177	300.261
21.5	105.6	0.204	303.839
19.9	106.3	0.188	273.805
18.3	107.4	0.171	294.479
17.6	100.8	0.175	274.708
18	105.9	0.17	271.334
17.8	98.9	0.18	251.989
21.3	105.6	0.202	292.172
	Min	0.167	242.786
	Max	0.204	309.843
	Avr.	0.1823	280.657

camera B	(App 8)	gamma 1	
case 1			
Target 3			
MinBr (W/m^2)	MaxBr (W/m^2)	Ratio	Grad.m
9.9	58.2	0.169	153.038
9.9	58.5	0.169	162.13
9.8	55.9	0.174	155.836
10.1	57.9	0.175	159.544
9.9	57.4	0.173	157.872
10.2	58.8	0.174	156.108
13	62.8	0.208	165.432
10.8	62	0.174	145.723
10.4	62.9	0.165	184.329
12.6	61.6	0.204	166.961
10.8	61.8	0.175	183.445
11	60.4	0.182	185.235
10.5	58	0.181	158.828
13.9	62.2	0.223	156.02
10.7	62.7	0.17	186.593
10.5	61.6	0.171	176.913
	Min	0.165	145.723
	Max	0.223	186.593
	Avr.	0.1804	165.875

camera B	(App 8)	gamma 0.45	
case 1			
Target 3			
MinBr (W/m^2)	MaxBr (W/m^2)	Ratio	Grad.m
11.7	66.4	0.176	225.975
11.1	65.6	0.169	213.54
11.3	65.6	0.172	196.673
12	64.2	0.187	156.029
11.7	63.3	0.184	172.646
13	66	0.197	191.833
14.1	64.7	0.218	177.326
13.1	66.6	0.197	174.748
13	66.5	0.195	170.965
11.1	64.6	0.172	185.569
11.1	63.3	0.176	181.217
12.2	61.4	0.198	126.279
10.5	58.1	0.181	149.487
10.3	60.8	0.17	159.487
14.6	65.1	0.225	162.717
13.6	65.6	0.208	167.597
	Min	0.169	126.279
	Max	0.225	225.975
	Avr.	0.1891	175.756

camera B	(App 5.6)	gamma 1	
case 2			
Target 3			
MinBr (W/m^2)	MaxBr (W/m^2)	Ratio	Grad.m
23.1	96.8	0.238	264.952
19.6	96.8	0.202	281.031
18.2	95	0.192	268.645
20.2	96.8	0.209	195.52
18.3	93.7	0.195	256.148
19.1	95	0.201	253.4
18.2	92.6	0.196	246.559
21.5	96.8	0.222	267.081
20.2	96.8	0.208	271.18
18	96.8	0.186	293.492
20.1	96.8	0.208	280.194
22.3	96.8	0.23	268.442
20.3	96.8	0.21	274.497
18.5	96.8	0.191	299.573
18.3	96.8	0.189	277.853
18.5	96.8	0.191	287.797
	Min	0.186	195.52
	Max	0.238	299.573
	Avr.	0.2043	267.898

camera B	(App 5.6)	gamma 0.45	
case 2			
Target 3			
MinBr (W/m^2)	MaxBr (W/m^2)	Ratio	Grad.m
22.5	105.9	0.212	290.181
20.2	108.3	0.187	303.938
20.2	100.7	0.2	278.421
20.7	102	0.202	285.992
20.2	102	0.198	280.809
20.5	95.6	0.214	233.209
23.3	107.2	0.217	292.393
20.6	106.4	0.193	324.957
19.9	104.8	0.19	314.354
20.1	105.2	0.191	298.924
20.7	103.2	0.2	262.051
20.3	104.8	0.194	280.735
22	107.2	0.205	317.706
22.6	110.9	0.203	313.184
22.7	109.5	0.207	310.795
24.5	110.2	0.222	312.74
	Min	0.187	233.209
	Max	0.222	324.957
	Avr.	0.2022	293.649

camera B	(App 8)	gamma 1	
case 1			
Target 4			
MinBr (W/m^2)	MaxBr (W/m^2)	Ratio	Grad.m
12.1	61.7	0.196	170.113
13.6	63	0.216	168.159
13	62.9	0.207	167.213
12.9	60	0.215	148.328
12.6	59.9	0.211	147.497
12	60.6	0.198	148.685
11.9	61.6	0.192	160.684
11.6	59.9	0.193	157.421
12.5	60.9	0.206	174.888
11.4	61.9	0.183	168.289
11.7	61.3	0.19	157.423
11.7	60.3	0.194	163.633
11.4	58.6	0.194	166.9
11.9	59.4	0.199	158.717
12.1	59.8	0.203	160.73
12.6	61.2	0.206	161.956
	Min	0.183	147.497
	Max	0.216	174.888
	Avr.	0.2002	161.29

camera B	(App 8)	gamma 0.45	
case 1			
Target 4			
MinBr (W/m^2)	MaxBr (W/m^2)	Ratio	Grad.m
16	67.1	0.239	175.431
15.3	66.8	0.229	178.12
15.4	67.5	0.228	172.785
15	66	0.227	167.877
14.2	62.8	0.226	155.401
14.1	64.1	0.219	152.099
13.2	62.6	0.211	163.439
13.2	63.7	0.208	180.878
13.4	65.9	0.203	165.817
13.1	65.3	0.2	171.366
14.1	65.4	0.215	168.223
16.3	66.3	0.246	164.961
14.5	66.3	0.22	174.791
15.1	65.7	0.23	171.403
15.3	66.6	0.229	158.666
14.1	66	0.213	166.876
	Min	0.2	152.099
	Max	0.246	180.878
	Avr.	0.2214	168.008

camera B	(App 5.6)	gamma 1	
case 2			
Target 4			
MinBr (W/m^2)	MaxBr (W/m^2)	Ratio	Grad.m
19.8	94.5	0.209	244.128
20.4	93.4	0.219	243.218
20.5	94.6	0.217	243.974
21.1	94.7	0.223	222.836
20.4	93.8	0.217	229.276
20	94.4	0.211	232.378
19.1	94.3	0.203	241.473
19.4	92.9	0.208	241.649
18.5	91.9	0.202	243.166
18.3	92.8	0.197	243.862
18.6	93.7	0.199	241.741
18.6	93.6	0.199	253.616
19.8	93.9	0.21	254.78
19.1	92.8	0.206	250.449
19.5	92.4	0.21	225.944
20.4	91.5	0.222	229.148
	Min	0.197	222.836
	Max	0.223	254.78
	Avr.	0.2095	240.102

camera B	(App 5.6)	gamma 0.45	
case 2			
Target 4			
MinBr (W/m^2)	MaxBr (W/m^2)	Ratio	Grad.m
28.2	118.5	0.238	298.069
27.7	119	0.233	304.309
26.2	114.8	0.229	296.629
26.8	116.9	0.229	265.614
25.4	115.5	0.22	275.135
24.7	113.6	0.217	303.778
24.3	113.5	0.214	311.108
23.7	114.6	0.207	322.667
23.9	117.9	0.203	307.05
24.9	117.2	0.212	308.839
27.6	118.1	0.234	301.929
25.2	117.8	0.214	317.522
26.5	118.1	0.224	320.077
26.3	117.4	0.224	278.37
25.1	116	0.217	273.587
24.9	115.3	0.216	311.863
	Min	0.203	265.614
	Max	0.238	322.667
	Avr.	0.2207	299.784

camera B gamma 1
case 1 (App 8)
Target 5

MinBr (W/m^2)	MaxBr (W/m^2)	Ratio	Grad.m
15.4	61.7	0.249	161.93
15.5	62	0.25	157.777
15.1	61.4	0.246	156.815
16.6	63.4	0.262	145.243
17.2	63	0.273	141.017
17.7	62.7	0.282	155.157
16.4	62.2	0.264	167.238
16	61.4	0.261	145.539
15.3	62	0.246	149.845
15.9	61	0.261	153.17
15.5	61.4	0.253	156.676
16.5	61.7	0.268	147.544
16.8	63.3	0.266	141.69
17.1	63	0.271	137.349
17.1	63.1	0.271	167.238
17.2	62.3	0.276	149.203
	Min	0.246	137.349
	Max	0.282	167.238
	Avr.	0.2624	152.214

camera B gamma 0.45
case 1 (App 8)
Target 5

MinBr (W/m^2)	MaxBr (W/m^2)	Ratio	Grad.m
19	65.2	0.292	155.611
18.4	65.1	0.282	155.492
19.5	65.7	0.297	164.971
19.6	67.4	0.29	147.999
18.4	67	0.274	149.582
18.6	65.6	0.284	158.488
17.3	65.4	0.265	161.575
17.3	65.2	0.266	159.501
17.5	66.2	0.264	158.422
17.6	64.3	0.274	159.449
17.6	64.5	0.273	171.362
17.2	64.9	0.266	162.146
19.2	68.2	0.281	157.288
19.4	69.4	0.28	157.805
18.9	68	0.278	176.402
18.6	67.3	0.276	162.26
	Min	0.264	147.999
	Max	0.297	176.402
	Avr.	0.2776	159.897

camera B gamma 1
case 2 (App 5.6)
Target 5

MinBr (W/m^2)	MaxBr (W/m^2)	Ratio	Grad.m
23.4	92.1	0.254	236.5
23.9	90.6	0.264	220.13
25.6	92.3	0.277	229.082
25.1	93.3	0.269	212.925
25.6	92.3	0.277	198.274
26.9	90.9	0.296	216.664
25.4	91.5	0.277	237.014
27.7	92.9	0.298	213.039
24.6	92.8	0.266	216.222
24.4	94.3	0.258	226.506
24.5	92.2	0.266	233.242
23.8	89.6	0.265	231.01
25.2	91.1	0.277	211.477
25.5	90.7	0.281	190.715
25.6	89	0.288	184.252
25.2	89.2	0.283	215.402
	Min	0.254	184.252
	Max	0.298	237.014
	Avr.	0.2748	217.028

camera B gamma 0.45
case 2 (App 5.6)
Target 5

MinBr (W/m^2)	MaxBr (W/m^2)	Ratio	Grad.m
28.7	113.7	0.253	290.358
29.3	115	0.255	280.796
29.9	115.6	0.259	284.36
32.4	121.1	0.268	247.299
32.9	121.3	0.271	245.076
33.7	121.1	0.278	284.043
32.3	118.6	0.272	283.114
30.7	116.2	0.265	273.69
29.3	116.9	0.251	270.15
30	115.3	0.26	284.293
29.2	117.6	0.249	287.434
31.1	118.3	0.263	280.842
31	122.9	0.252	239.982
31.3	124.2	0.252	291.118
32	121.5	0.264	285.125
30.7	121.5	0.252	282.734
	Min	0.249	239.982
	Max	0.278	291.118
	Avr.	0.2603	275.65

camera B gamma 1
case 1 (App 8)
Target 6

MinBr (W/m^2)	MaxBr (W/m^2)	Ratio	Grad.m
20.3	61.5	0.329	123.343
20	61.3	0.326	129.239
20.2	61.6	0.327	125.225
19.6	60.9	0.322	147.016
17.9	59.7	0.3	137.579
18.7	58.3	0.321	119.096
18.9	58.9	0.321	130.806
19	59.6	0.318	133.537
20.1	60.3	0.333	137.272
20.4	61.6	0.331	137.022
18.9	61.4	0.307	138.342
18.5	61.3	0.302	128.509
18.9	59.8	0.316	135.97
18.7	58.9	0.318	141.444
18.4	59.7	0.308	146.274
17.9	58.1	0.309	131.577
	Min	0.3	119.096
	Max	0.333	147.016
	Avr.	0.318	133.891

camera B gamma 0.45
case 1 (App 8)
Target 6

MinBr (W/m^2)	MaxBr (W/m^2)	Ratio	Grad.m
21	63.3	0.332	146.096
21.4	64	0.334	153.636
22.2	64.7	0.343	139.786
22.6	66.3	0.341	137.669
21.5	64.8	0.331	136.682
21.1	65.3	0.323	155.248
20.4	63.9	0.32	147.72
20.8	62.2	0.335	144.743
20.6	62.3	0.331	143.736
21.3	65.2	0.326	135.543
20.9	64.6	0.324	134.143
20.3	62.8	0.324	147.33
20	60.7	0.329	145.364
19.7	61.6	0.32	147.707
19.9	61.3	0.325	139.461
20	61.6	0.325	142.814
	Min	0.32	134.143
	Max	0.343	155.248
	Avr.	0.3269	143.606

camera B gamma 1
case 2 (App 5.6)
Target 6

MinBr (W/m^2)	MaxBr (W/m^2)	Ratio	Grad.m
28.1	89.6	0.314	197.486
28.4	91.9	0.309	212.051
30.2	92.1	0.328	206.516
30.5	94	0.324	190.429
30	94.5	0.317	194.95
31.3	94.5	0.331	203.604
31.5	93.8	0.336	197.216
32	93.8	0.341	206.063
29.3	93.1	0.315	209.911
28.4	91.6	0.31	206.146
30.3	91.4	0.332	200.985
29.4	93.7	0.314	194.486
30.7	93.7	0.328	220.119
31.9	94.5	0.337	194.523
32	95.5	0.335	187.062
32.9	94.6	0.348	203.772
	Min	0.309	187.062
	Max	0.348	220.119
	Avr.	0.3262	201.583

camera B gamma 0.45
case 2 (App 5.6)
Target 6

MinBr (W/m^2)	MaxBr (W/m^2)	Ratio	Grad.m
33	108.6	0.304	239.175
33.8	112.2	0.301	254.657
40.9	116.9	0.35	145.234
36.5	115.5	0.316	216.779
40.7	117.1	0.348	240.385
41.6	115.5	0.361	228.028
37	114.6	0.323	242.835
34.4	111	0.309	236.859
34.7	111.2	0.312	235.328
35.4	110.4	0.321	226.076
34.2	111.8	0.306	237.607
37.3	116	0.322	260.202
39.6	116.9	0.339	218.965
41.5	117.2	0.354	205.312
40.7	118.3	0.344	245.488
37.4	115.5	0.324	237.908
	Min	0.301	145.234
	Max	0.361	260.202
	Avr.	0.3271	229.427

camera B		gamma 1	
case 1	(App 8)		
Target 7			
MinBr (W/m^2)	MaxBr (W/m^2)	Ratio	Grad.m
23.1	63.2	0.366	126.296
22.9	63.4	0.36	135.994
22.6	62.1	0.364	127.859
20.5	63.6	0.322	161.594
19.4	62.4	0.311	148.384
19.7	63.1	0.312	145.076
18.7	61.1	0.306	126.727
18.5	59.2	0.312	140.202
19.4	60.8	0.318	140.954
19	61.4	0.309	142.087
19.4	62.2	0.311	156.882
20.6	62.4	0.33	155.439
21.7	62.5	0.347	124.322
22.3	62.4	0.357	122.595
21	61.9	0.339	142.741
20.6	63	0.328	146.609
	Min	0.306	122.595
	Max	0.366	161.594
	Avr.	0.3308	140.235

camera B		gamma 0.45	
case 1	(App 8)		
Target 7			
MinBr (W/m^2)	MaxBr (W/m^2)	Ratio	Grad.m
20.8	62.8	0.331	150.054
23.7	63.9	0.37	122.736
21.2	62.4	0.339	175.041
20.4	59.3	0.344	139.717
20.5	61.5	0.334	155.823
18.8	59.1	0.318	142.83
19.5	58.1	0.336	130.156
19.8	60.7	0.326	145.511
20.1	61.5	0.327	143.976
20.7	62.5	0.332	148.064
21.2	62.7	0.339	153.383
25.2	63.8	0.396	115.094
23.3	63.5	0.366	121.487
22.4	61.3	0.366	131.4
21.4	61.8	0.347	155.215
21.3	60.9	0.35	159.789
	Min	0.318	115.094
	Max	0.396	175.041
	Avr.	0.3451	143.142

camera B		gamma 1	
case 2	(App 5.6)		
Target 7			
MinBr (W/m^2)	MaxBr (W/m^2)	Ratio	Grad.m
25.6	81.8	0.313	214.634
25.4	82	0.31	212.431
26	83.3	0.312	207.138
31.2	84	0.372	168.365
30.7	83.6	0.368	177.133
26.4	83.1	0.318	214.16
25.9	81.7	0.317	206.321
25.1	82.3	0.305	218.544
24.4	81.1	0.3	182.563
24.4	76.2	0.32	164.963
25.2	81.8	0.308	202.885
26.5	83.2	0.319	206.275
26	83.6	0.312	177.33
29.1	83.6	0.349	156.094
30.9	83.7	0.37	172.657
27.9	83.2	0.335	175.641
	Min	0.3	156.094
	Max	0.372	218.544
	Avr.	0.3268	191.071

camera B		gamma 0.45	
case 2	(App 5.6)		
Target 7			
MinBr (W/m^2)	MaxBr (W/m^2)	Ratio	Grad.m
29.3	84.3	0.348	174.235
28.1	83.9	0.335	161.985
26.3	83.3	0.316	228.267
27.6	83.9	0.329	196.933
26.3	83.3	0.316	228.267
25.6	83	0.309	183.057
25.5	80.6	0.317	192.197
25.8	81.6	0.316	190.538
27.8	82.2	0.338	199.147
26.6	82.6	0.322	207.416
27.8	83.5	0.333	209.954
29.7	84	0.353	159.855
28.9	83.7	0.346	164.95
28.3	83	0.341	190.37
26.8	80.4	0.333	189.567
27.1	81.1	0.334	208.131
	Min	0.309	159.855
	Max	0.353	228.267
	Avr.	0.3304	192.804

camera B		gamma 1	
case 1	(App 8)		
Target 8			
MinBr (W/m^2)	MaxBr (W/m^2)	Ratio	
23.5	58.7	0.401	118.363
23.2	58.7	0.396	118.755
22.6	58.2	0.389	116.766
23.3	61.7	0.377	142.565
23.7	62	0.382	145.803
24.5	62.4	0.393	135.649
27.8	61.4	0.453	115.07
28.7	61.1	0.47	108.47
24.1	61.8	0.39	147.898
23.6	61.9	0.381	147.039
23	61.3	0.374	149.067
24.1	61.1	0.394	131.501
23.2	60.5	0.384	129.444
22.8	60.3	0.378	134.326
22.4	58.5	0.382	123.694
22.2	57.8	0.384	119.574
	Min	0.374	108.47
	Max	0.47	149.067
	Avr.	0.3955	130.124

camera B		gamma 0.45	
case 1	(App 8)		
Target 8			
MinBr (W/m^2)	MaxBr (W/m^2)	Ratio	Grad.m
24.4	58.3	0.419	117.707
24.3	58.5	0.415	119.185
23.8	57	0.418	109.055
23.7	60.3	0.394	152.661
23.4	62.5	0.374	151.932
24.7	60.3	0.409	153.597
26.6	62.6	0.425	114.363
27	61.1	0.442	108.076
24.9	62.2	0.401	148.673
24.4	62.6	0.389	148.479
24.1	62	0.389	139.21
23.6	60.1	0.394	149.877
27.3	61.7	0.443	107.011
27.1	61	0.445	107.012
26.9	61.3	0.438	102.435
24.2	59.1	0.409	131.058
	Min	0.374	102.435
	Max	0.445	153.597
	Avr.	0.4128	128.771

camera B		gamma 1	
case 2	(App 5.6)		
Target 8			
MinBr (W/m^2)	MaxBr (W/m^2)	Ratio	Grad.m
31	80.9	0.383	141.746
31.5	80.4	0.391	148.275
30.9	81	0.381	175.783
31.1	80.9	0.384	176.154
32.1	81.8	0.393	169.947
38.9	82.1	0.474	135.145
39.6	81.6	0.485	130.647
32.2	81.9	0.393	198.659
31.6	82.6	0.382	197.809
30.9	81.4	0.38	204.374
34.6	81.2	0.425	131.063
33.1	81.1	0.408	133.937
30.8	81.9	0.376	190.024
30.5	80.7	0.378	190.052
28.6	75.1	0.382	145.784
28.9	74.9	0.386	144.963
	Min	0.376	130.647
	Max	0.485	204.374
	Avr.	0.4001	163.398

camera B		gamma 0.45	
case 2	(App 5.6)		
Target 8			
MinBr (W/m^2)	MaxBr (W/m^2)	Ratio	Grad.m
29.8	77.1	0.386	159.39
29	77.4	0.374	159
29.6	79.3	0.373	184.1
29.6	78.9	0.376	181.814
29.8	79.9	0.373	192.181
32.8	82.5	0.397	149.082
33.8	82.3	0.41	140.586
32.2	83.2	0.387	167.905
31.1	82.3	0.377	175.214
30.2	82.6	0.365	183.591
34.8	82.6	0.421	138.308
33.7	82.9	0.407	132.438
33.1	83.2	0.398	139.691
31.3	80.8	0.388	174.291
30.6	80.4	0.38	176.572
30.4	78.2	0.389	157.47
	Min	0.365	132.438
	Max	0.421	192.181
	Avr.	0.3876	163.227

camera B		gamma 1	
case 1	(App 8)		
Target 9			
MinBr [W/m^2]	MaxBr [W/m^2]	Ratio	Grad.m
32.3	64.6	0.499	98.711
29.2	64.5	0.452	138.138
29.3	63.2	0.464	122.918
27.6	60.3	0.458	97.989
28.6	61.2	0.466	104.52
31	63.9	0.485	117.687
30.9	64	0.482	119.604
29.2	64	0.456	128.227
32.1	64.7	0.496	101.823
30.1	64.3	0.468	90.183
28.9	63.4	0.455	119.323
27.5	62.6	0.439	120.068
27.8	61.7	0.451	113.212
27.6	61.4	0.449	115.621
28.1	62.6	0.448	119.619
29.3	62.9	0.465	115.769
	Min	0.439	90.183
	Max	0.499	138.138
	Avr.	0.4646	113.962

camera B		gamma 0.45	
case 1	(App 8)		
Target 9			
MinBr [W/m^2]	MaxBr [W/m^2]	Ratio	Grad.m
30.3	67	0.452	112.784
28.5	64.4	0.443	62.015
28.6	65.7	0.436	146.212
28.5	64.1	0.445	155.414
28.5	63.7	0.447	136.028
27.2	58.1	0.469	107.919
27.6	60.7	0.456	110.823
28.5	62.6	0.456	121.228
29.4	63.2	0.466	134.606
27.7	65	0.427	125.185
30.3	67	0.452	113.275
30.6	64.7	0.473	128.343
28.5	63.9	0.446	131.149
27.3	63.9	0.427	120.168
27	63.2	0.428	133.445
27.1	60.3	0.45	105.97
	Min	0.427	62.015
	Max	0.473	155.414
	Avr.	0.4483	121.535

camera B		gamma 1	
case 2	(App 5.6)		
Target 9			
MinBr [W/m^2]	MaxBr [W/m^2]	Ratio	Grad.m
38.4	83.7	0.459	156.431
36.6	80.4	0.455	146.22
37.7	81.6	0.462	128.321
37.4	83.9	0.445	183.924
38.6	86.3	0.447	162.46
41.6	86.4	0.481	135.175
46.3	86.5	0.535	121.281
45.5	86.5	0.526	130.262
41.9	85.2	0.492	147.804
39.6	84.1	0.471	169.63
39.4	84.9	0.464	149.139
39	83.6	0.466	152.512
37	83.9	0.441	157.032
38.2	85	0.45	149.764
37.5	80.8	0.464	137.681
36.3	83	0.438	158.939
	Min	0.438	121.281
	Max	0.535	183.924
	Avr.	0.4685	149.161

camera B		gamma 0.45	
case 2	(App 5.6)		
Target 9			
MinBr [W/m^2]	MaxBr [W/m^2]	Ratio	Grad.m
44.3	88.9	0.498	124.358
45	88.2	0.511	138.212
41.3	87.2	0.474	190.252
40.2	86.5	0.466	177.546
39.6	86.7	0.457	178.305
37.9	81.8	0.463	131.801
38.5	81.2	0.474	133.103
40.7	84.7	0.48	131.998
40.1	85.5	0.469	141.382
42.2	85.3	0.495	155.401
45.5	88.5	0.514	134.964
41	83.4	0.491	140.608
39.5	85.3	0.463	151.503
38.5	84.7	0.454	165.382
37.1	84.3	0.441	145.233
37.9	84	0.451	137.184
	Min	0.441	124.358
	Max	0.514	190.252
	Avr.	0.4751	148.577

camera B		gamma 1	
case 1	(App 8)		
Target 10			
MinBr [W/m^2]	MaxBr [W/m^2]	Ratio	Grad.m
36.7	62.9	0.584	83.602
36.5	62.8	0.581	85.192
37.6	63.5	0.592	64.831
33.9	62.3	0.545	90.272
34	61.1	0.556	90.656
34.4	62.4	0.552	86.135
36.1	62.3	0.581	64.722
33.9	60	0.565	75.508
34.9	61.8	0.565	79.481
35.2	61.9	0.569	86.522
34.1	61.8	0.552	93.282
38.1	63.7	0.598	79.088
34.3	63.1	0.544	87.637
37.1	64.1	0.578	90.612
34.4	64.6	0.533	108.158
33.6	62.5	0.537	97.878
	Min	0.533	64.722
	Max	0.598	108.158
	Avr.	0.5645	85.2235

camera B		gamma 0.45	
case 1	(App 8)		
Target 10			
MinBr [W/m^2]	MaxBr [W/m^2]	Ratio	Grad.m
33	65.7	0.502	110.208
35.6	64.5	0.552	103.021
31.9	64.1	0.497	125.422
31.6	64.6	0.488	124.464
33	63	0.524	118.114
32.2	62.5	0.515	85.837
31.3	60.1	0.521	88.304
31.2	58.8	0.53	81.665
31.2	62	0.503	109.921
31.1	63.3	0.492	101.504
32.3	62.6	0.516	118.848
33.5	65.6	0.511	102.931
32.5	63.2	0.514	92.953
31	62.7	0.495	104.538
32.2	62	0.519	91.542
31.2	62.1	0.503	93.325
	Min	0.488	81.665
	Max	0.552	125.422
	Avr.	0.5114	103.287

camera B		gamma 1	
case 2	(App 5.6)		
Target 10			
MinBr [W/m^2]	MaxBr [W/m^2]	Ratio	Grad.m
46.4	83.3	0.557	115.924
47.8	83.5	0.573	122.034
45.4	81.7	0.556	126.169
45.1	81	0.557	120.92
45	79.6	0.565	107.442
45	80.3	0.561	109.758
45.5	82	0.555	103.275
46.1	81	0.569	106.943
44.9	81.3	0.552	117.22
47.8	83	0.576	113.853
45.6	82.3	0.554	121.705
48.3	84.9	0.569	121.389
46.4	84.7	0.548	118.465
45.7	85.4	0.534	142.591
45	85	0.53	134.047
45.7	83	0.55	129.998
	Min	0.53	103.275
	Max	0.576	142.591
	Avr.	0.5566	119.483

camera B		gamma 0.45	
case 2	(App 5.6)		
Target 10			
MinBr [W/m^2]	MaxBr [W/m^2]	Ratio	Grad.m
50.2	86.2	0.583	110.494
50.4	85.9	0.587	117.842
49	83.2	0.589	115.757
47.9	83.2	0.576	117.895
48	83	0.578	118.431
48	79.9	0.601	91.762
49	83	0.59	96.502
48.6	83	0.585	119.999
47.9	83.3	0.575	110.528
52.2	87.6	0.596	112.97
50.2	86.9	0.578	119.666
48.4	84.9	0.57	129.936
49.4	86	0.574	121.544
47.7	85	0.561	129.411
49.7	81.5	0.61	90.573
48.7	83.3	0.585	102.387
	Min	0.561	90.573
	Max	0.61	129.936
	Avr.	0.5836	112.856

APPENDIX B

TARGET PLASTIFYING OR LAMINATING (EFFECTS)

Other set of measurements in terms of brightness measurements was done to find the effects of laminating/plastifying of targets. Targets were covered with reflecting or nonreflecting (mate) tape. A comparation was made among the brightness measurements resulted in testing a plain target, target covered with reflecting tape and target covered with mate or nonreflecting tape. Conclusion of these measurements is that covering the surface of targets using either shiny or mate tape has an effect of slightly reducing the brightness of the images with an approx. 2-3%. The results of tests are annexed. One inconvenient of covering targets with reflectance tape is that incident lighting is uncontrollably reflected and this has a negative effect on recognition.

Data is presented on the following pages along with charts that graphically present the changes caused by the laminating done to the target's surface.

camera A gamma 1

case 1 (App 8)

	Target 1			
	MinBr (W/m²)	MaxBr (W/m²)	Ratio	Grad.m
	5.9	74.6	0.089	210.286
	7.2	76.8	0.093	227.282
	7.7	76.3	0.101	237.523
	6.5	75.5	0.087	259.644
	7	76.8	0.092	260.924
	7	76.2	0.092	255.612
	6.9	75.8	0.092	242.474
	7	74.8	0.094	224.42
	6.3	72.5	0.088	236.469
	7.9	74.1	0.107	162.734
	7.5	73.1	0.102	206.808
	7.7	74.8	0.103	204.883
	6	75.6	0.101	256.608
	6	76.7	0.091	259.48
	5.9	74.6	0.092	267.94
	5.8	74.7	0.099	271.284
	6.2	77.4	0.101	281.472
	6.4	76.2	0.084	278.921
Min			0.084	162.734
Max			0.107	281.472
Avr.			0.095	241.487

camera A gamma 1

case 1 (App 8)

	Target 1(tape 1)				Target 1(tape2)			
	MinBr (W/m²)	MaxBr (W/m²)	Ratio	Grad.m	MinBr (W/m²)	MaxBr (W/m²)	Ratio	Grad.m
	7.5	66.8	0.113	217.448	9.3	70	0.133	184.925
	6.8	64.1	0.107	192.481	9	70.1	0.128	183.051
	7.1	69.8	0.102	191.396	9.4	70.8	0.132	178.239
	7.1	69.8	0.102	217.448	9.4	70.8	0.132	208.871
	8.5	68.9	0.124	213.463	9.3	64.7	0.143	202.399
	7.5	66.8	0.113	213.463	8.5	66	0.129	203.193
	7.4	68	0.109	217.448	10.9	69.3	0.131	200.256
	8.5	68.9	0.124	192.481	10	69.7	0.122	201.159
	7.1	69.8	0.102	191.396	9.9	69.9	0.128	199.521
	8.5	68.9	0.124	224.819	9.3	64.7	0.143	171.502
	8.8	64.6	0.136	197.406	8.5	66	0.129	182.239
	6.8	64.1	0.107	192.481	10.9	69.3	0.131	127.44
	7.5	66.8	0.113	221.168	10	69.7	0.122	212.965
	7.4	68	0.109	206.847	9.9	69.9	0.128	216.272
	8.5	68.9	0.124	224.819	9.3	70	0.133	214.603
	8.2	69.1	0.119	228.122	9	70.1	0.128	220.767
	8.3	71.5	0.116	229.32	9.4	70.8	0.132	221.604
	7.5	66.8	0.113	233.268	9.4	70.8	0.132	221.604
Min			0.102	191.396			0.122	127.44
Max			0.136	233.268			0.143	221.604
Avr.			0.114	211.404			0.131	197.256

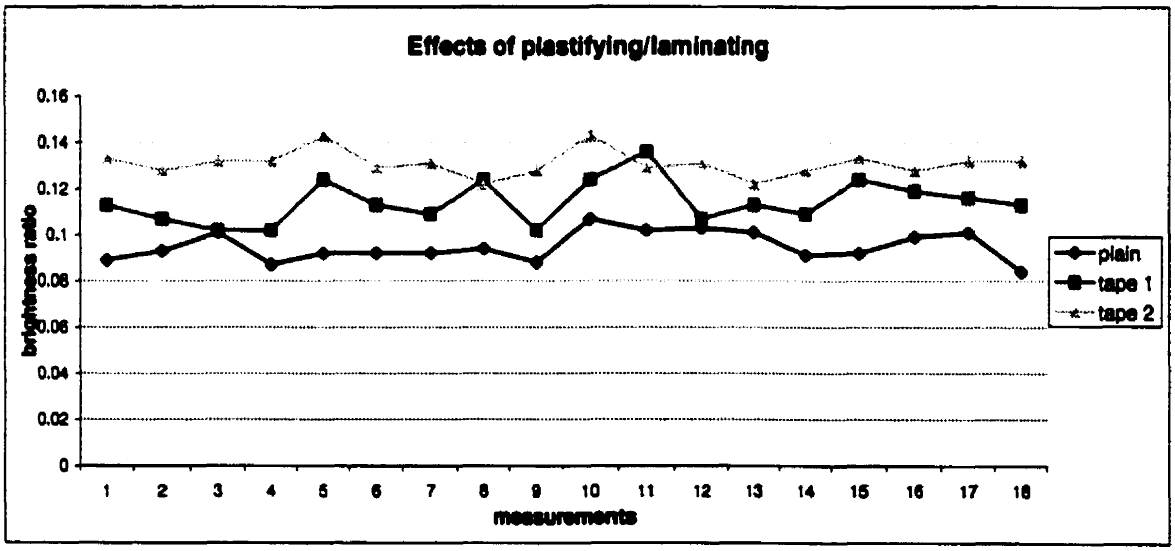

camera A gamma 1

case 1 (App 6)

	Target 6			
	MinBr [W/m^2]	MaxBr [W/m^2]	Ratio	Grad.m
	8.5	63.9	0.134	192.879
	8.1	63.6	0.127	176.499
	8.5	63.9	0.134	166.691
	9.7	65.6	0.148	194.131
	9.4	65.7	0.143	193.715
	9.7	65.6	0.147	196.576
	9.5	65.5	0.145	194.517
	9.5	64.8	0.147	195.006
	9.5	64.6	0.147	195.428
	8.5	63.9	0.134	117.425
	8.8	66.6	0.131	158.962
	8.5	63.9	0.134	147.532
	8.2	63.1	0.129	197.042
	8.5	63.9	0.134	203.119
	8.5	63.9	0.134	190.545
	8.5	63.9	0.134	180.227
	8.5	63.9	0.134	194.523
	8.8	66.6	0.131	196.202
Min			0.127	117.425
Max			0.148	203.119
Avr.			0.137	182.834

camera A gamma 1

case 1 (App 6)

	Target 6(tape 1)				Target 6(tape2)			
	MinBr [W/m^2]	MaxBr [W/m^2]	Ratio	Grad.m	MinBr [W/m^2]	MaxBr [W/m^2]	Ratio	Grad.m
	10.3	66.5	0.154	179.084	11	69	0.16	182.331
	10.4	66.1	0.157	179.782	11.2	67.6	0.166	172.008
	11.4	71.8	0.159	222.1	11.8	69.9	0.169	171.963
	10.2	66.4	0.153	201.489	11.2	70	0.16	210.164
	10.8	65.3	0.166	197.021	11.3	65.3	0.172	183.061
	10.3	66.5	0.154	206.808	10.9	70.6	0.154	210.523
	10.4	66.1	0.157	204.459	10.9	70.4	0.155	211.744
	10.4	65.1	0.159	202.353	10.9	70.9	0.154	216.23
	11.4	70.8	0.161	176.154	11.5	71.8	0.161	214.584
	11.4	71.8	0.159	222.1	11.8	69.9	0.169	171.963
	11.4	70.8	0.161	186.958	11.3	65.3	0.172	183.061
	10.7	63.8	0.168	184.143	11.8	69.9	0.169	171.963
	11.4	70.8	0.161	222.422	12.3	68.7	0.179	197.823
	12.1	71.6	0.169	226.9	11.9	69	0.172	200.266
	11.4	71.8	0.159	222.1	11.6	69	0.168	199.437
	11.4	70.8	0.161	229.996	11.1	69.4	0.16	195.757
	10.4	66.1	0.157	204.459	10.8	69.7	0.155	193.369
	10.2	66.4	0.153	234.286	10.8	69.7	0.155	193.369
Min			0.153	176.154			0.154	171.963
Max			0.169	234.286			0.179	216.230
Avr.			0.159	205.645			0.164	193.309

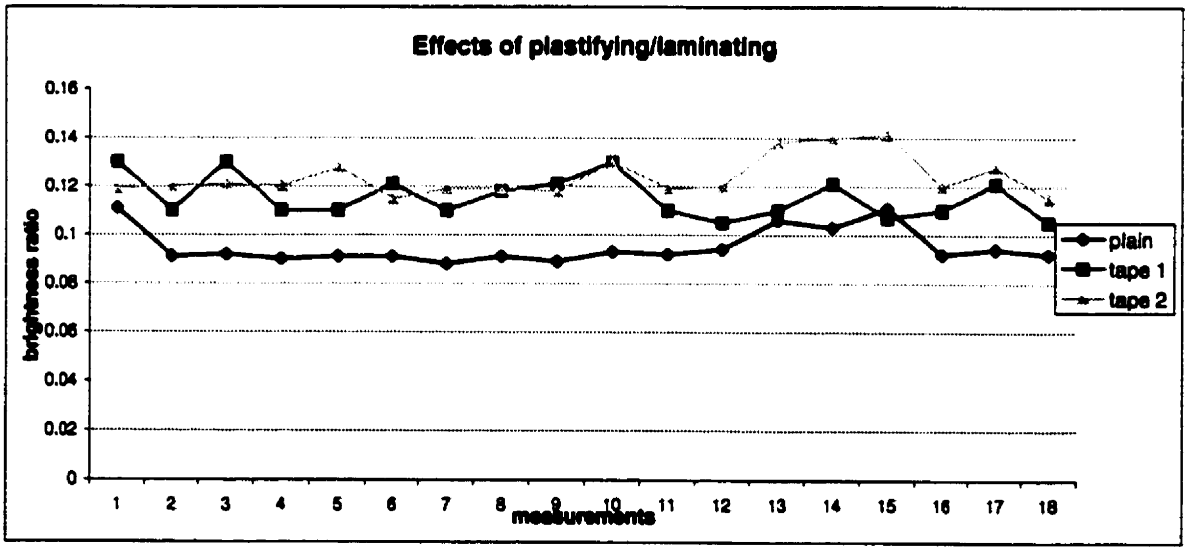

camera B gamma 1

case 1 (App 8)

	Target 1			
	MinBr [W/m²]	MaxBr [W/m²]	Ratio	Grad.m
	5.7	51.8	0.111	168.971
	4.8	52.8	0.091	148.91
	4.9	52.9	0.092	152.921
	4.8	53.6	0.09	164.585
	4.9	53.5	0.091	159.63
	4.9	53.5	0.091	159.63
	4.4	49.3	0.088	148.495
	4.5	49.5	0.091	148.495
	4.5	50.5	0.089	158.779
	4.7	50.1	0.093	160.509
	4.6	50.2	0.092	159.167
	4.8	50.9	0.094	161.413
	5.6	52.9	0.106	175.694
	5.3	51.8	0.103	173.429
	5.7	51.8	0.111	168.971
	4.9	52.9	0.092	166.396
	4.8	50.9	0.094	160.502
	4.9	52.9	0.092	152.921
Min			0.088	148.495
Max			0.111	175.694
Avr.			0.096	160.523

camera B gamma 1

case 1 (App 8)

	Target 1(tape 1)				Target 1(tape2)			
	MinBr [W/m²]	MaxBr [W/m²]	Ratio	Grad.m	MinBr [W/m²]	MaxBr [W/m²]	Ratio	Grad.m
	5.6	43	0.13	157.455	5.5	46.6	0.119	122.669
	5.3	47.8	0.11	157.455	5.6	46.6	0.12	119.936
	5.6	43	0.13	141.447	5.8	48.1	0.121	118.287
	5.3	47.8	0.11	141.447	5.6	46.6	0.12	119.936
	5.3	47.8	0.11	144.901	6.2	48.5	0.128	153.921
	5.8	48	0.121	157.455	5.6	48.6	0.116	156.518
	5.3	47.8	0.11	157.455	5.8	49	0.119	154.384
	5.6	47.4	0.118	154.735	5.9	49.7	0.119	156.044
	5.8	48	0.121	151.248	5.8	49	0.118	149.434
	5.6	43	0.13	120.959	5.9	45.7	0.13	125.724
	5.3	47.8	0.11	157.455	5.5	46.6	0.119	122.669
	4.5	42.8	0.105	128.619	5.6	46.6	0.12	119.936
	5.3	47.8	0.11	161.02	6.8	49.4	0.138	146.679
	5.8	48	0.121	165.476	7	50	0.14	149.802
	5.2	48.8	0.107	165.505	7.1	50.4	0.141	150.262
	5.3	47.8	0.11	157.455	5.6	46.6	0.12	119.936
	5.8	48	0.121	151.248	6.2	48.5	0.128	153.921
	4.5	42.8	0.105	168.107	5.6	48.6	0.115	156.518
Min			0.105	120.959			0.115	118.287
Max			0.13	168.107			0.141	156.518
Avr.			0.116	152.080			0.124	138.699

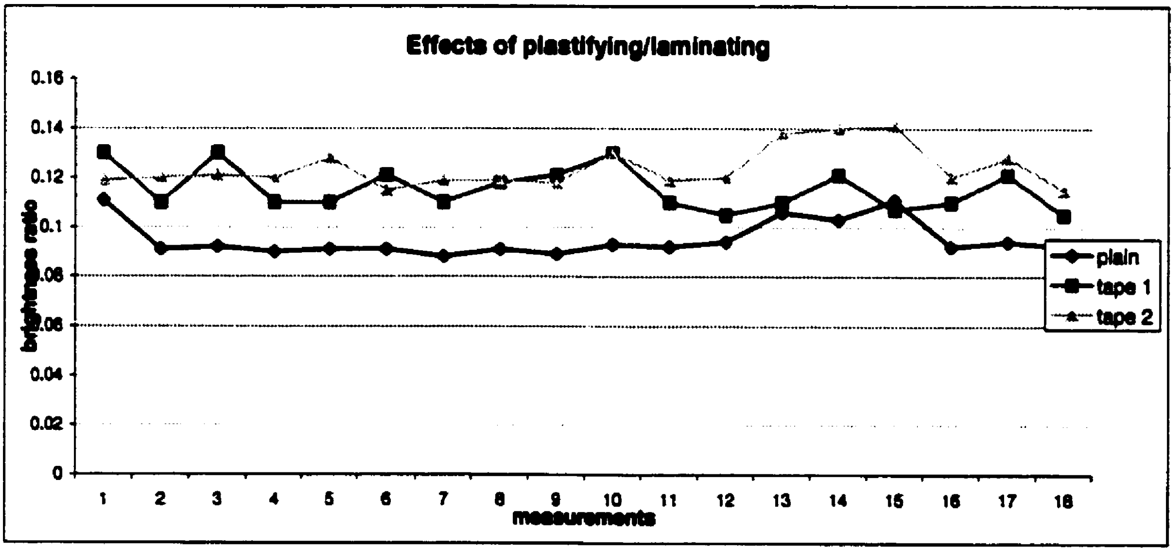

camera 8 gamma 1

case 1 (App 8)

	Target 5			
	MinBr (W/m²)	MaxBr (W/m²)	Ratio	Grad.m
	9.2	64.9	0.142	193.999
	8.9	64.5	0.137	192.632
	9.2	64.9	0.142	193.999
	9.1	65.2	0.139	193.046
	9.2	64.9	0.142	193.999
	9.2	64.9	0.142	193.999
	9.1	65.2	0.139	193.046
	9.2	64.9	0.142	193.999
	8.9	64.5	0.137	192.632
	10.5	58.8	0.178	164.066
	9.2	64.9	0.142	193.999
	8.9	64.5	0.137	192.632
	8.7	63	0.138	209.571
	8.7	63.1	0.138	210.5
	8.4	63.8	0.131	216.265
	8.4	64.3	0.131	212.283
	9.2	64.9	0.142	193.999
	8.9	64.5	0.137	192.632
Min			0.131	164.066
Max			0.178	216.265
Avr.			0.141	195.961

camera 8 gamma 1

case 1 (App 8)

	Target 5(tape 1)				Target 5(tape2)			
	MinBr (W/m²)	MaxBr (W/m²)	Ratio	Grad.m	MinBr (W/m²)	MaxBr (W/m²)	Ratio	Grad.m
	8.4	51.7	0.162	131.745	8.1	50	0.163	144.449
	7.2	49.5	0.146	135.123	8.6	49.9	0.172	131.849
	7.7	51.7	0.15	136.954	7.8	46.4	0.169	133.752
	7.6	50.8	0.15	143.116	8.4	49.2	0.17	133.364
	7.6	49.1	0.155	160.522	8.1	46.5	0.175	129.294
	8.4	51.7	0.162	131.745	7.7	46.9	0.164	133.752
	8.2	49.2	0.167	154.268	7.7	46.3	0.167	133.304
	7.2	48.7	0.148	158.756	7.8	46.4	0.169	133.752
	7	48.4	0.145	153.03	7.8	47.3	0.165	134.747
	7.3	48.2	0.152	151.648	9.1	48.2	0.186	138.689
	8.3	49.5	0.168	123.18	8.7	48.2	0.181	139.171
	8.4	51.7	0.162	131.745	8.4	49.2	0.17	133.364
	8.6	51.9	0.165	127.52	8.2	49.1	0.168	121.719
	7.6	50.8	0.15	143.118	9.1	48.2	0.188	138.689
	7.6	49.1	0.155	160.522	8.4	49.2	0.17	124.836
	7.9	52.4	0.15	157.521	9.1	48.2	0.188	138.689
	8.6	51.9	0.165	158.739	8.6	49.9	0.172	131.849
	8.6	51.9	0.165	159.237	8.6	49.9	0.172	131.849
Min			0.145	123.18			0.163	121.719
Max			0.168	160.522			0.188	144.449
Avr.			0.157	145.416			0.173	133.729

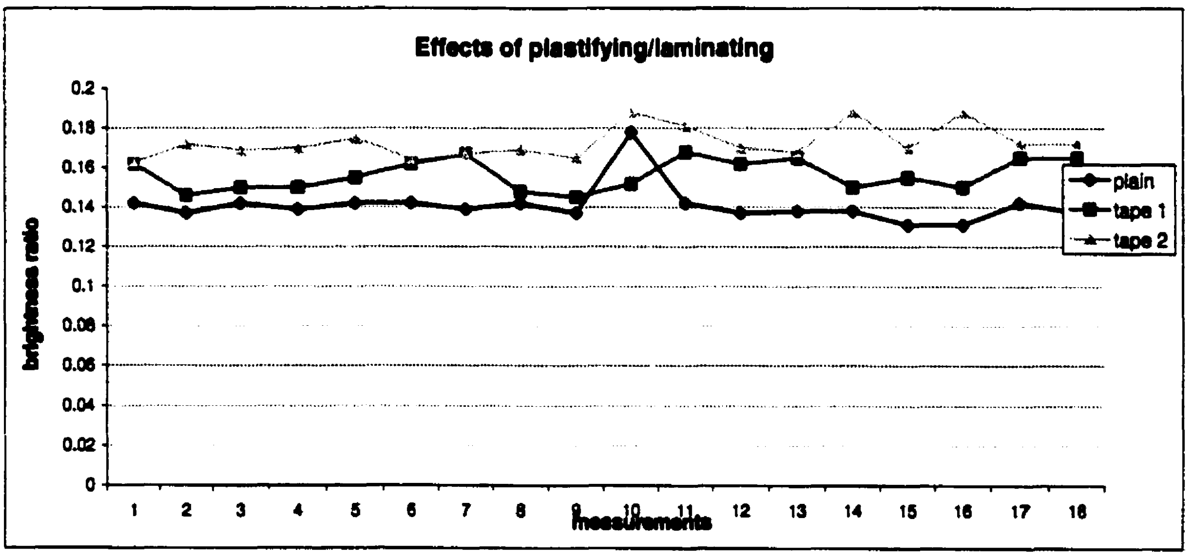

camera A gamma 1

case 1 (App 8)

Target 9				
	MinBr (W/m²)	MaxBr (W/m²)	Ratio	Grad.m
	14	69	0.203	194.11
	14.4	68.3	0.211	164.364
	14.6	68.7	0.212	174.077
	14.4	73.1	0.198	199.1
	14.6	68.7	0.212	174.077
	14.2	72.9	0.195	196.161
	14.4	73.1	0.198	199.1
	14.6	73.1	0.2	207.795
	14.6	73.1	0.2	207.795
	14.6	73.1	0.2	210.586
	14.8	72.2	0.205	207.666
	14.6	73.1	0.2	207.795
	14.6	73.1	0.2	207.795
	14.6	68.7	0.212	174.077
	13.8	64.5	0.213	176.116
	15	65.6	0.228	192.927
	14.3	67.3	0.213	205.193
	13.8	67	0.206	216.267
Min			0.195	174.077
Max			0.228	216.267
Avr.			0.206	196.500

camera A gamma 1

case 1 (App 8)

	Target 9(tape1)				Target 9(tape2)			
	MinBr (W/m²)	MaxBr (W/m²)	Ratio	Grad.m	MinBr (W/m²)	MaxBr (W/m²)	Ratio	Grad.m
	16.9	74.9	0.226	225.665	16.8	70.8	0.236	176.906
	16.5	73.7	0.224	181.045	16.1	68.2	0.237	172.827
	15.4	72.4	0.212	186.748	15.6	72.3	0.216	206.447
	15.8	76.3	0.207	225.298	14.7	72.7	0.202	212.965
	16.8	74.2	0.226	225.231	15.3	72.5	0.211	216.691
	16.9	75.6	0.223	225.279	15.5	70.7	0.22	209.704
	16.9	75.6	0.223	225.279	14.9	70.5	0.211	203.958
	16.9	74.9	0.226	225.665	14.8	69.2	0.214	207.287
	16.9	74.9	0.226	225.665	15.1	69.7	0.217	201.501
	16.9	74.9	0.226	225.665	15.9	67.8	0.235	184.721
	16.5	67	0.246	166.115	16	67.9	0.236	181.42
	16.9	74.9	0.226	225.665	17.7	66	0.269	159.569
	17.9	74.1	0.241	211.76	17.4	72	0.242	182.13
	17.7	74.3	0.238	197.394	16.9	71.6	0.235	186.82
	16.3	72.7	0.224	198.307	16	72.2	0.222	184.392
	17	72.7	0.234	198.735	16	70.7	0.226	186.139
	16.5	73	0.226	197.992	15.8	71	0.222	174.639
	15.4	73.4	0.21	212.092	18	72.3	0.249	190.89
Min			0.207	166.115			0.202	159.569
Max			0.246	225.665			0.269	216.691
Avr.			0.226	209.867			0.226	191.000

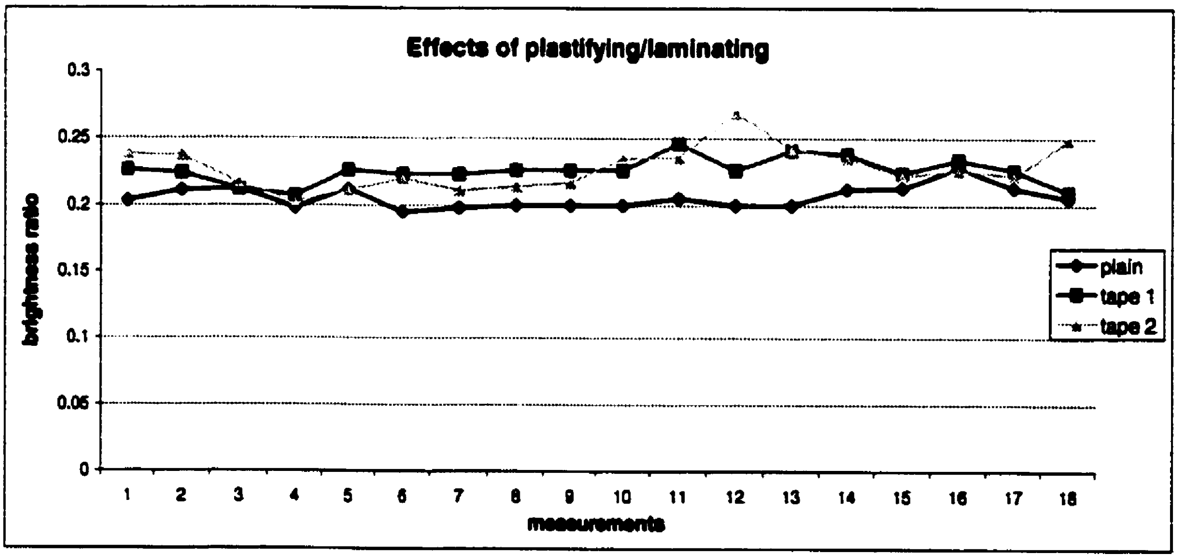

camera A **gamma 1**

case 1 **(App 8)**

	Temp. 13 - bar 1			
	MinBr [W/m²]	MaxBr [W/m²]	Ratio	Grad.m
	28.6	71.1	0.402	136.016
	25.9	69.9	0.371	171.189
	25.5	70.4	0.362	171.605
	25.5	70.4	0.362	171.605
	26.1	72.1	0.348	171.171
	25.3	70.8	0.358	166.029
	25.3	69.6	0.363	165.471
	23.3	70.1	0.332	168.841
	25.2	69.8	0.362	159.385
	25.9	69	0.375	158.069
	24.9	68.8	0.362	153.293
	27	72.1	0.375	122.678
	27.1	70	0.388	147.898
	26.3	68	0.386	151.925
	24.6	70.9	0.348	144.228
	24.5	70.6	0.348	135.175
	28.3	71.2	0.398	133.588
	28.2	70.3	0.401	136.776
Min			0.332	122.678
Max			0.402	171.605
Avr.			0.369	153.552

camera A **gamma 1**

case 1 **(App 8)**

	Temp. 13 - bar 1 (tape1)				Temp. 13 - bar 2 (tape 2)			
	MinBr [W/m²]	MaxBr [W/m²]	Ratio	Grad.m	MinBr [W/m²]	MaxBr [W/m²]	Ratio	Grad.m
	25.7	74.3	0.346	154.043	27.5	66.9	0.411	142.565
	33.4	75.1	0.444	130.739	30.8	69.3	0.445	124.499
	32.5	75.6	0.429	136.112	30.5	69.3	0.44	129.828
	31.9	74.5	0.428	142.102	27.8	68.3	0.407	147.42
	33.8	75.1	0.45	129.775	27.3	68.8	0.397	154.027
	33.8	75.6	0.447	166.958	27	67.5	0.401	149.473
	25.9	75.8	0.342	163.289	27.3	67.9	0.403	147.957
	28.7	72.8	0.395	178.73	27.5	66.9	0.411	142.565
	28.7	72.8	0.396	178.73	26.4	66.3	0.398	141.725
	25.2	74.8	0.337	189.698	27.1	60.7	0.447	111.387
	25.2	74.8	0.337	189.698	27.6	60.3	0.457	106.061
	26.7	71	0.376	152.413	26.8	63.8	0.421	111.459
	26.7	71	0.376	152.413	24.7	65.1	0.38	174.05
	26.5	70.5	0.377	156.024	25	65.8	0.38	178.559
	29.1	70.7	0.411	135.492	25	66.5	0.376	174.05
	27.5	67.3	0.409	128.19	25.5	66.2	0.384	174.869
	25.3	70.7	0.358	140.842	25.8	67.5	0.382	173.432
	22.1	72.4	0.306	169.663	25.8	67.5	0.382	173.432
Min			0.306	128.19			0.376	106.061
Max			0.45	189.698			0.457	178.559
Avr.			0.387	156.384			0.407	147.631

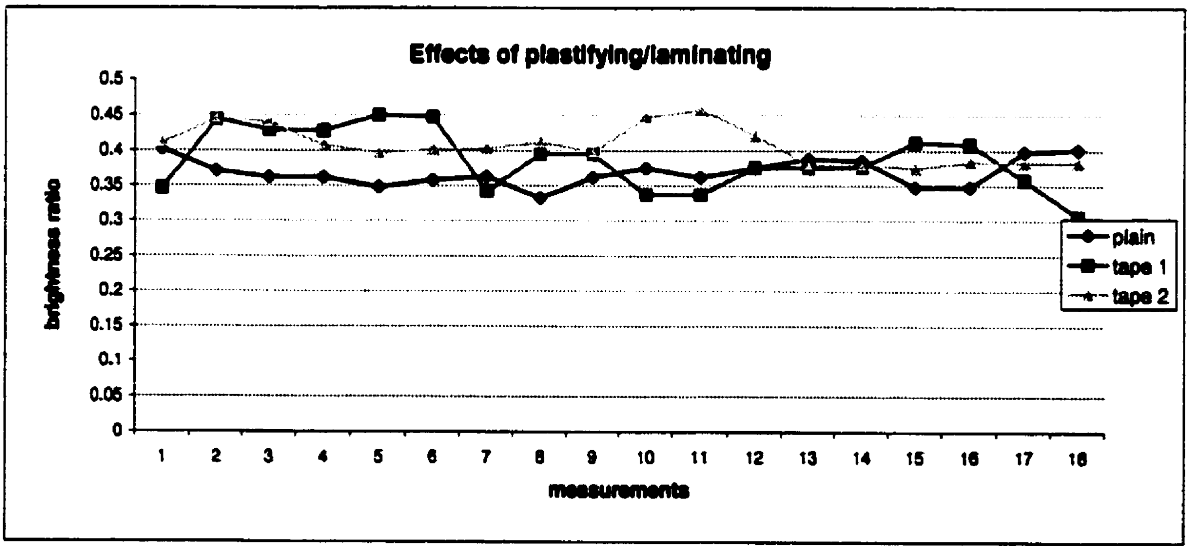

camera 8 gamma 1

case 1 (App 8)

Temp. 9 - bar 1				
	MinBr [W/m²]	MaxBr [W/m²]	Ratio	Grad.m
	10.7	47.7	0.226	130.293
	10.9	49.9	0.219	130.21
	11.1	49.9	0.222	127.508
	10.5	49.3	0.213	146.409
	10.6	48.6	0.218	142.844
	10.6	48.6	0.218	142.844
	11.2	47.1	0.238	131.539
	10.8	45.8	0.237	119.752
	10.7	47.7	0.226	130.293
	11.5	45.4	0.254	119.513
	10.7	47.7	0.226	130.293
	10.9	43.8	0.25	107.092
	9.7	47.8	0.202	149.466
	9.7	47.9	0.202	144.548
	10.7	47.7	0.226	130.293
	10	48.4	0.206	126.629
	11.1	49.3	0.225	139.125
	10.3	49.1	0.21	148.059
Min			0.202	107.092
Max			0.254	149.466
Avr.			0.223	133.095

camera 8 gamma 1

case 1 (App 8)

Temp. 9 - bar 1 (tape1)					Temp. 9 - bar 2 (tape2)			
	MinBr [W/m²]	MaxBr [W/m²]	Ratio	Grad.m	MinBr [W/m²]	MaxBr [W/m²]	Ratio	Grad.m
	11.4	53.2	0.214	119.929	12.3	52.4	0.236	122.702
	15.4	53.4	0.289	109.968	10.8	51.4	0.21	124.861
	13.5	52	0.26	117.256	11.1	49.7	0.223	117.703
	14.9	55.2	0.27	149.43	10.7	51.7	0.208	123.053
	11.2	54	0.207	151.625	10.5	49.8	0.211	138.211
	11.2	54	0.207	151.625	10.4	49.4	0.21	135.094
	9.4	51.7	0.182	153.264	10.7	52	0.207	132.868
	11.4	53.5	0.214	155.626	10.6	49	0.216	134.202
	10	53	0.189	150.066	10.6	52.1	0.202	129.291
	10.1	50.5	0.2	150.733	10.4	47.8	0.218	125.838
	10.2	49.7	0.205	135.606	10.3	47.3	0.218	125.775
	10	50.8	0.197	137.034	10.6	47.7	0.221	127.62
	10.3	51.3	0.2	135.105	10.8	46.5	0.233	122.161
	14	50.5	0.277	125.645	13.4	47	0.285	112.35
	15.7	54.2	0.289	131.184	11.1	46.9	0.238	119.929
	15.6	54.7	0.284	126.695	12	52.6	0.228	131.567
	13.8	54	0.255	131.793	11.5	52.6	0.218	131.969
	12.2	53.9	0.226	138.212	11.3	52.5	0.216	133.824
Min			0.182	109.968			0.202	112.35
Max			0.289	155.626			0.285	138.211
Avr.			0.231	137.268			0.222	127.167

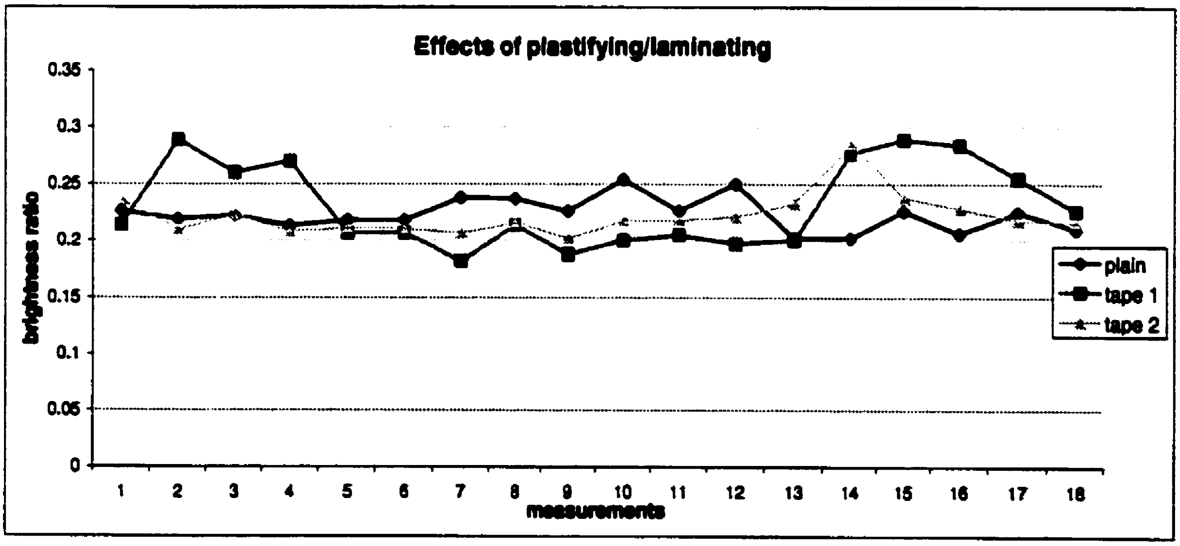

camera B gamma 1

case 1 (App 8)

	Temp. 13 - bar 1			
	MinBr $[W/m^2]$	MaxBr $[W/m^2]$	Ratio	Grad.m
	19.6	52.7	0.371	95.724
	19.8	53.9	0.367	111.912
	21.1	53.7	0.392	101.642
	18.5	52.8	0.35	129.866
	18.3	53.5	0.342	136.102
	18.4	54.7	0.337	127.973
	17.3	49.8	0.347	114.649
	17.8	50.1	0.355	118.36
	17.8	50.1	0.355	118.36
	19.3	49.6	0.39	101.665
	21.2	50.3	0.422	94.535
	19.7	50.4	0.391	96.976
	19.2	52.8	0.364	89.453
	19	52	0.366	115.409
	19	52	0.366	115.409
	17.8	52.6	0.339	122.483
	18.1	50.8	0.357	111.976
	20.3	53.8	0.377	104.183
Min			0.337	89.453
Max			0.422	136.102
Avr.			0.366	111.482

camera B gamma 1

case 1 (App 8)

	Temp. 13 - bar 1 (tape1)				Temp. 13 - bar 2 (tape 2)			
	MinBr $[W/m^2]$	MaxBr $[W/m^2]$	Ratio	Grad.m	MinBr $[W/m^2]$	MaxBr $[W/m^2]$	Ratio	Grad.m
	23.4	52.1	0.449	92.34	22.8	52	0.438	89.384
	23.3	52.3	0.446	92.374	21.8	51.4	0.424	89.171
	22.8	52.3	0.436	91.859	21.8	51	0.428	92.772
	20.6	52.4	0.394	129.319	18.7	51	0.366	112.523
	20.8	51.4	0.404	128.449	18.6	50.4	0.368	107.924
	20.3	51.6	0.394	128.403	18.5	50.8	0.365	110.129
	20.6	50.1	0.41	123.049	18.6	50.9	0.366	111.034
	20.1	49.8	0.403	123.049	18.7	51.1	0.367	109.273
	20.4	50.2	0.406	122.171	18.9	51	0.371	109.339
	21	48.7	0.431	84.358	19.7	50.4	0.391	98.295
	20.7	49.2	0.421	85.641	19.5	50	0.389	102.104
	21.3	49.2	0.433	89.622	19.1	50.3	0.379	100.821
	20.2	50.5	0.399	122.317	18.9	51.2	0.369	102.213
	20.3	50.8	0.399	120.867	18.8	51.6	0.364	105.738
	19.8	51	0.387	127.089	19	51.9	0.367	110.696
	19.8	51.1	0.388	124.067	18.8	51.7	0.364	113.246
	20.1	51.6	0.389	126.171	19.3	51.9	0.371	111.013
	19.5	51.9	0.376	129.744	19.2	51.8	0.371	109.237
Min			0.376	84.358			0.364	89.171
Max			0.449	129.744			0.438	113.246
Avr.			0.409	113.382			0.381	104.717

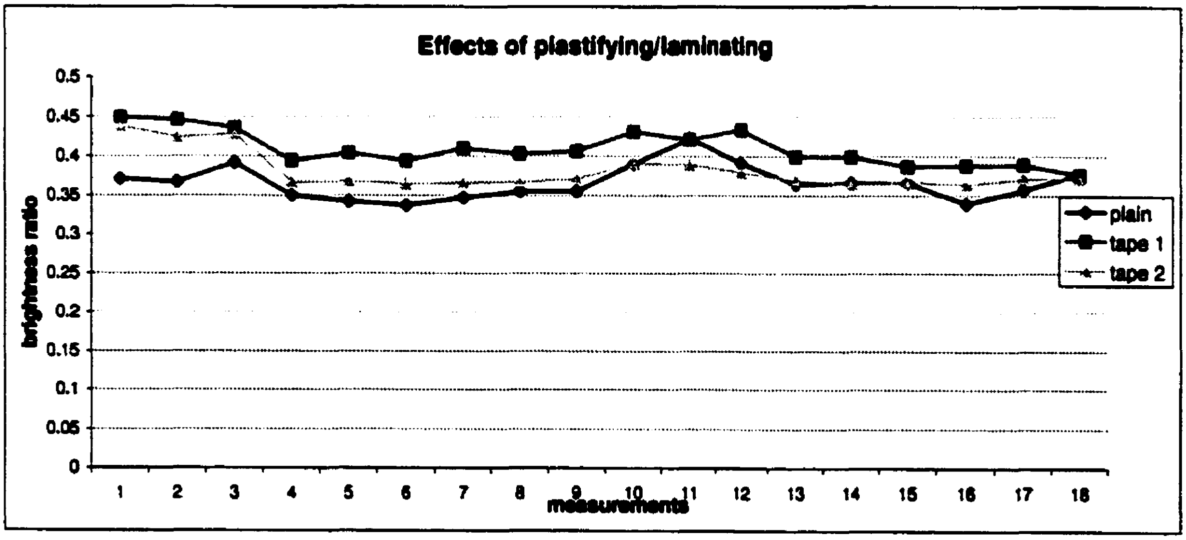

APPENDIX C

POSITION COMPUTATION ALGORITHM

Triangulation refers to the process of determining the (x, y, z) coordinates of a three-dimensional point from the observed position of two perspective projections of the point. The routine uses an algorithm [56] developed by Sensor Adaptive incorporation. The routine is based on the following camera model mapping (x,y,z) to undistorted pixel (f,g):

$$f(u)=\frac{a(0)\cdot x+a(1)\cdot y+a(2)\cdot z+a(3)}{a(8)\cdot x+a(9)\cdot y+a(10)\cdot z+1} \quad \text{(A.3)}$$

$$f(u) = f+D(f)(df,order,f,g) \quad \text{(A.4)}$$

$$g(u)=\frac{a(4)\cdot x+a(5)\cdot y+a(6)\cdot z+a(7)}{a(8)\cdot x+a(9)\cdot y+a(10)\cdot z+1} \quad \text{(A.5)}$$

$$g(u) = g+D(g)(dg,order,f,g) \quad \text{(A.6)}$$

Where:

- (f,g) is frame buffer pixel coordinate(column,row) with arbitrary origin.
- (x,y,z) is world coordinate ie(mm).
- a(k) k = 0...10 are unknown camera parameters.
- D(f)(df,order,f,g) is a polynomial lens distortion model in f .

- D(g)(dg,order,f,g) is a polynomial lens distortion model in, g.

Using the previously calculated a (k) parameters and assuming that (F_1, G_1) and (F_2, G_2) is the perspective projection of a 3D point (x, y, z) the position of target is calculated by solving the set of equations (A.3, …A.6)

The C++ (Borland) algorithm

```
//transforms pixel locations into world coordinates//
#include <alloc.h>
#include <windows.h>
#include <string.h>
#include <stdlib.h>
#include <stdio.h>
#include <process.h>
#include <math.h>
#include <dos.h>    // used for computing the time ...
#include <time.h>


double **M;
double B[8][2];

int dvector(int, int, double **);
int dmatrix(int, int, int, int, double ***);
void nrerror(char);
void free_dvector(double *, int, int);
void free_dmatrix(double **,int, int, int, int);
//void svdcmp(float a,int,int,float w,float v);
void dsvdcmp(double **a, int m, int n, double w[], double **v);

int dsvbksb(double **,double *,double **,int,int,double *,double *);

void get_coeficients();
void get_pixels();
int convert();

int main()
{
   #define SINGULARITY_THRESHOLD (float)1e-8;
 // #define ERROR_CODE error = 0;

   int error;

   double ** C, **a, **u; // xyz_fg mapping equations
   double ** V; // output from svdcmp
   double * w, *v;
   double * x;    // world points
   double * b;
```

```
double * testVect;
double temp1,temp2;
double F1,F2,G1,G2;
double scaled_cam1_x, scaled_cam2_x,
     scaled_cam1_y, scaled_cam2_y ;
double rSensorCoordinate_x, rSensorCoordinate_y, rSensorCoordinate_z;
   int thaa;
FILE *ftr;

get_coeficients();

get_pixels();


// if ( m_CalCoeffs.camera[0].fg_factors.f.offset == DBL_MAX )
//    error = SENSOR_IS_NOT_CALIBRATED;
// else
ftr=fopen("coord.dat","w");

   if( !(error = dmatrix(1, 4, 1, 3, &C)) )
   {
      if( !(error = dmatrix(1, 3, 1, 3, &V)) )
     {
        if( !(error = dvector(1, 3, &w)) )
        {
           if( !(error = dvector(1, 3, &x)) )
           {
              if( !(error = dvector(1, 4, &b)) )
              {


                 scaled_cam1_x = ( B[0][0] - M[4][0])/M[4][1];
                 scaled_cam1_y = ( B[0][1] - M[5][0])/M[5][1];



                 scaled_cam2_x = ( B[3][0] - M[9][0])/M[9][1];
                 scaled_cam2_y = ( B[3][1] - M[10][0])/M[10][1];

                 temp1 = scaled_cam1_x * scaled_cam1_x;
                 temp2 = scaled_cam1_y * scaled_cam1_y;

                 F1 = scaled_cam1_x +
                   (M[2][0]+ scaled_cam1_x * M[2][1]+ scaled_cam1_y * M[2][2]+
                    temp1 * M[2][3] + scaled_cam1_x * scaled_cam1_y * M[2][4] +
                    temp2 * M[2][5] + scaled_cam1_x * temp1 * M[2][6] +
                    scaled_cam1_y * temp1 * M[2][7] +
                    scaled_cam1_x * temp2 * M[2][8] +
                    scaled_cam1_y * temp2 * M[2][9]);


                 G1 = scaled_cam1_y +
                  (M[3][0]+ scaled_cam1_x * M[3][1]+ scaled_cam1_y * M[3][2]+
                    temp1 * M[3][3] + scaled_cam1_x * scaled_cam1_y * M[3][4] +
                    temp2 * M[3][5] + scaled_cam1_x * temp1 * M[3][6] +
                    scaled_cam1_y * temp1 * M[3][7] +
```

```
            scaled_cam1_x * temp2 * M[3][8] +
            scaled_cam1_y * temp2 * M[3][9]);

        temp1 = scaled_cam2_x * scaled_cam2_x;
        temp2 = scaled_cam2_y * scaled_cam2_y;

        F2 = scaled_cam2_x +
          ( M[7][0]+ scaled_cam2_x * M[7][1]+ scaled_cam2_y * M[7][2]+
            temp1 * M[7][3] +  scaled_cam2_x * scaled_cam2_y * M[7][4] +
            temp2 * M[7][5] +  scaled_cam2_x * temp1 * M[7][6] +
            scaled_cam2_y * temp1 * M[7][7] +
            scaled_cam2_x * temp2 * M[8][8] +
            scaled_cam2_y * temp2 * M[7][9]);


        G2 = scaled_cam2_y +
          (  M[8][0]+ scaled_cam2_x * M[8][1]+ scaled_cam2_y * M[8][2]+
            temp1 * M[8][3] +  scaled_cam2_x * scaled_cam2_y * M[8][4] +
            temp2 * M[8][5] +  scaled_cam2_x * temp1 * M[8][6] +
            scaled_cam2_y * temp1 * M[8][7] +
            scaled_cam2_x * temp2 * M[8][8] +
            scaled_cam2_y * temp2 * M[8][9]);


        b[1] = F1 - M[1][3];
        b[2] = G1 - M[1][7];
        b[3] = F2 - M[6][3];
        b[4] = G2 - M[6][7];

        C[1][1] = M[1][0] - ( M[1][8] * F1);
        C[1][2] = M[1][1] - ( M[1][9] * F1);
        C[1][3] = M[1][2] - ( M[1][10] * F1);

        C[2][1] = M[1][4] - ( M[1][8] * G1);
        C[2][2] = M[1][5] - ( M[1][9] * G1);
        C[2][3] = M[1][6] - ( M[1][10] * G1);

        C[3][1] = M[6][0] - ( M[1][8] * F2);
        C[3][2] = M[6][1] - ( M[1][9] * F2);
        C[3][3] = M[6][2] - ( M[1][10] * F2);

        C[4][1] = M[6][4] - ( M[1][8] * G2);
        C[4][2] = M[6][5] - ( M[1][9] * G2);
        C[4][3] = M[6][6] - ( M[1][10] * G2);

        // find (x,y,z) coord.

        dsvdcmp(C,4,3,w,V);
//                puts("check");

//scanf("%d", &thaa);
              // {

            if( !(error = dsvbksb(C,w,V,4,3,b,x)) )
            {
```

```
                    printf("x[1] = %lf,x[2] = %lf,x[3] = %lf", x[1],x[2],x[3]);
                    scanf("%lf", &x[1]);

                      rSensorCoordinate_x = (double)( x[1] * M[11][1] + M[11][0]);
                      rSensorCoordinate_y = (double)( x[2] * M[12][1] + M[12][0]);
                      rSensorCoordinate_z = (double)( x[3] * M[13][1] + M[13][0]);


                      fprintf(ftr,"%lf  %lf %lf ",rSensorCoordinate_x,rSensorCoordinate_y,
                      rSensorCoordinate_z);

                    }
                  // }
                  free_dvector( b, 1, 4);
                }
                free_dvector( x, 1, 3);
              }
              free_dvector( w, 1, 3);
            }
            free_dmatrix( V, 1, 3, 1, 3);
          }
          free_dmatrix( C, 1, 4, 1, 3);
        }

    fclose(ftr);

  // return error;

  return 0;
}


void nrerror(char error_text[])

//numerical recipes standard error handler
{
 //       void exit();

  fprintf(stderr,"Numerical Recipes run-time error...\n");
  fprintf(stderr,"%s\n",error_text);
  fprintf(stderr,"...now exiting to system...\n");
  exit(1);
}


int dvector(int nl, int nh, double **v)

//allocates a double vector with range [nl..nh]
{
  *v = (double *)malloc((unsigned) (nh-nl+1+1)*sizeof(double));
  if ( !(*v) )
  {
        nrerror("allocation failure in vector()");
    return 1;
```

```
  }

  (*v) -= nl;

  return 0;
}


/*
double *dvector(int nl, int nh)
//allocates a double vector with range [nl...nh.
{
        double *v;
  v = (double *)malloc((unsigned) (nh-nl+1)*sizeof(double));
   if ( !v ) nrerror("allocation failure in vector()");
   return v-nl;
}
*/

int dmatrix(int nrl, int nrh, int ncl, int nch, double ***m)

//allocates a double matrix with range [nrl..nrh][ncl..nch]
{
        int i;

  //allocate pointers to rows
  *m = (double **)malloc((unsigned)(nrh-nrl+1+1)*sizeof(double*));
  if (!(*m) )
    {
        nrerror("allocation failure 2 in matrix()");
    return 1;
    }
         (*m)-=nrl;

        //allocate rows and set pointers to them
  for(i=nrl;i<=nrh;i++){
        (*m)[i]=(double *)malloc((unsigned)(nch-ncl+1+1)*sizeof(double));
    if (!(*m)[i])
        {
        nrerror("allocation failure 2 in matrix()");
      return 1;
      }
         (*m)[i]-=ncl;

    }
  //return pointer to array of pointers to rows
  return 0;
}


void free_dvector(double *v, int nl, int nh)

//frees a double vector allocated by vector()
{
        free(((v+nl)));
}
```

```
void free_dmatrix(double **m,int nrl, int nrh, int ncl, int nch)

//frees a matrix allocated with dmatrix
{
	int i;

  for (i=nrh;i>=nrl;i--)free((m[i]+ncl));
  free((m+nrl));
}



static double at,bt,ct;
#define PYTHAG(a,b)
((at=fabs(a))>(bt=fabs(b))?(ct=bt/at,at*sqrt(1.0+ct*ct)):(bt?(ct=at/bt,bt*sqrt(1.0+ct*ct)):0.0))
static double maxarg1,maxarg2;
#define MAX(a,b)(maxarg1=(a),maxarg2=(b),(maxarg1)>(maxarg2)?(maxarg1):(maxarg2))
static double minarg1,minarg2;
#define MIN(a,b)(minarg1=(a),minarg2=(b),(minarg1)<(minarg2)?(minarg1):(minarg2))
#define SIGN(a,b) ((b)>=0.0 ? fabs(a):-fabs(a))


///*************************************************************

void dsvdcmp(double **a, int m, int n, double w[], double **v)
{
//	float PYTHAG(float a, float b);
	int flag,i,its,j,jj,k,l,nm;
	double anorm,c,f,g,h,s,scale,x,y,z,*rv1;

	dvector(1,n,&rv1);
	g=scale=anorm=0.0;
	for (i=1;i<=n;i++) {
		l=i+1;
		rv1[i]=scale*g;
		g=s=scale=0.0;
		if (i <= m) {
			for (k=i;k<=m;k++) scale += fabs(a[k][i]);
			if (scale) {
				for (k=i;k<=m;k++) {
					a[k][i] /= scale;
					s += a[k][i]*a[k][i];
				}
				f=a[i][i];
				g = -SIGN(sqrt(s),f);
				h=f*g-s;
				a[i][i]=f-g;
				for (j=l;j<=n;j++) {
					for (s=0.0,k=i;k<=m;k++) s += a[k][i]*a[k][j];
					f=s/h;
					for (k=i;k<=m;k++) a[k][j] += f*a[k][i];
				}
				for (k=i;k<=m;k++) a[k][i] *= scale;
```

```
				}
			}
			w[i]=scale *g;
			g=s=scale=0.0;
			if (i <= m && i != n) {
				for (k=l;k<=n;k++) scale += fabs(a[i][k]);
				if (scale) {
					for (k=l;k<=n;k++) {
						a[i][k] /= scale;
						s += a[i][k]*a[i][k];
					}
					f=a[i][l];
					g = -SIGN(sqrt(s),f);
					h=f*g-s;
					a[i][l]=f-g;
					for (k=l;k<=n;k++) rv1[k]=a[i][k]/h;
					for (j=l;j<=m;j++) {
						for (s=0.0,k=l;k<=n;k++) s += a[j][k]*a[i][k];
						for (k=l;k<=n;k++) a[j][k] += s*rv1[k];
					}
					for (k=l;k<=n;k++) a[i][k] *= scale;
				}
			}
			anorm=MAX(anorm,(fabs(w[i])+fabs(rv1[i])));
		}
		for (i=n;i>=1;i--) {
			if (i < n) {
				if (g) {
					for (j=l;j<=n;j++)
						v[j][i]=(a[i][j]/a[i][l])/g;
					for (j=l;j<=n;j++) {
						for (s=0.0,k=l;k<=n;k++) s += a[i][k]*v[k][j];
						for (k=l;k<=n;k++) v[k][j] += s*v[k][i];
					}
				}
				for (j=l;j<=n;j++) v[i][j]=v[j][i]=0.0;
			}
			v[i][i]=1.0;
			g=rv1[i];
			l=i;
		}
		for (i=MIN(m,n);i>=1;i--) {
			l=i+1;
			g=w[i];
			for (j=l;j<=n;j++) a[i][j]=0.0;
			if (g) {
				g=1.0/g;
				for (j=l;j<=n;j++) {
					for (s=0.0,k=l;k<=m;k++) s += a[k][i]*a[k][j];
					f=(s/a[i][i])*g;
					for (k=i;k<=m;k++) a[k][j] += f*a[k][i];
				}
				for (j=i;j<=m;j++) a[j][i] *= g;
			} else for (j=i;j<=m;j++) a[j][i]=0.0;
			++a[i][i];
		}
```

```
for (k=n;k>=1;k--) {
	for (its=1;its<=30;its++) {
		flag=1;
		for (l=k;l>=1;l--) {
			nm=l-1;
			if ((float)(fabs(rv1[l])+anorm) == anorm) {
				flag=0;
				break;
			}
			if ((float)(fabs(w[nm])+anorm) == anorm) break;
		}
		if (flag) {
			c=0.0;
			s=1.0;
			for (i=l;i<=k;i++) {
				f=s*rv1[i];
				rv1[i]=c*rv1[i];
				if ((float)(fabs(f)+anorm) == anorm) break;
				g=w[i];
				h=PYTHAG(f,g);
				w[i]=h;
				h=1.0/h;
				c=g*h;
				s = -f*h;
				for (j=1;j<=m;j++) {
					y=a[j][nm];
					z=a[j][i];
					a[j][nm]=y*c+z*s;
					a[j][i]=z*c-y*s;
				}
			}
		}
		z=w[k];
		if (l == k) {
			if (z < 0.0) {
				w[k] = -z;
				for (j=1;j<=n;j++) v[j][k] = -v[j][k];
			}
			break;
		}
		if (its == 30) nrerror("no convergence in 30 svdcmp iterations");
		x=w[l];
		nm=k-1;
		y=w[nm];
		g=rv1[nm];
		h=rv1[k];
		f=((y-z)*(y+z)+(g-h)*(g+h))/(2.0*h*y);
		g=PYTHAG(f,1.0);
		f=((x-z)*(x+z)+h*((y/(f+SIGN(g,f)))-h))/x;
		c=s=1.0;
		for (j=l;j<=nm;j++) {
			i=j+1;
			g=rv1[i];
			y=w[i];
			h=s*g;
			g=c*g;
```

```
						z=PYTHAG(f,h);
						rv1[j]=z;
						c=f/z;
						s=h/z;
						f=x*c+g*s;
						g = g*c-x*s;
						h=y*s;
						y *= c;
						for (jj=1;jj<=n;jj++) {
							x=v[jj][j];
							z=v[jj][i];
							v[jj][j]=x*c+z*s;
							v[jj][i]=z*c-x*s;
						}
						z=PYTHAG(f,h);
						w[j]=z;
						if (z) {
							z=1.0/z;
							c=f*z;
							s=h*z;
						}
						f=c*g+s*y;
						x=c*y-s*g;
						for (jj=1;jj<=m;jj++) {
							y=a[jj][j];
							z=a[jj][i];
							a[jj][j]=y*c+z*s;
							a[jj][i]=z*c-y*s;
						}
					}
					rv1[l]=0.0;
					rv1[k]=f;
					w[k]=x;
				}
			}
	free_dvector(rv1,1,n);
}


int dsvbksb(double **u, double *w, double **v,int m,int n,double *b,double *x)

/*solves A*X=B for a vector X, where A is specified by the arrays
  u[1..m],w[1..n],v[1..n][1..n] as returned by svdcmp.  m and n are the
  dimensions of A, and will be equal for square matrices.  b[1..m]
  is the input right-hand side.  x[1..n] is the output solution vector.*/

 {
	int jj,j,i;
  double s,*dtmp;

  dvector(1,n, &dtmp);

  for (j=1;j<=n;j++){  //calculate  transpuse of U*B
	s=0.0;
    if (w[j]) {
	for (i=1; i<=m; i++)
```

```
          s += u[i][j]*b[i];
        s/= w[j];
      }
      dtmp[j]=s;
    }

    for (j=1 ; j<=n; j++){    //matrix multiply by V to get ansver.
            s=0.0;
      for (jj=1; jj<=n; jj++) s += v[j][jj]*dtmp[jj];
      x[j]=s;
    }
    free_dvector(dtmp,1,n);

    return 0;
}

void get_coeficients()
{
            FILE *Input_file ;

            int i,j , jj ;
            int mm[15] = {6,11,10,10, 2,2,11,10,10, 2,2, 2,2,2, 1}      ;

            //Input_file = fopen("coeffs.txt", "r")          ;
    //Input_file = fopen("verniercoefs.txt", "r")          ;
    Input_file = fopen("cmmcoefs.txt", "r")  ;
    //Input_file = fopen("rulercoefs.txt", "r") ;

            M = (double **)calloc(15, sizeof(double *));

            j=0       ;
            for ( i = 0 ; i < 15 ; i++ )
  {
                        M[i] = (double *)calloc( mm[j] , sizeof(double));
                        j++       ;
  }

            jj=0      ;
            for ( i = 0 ; i < 15 ; i++ )
            {
                        for ( j = 0 ; j < mm[jj] ; j++ )
                        {                      fscanf(Input_file, "%lf", &M[i][j]);   }
                        jj++      ;
            }

    fclose(Input_file);

}

void get_pixels()
{
            FILE *fp;
    char buffer[80];
    int i = 0;

    fp = fopen("Pixel_lo.dat", "r");
```

```
        while( fgets(buffer, 80, fp) != NULL )
  {
        sscanf(buffer, "%lf%lf", &(B[i][0]), &(B[i][1]) );

    i++;
  }

  fclose(fp);
}
```

VITA AUCTORIS

NAME:	Melinda Harmos
PLACE OF BIRTH:	Tg. Mures, Romania
EDUCATION:	University of Transilvania, BRASOV, Romania Mechanical Engineering, 1989-1994, B.Sc.
	University of Windsor, Windsor, Ontario 1996-1999, M.A.Sc.